이학박사 학위논문

Present and past organic carbon cycling on the Amundsen Shelf, Antarctica: Implications from radiocarbon and sterols

방사성탄소동위원소와 스테롤을 통한 현재와 과거 남극 아문젠해 유기탄소 순환 고찰

August 2019

Graduate School

Seoul National University

Earth and Environmental Sciences

MINKYOUNG KIM

Abstract

Present and past organic carbon cycling on the Amundsen Shelf, Antarctica: Implications from radiocarbon and sterols

Minkyoung Kim
School of Earth and Environmental Sciences
The Graduate School
Seoul National University

The Amundsen Sea in the west Antarctic is experiencing rapid glacial melting and declining in sea-ice according to the climate change. This physical change is expected to influence the carbon cycling in the Amundsen Sea. The change is not one dimensional and therefore, it is important to understand the past and present organic carbon cycling in the Amundsen Sea to project the role of the Amundsen Sea in the future.

To further our understanding of organic carbon cycling on the Amundsen Shelf, a research was carried out in collaboration with KOPRI (Korea Polar Research Institute), ETH Zürich, and BAS (British Antarctic Survey) adopting multidimensional and multidisciplinary approaches. Various aspects of particulate organic carbon (POC) and sedimentary organic carbon (SOC) cycling in present and past were investigated. Sinking particles and sediment samples were collected during 4 cruises and sediment trap moorings from 2011 to 2018.

Sediment trap is the only way to investigate year-round biological pump system in this region due to observational constraints. I tried to extend spatial and temporal understanding of sinking particles from one year study in perennial sea ice zone. Sinking particles, collected by a sediment trap deployed at three different sites (perennial sea ice zone, Amundsen Sea Polynya (ASP), and in front of the Dotson Ice Shelf). POC flux in the perennial ice-covered area where diatoms are dominant phytoplankton species can be high and comparable to that of the central polynya. Two years of sediment trap data covering three summers were obtained and examined sea ice evolution and POC export and their relationship. The summertime POC flux showed high interannual variability with the reduction in sea ice cover in early summer for sufficient insolation being critical to enhanced sinking POC flux (Chapter 3, as it is published in *Journal of Marine Systems*).

Collection of large benthic invertebrates including juvenile scallops, a sea urchin, and long and slender worms in sediment traps for 2 years at three locations in the Amundsen Shelf also have been reported (Chapter 4). To our

knowledge, this is the first reporting of collection of benthic macro organisms without swimming capability in the sediment trap. Organic carbon supplied by worms accounted for up to 5-fold the POC flux derived from primary production in the overlying water column. The collection of these organisms occurred predominantly during the austral winter. Plausible source region and transport mechanisms of these benthic organisms and the impacts on Antarctic biology, as a disturbance to benthic ecosystems, a dispersal mechanism for benthic invertebrates, and an energy supply to the deeper benthic ecosystems were investigated (Chapter 4, as it is published in *Biogeosciences*).

Sediment samples collected by gravity core and boxcore were used to investigate recent and Holocene organic carbon cycling in this region. High resolution radiocarbon ages in depth for the cores were analyzed. History of the ASP formation and sedimentation characteristics were examined from three gravity cores recovered in the shelf break, inside the polynya, and near the Dotson Ice Shelf (Chapter 5). The up-core variation of biogeochemical proxies implied that the shelf break region and the ASP experienced different environment after deglaciation. Based on paleoproductivity proxies (ratio of Br/Ti, Ba/Al), OC normalized brassicasterol, and diatom valve abundances, temporal evolution of the ASP were suggested. The ASP suspected to be exist right after the deglaciation and the dominant plankton species may be shifted 9~6 kyr cal BP.

In addition, box core samples from various locations of different surface water conditions in the western Amundsen Shelf were investigated to complement the spatial limitation of gravity cores. Radiocarbon, biomarkers representing phytoplankton communities and paleoproductivity (brassicasterol, cholesterol, and dinosterol), and grain size were analyzed for a high spatial-resolution of SOC accumulation characteristics on the Amundsen Shelf (Chapter 6).

This study contributes to further advance our understanding and future climate model of the organic carbon cycling in the Amundsen Sea, one of the most rapidly changing, the least affected by human activity region around the Antarctica.

Keywords: particulate organic carbon, radiocarbon, sediment trap, gravity core, Amundsen Sea

***Student Number**: 2014-31014*

TABLE OF CONTENTS

LIST OF FIGURES

LIST OF TABLES

`

Chapter 1. Introduction

1.1. Background and motivation

Changing Antarctic

Southern Ocean sea ice exhibits marked regional variations, with some sectors decreasing in sea ice extent and duration, and others increasing (Thomas et al., 2004; Turner et al., 2009). Western part of Antarctica suffers ice sheet loss driven by basal melting of ice shelves, ice thickness decreasing, coincident with warming in recent decades (Rignot et al., 2008; Pritchard et al., 2009; Stammerjohn 2012).

Especially the Amundsen Sea, in the west Antarctic shows significant sea ice retreat, ice sheet melting, and glacier melting that causing over 1 mm/yr of global sea level rise (Pritchard et al., 2012; Joughin et al., 2014). Inflow and upwelling of warm, dense circumpolar deep water (CDW) through bottom glacial troughs onto the continental shelf suspected as the main driver of these environmental change (Pritchard et al., 2012; Dutrieux et al., 2014).

`

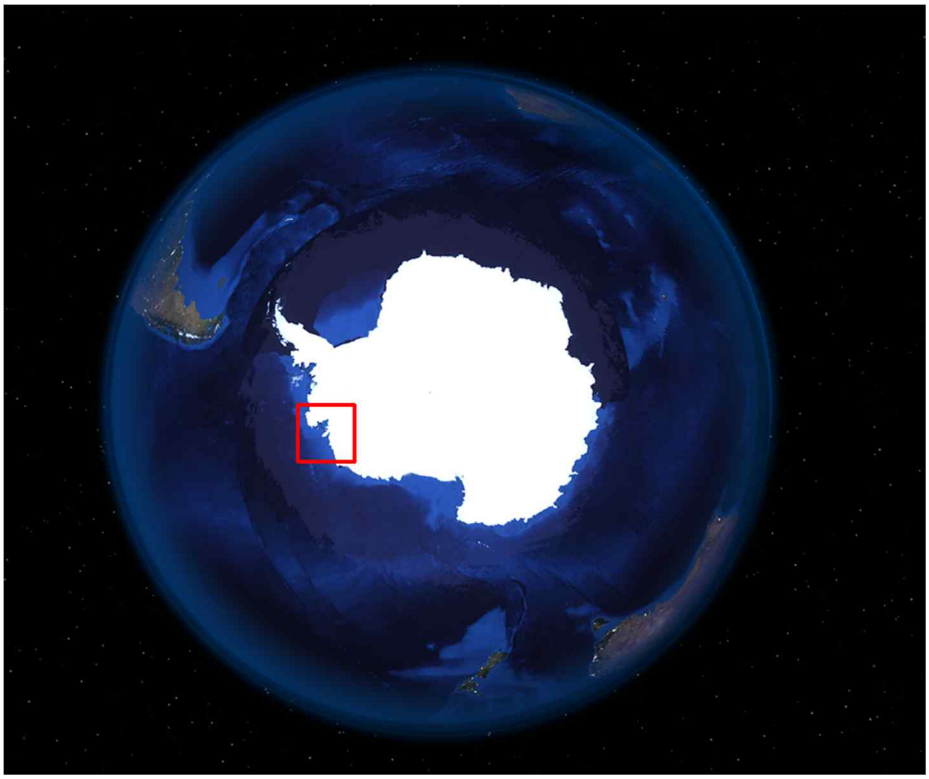

Figure 1.1. Location of the Amundsen Sea, in the west Antarctic.

Antarctic Polynyas

Polynyas, seasonally open water area surrounded by sea ice and/or land in the polar regions, are known to be associated with intensively high primary productivity in summer (Arrigo and Van Dijken 2003; Smith and Barber, 2007). Polynyas categorized into latent heat polynyas and sensible heat polynyas based on the formation process (Smith and Barber, 2007). Most of latent heat polynyas in the Antarctic are formed through katabatic wind, encountered to the coastline and on the narrow continental shelf (Massom et al., 1998). Reduced sea ice coverage in austral summer and supply of nutrients fueled the phytoplankton bloom in the polynyas

`

(Arrigo et al., 2012). Primary production in Antarctic polynyas typically exceeds 1 gC $m^{-2}d^{-1}$ on average, much higher than offshore waters of the Southern Ocean (0.2~0.4 gC $m^{-2}d^{-1}$; Arrigo et al., 2008).

The Amundsen Sea in the west Antarctic hosts two large and persistent polynyas: Amundsen Sea Polynya (ASP) in the West and the Pine Island Polynya (PIP) in the East. The ASP is one of the most productive coastal polynya around Antarctica (Arrigo and Van Dijken 2003; Arrigo et al., 2012; Mu et al., 2014). It is therefore important to understand the fate of the extensive phytoplankton blooms occurring in the ASP both in the present and the past.

Amundsen Sea

The Amundsen Sea has been explored by a few international programs: United State Amundsen Sea Polynya International Research Expedition (ASPIRE; Yager et al., 2016) and Rutgers, United Kingdom Ice Sheet Stability program (iSTAR), the Sweden/US Oden Southern Ocean expeditions, and Korea Polar Research Institute (KOPRI) Amundsen project (Lee et al., 2017). This research was performed as part of the major research objectives of KOPRI Amundsen project: Characteristics of biological pump system of the Amundsen Sea.

The magnitude and carbon export efficiency in the polynyas vary seasonally and interannually (Smith and Barber, 2007). Sediment trap study was vital because it is the only feasible way to collect year-round sinking particle samples. Especially because of difficulty of deployment and recovery of moorings, perennially sea-ice-covered area in the Amundsen Sea (and around Antarctica in general) has been poorly studied. KOPRI successfully recovered sediment trap samples from 4

`

locations, between 2011 and 2018 at different surface water conditions on the Amundsen Shelf. Previously, Kim et al. (2015) compared the sinking particle flux between in the SIZ (sea ice zone) and inside the ASP and suggested that POC flux at both sites in summer were comparable despite the considerable difference in primary productivity. In this dissertation, temporally expanded two-year data covering three summers were obtained in the perennial SIZ. Sea ice evolution and POC export and their relationship in perennial SIZ was examined, too. Spatial comparisons among the sinking particles obtained in perennial SIZ, inside the ASP and in front of DIS were also made.

It is important to understand how much OC is finally deposited and sequestrated in sediment. Most of freshly produced organic matter is recycled within the water column and a small fraction is deposited in sediment in the Southern Ocean (Nelson et al., 1996). Lee et al. (2017) also showed low carbon sequestration on the Amundsen Shelf. Several studies investigated the deglaciation in the western Amundsen Sea embayment (Hillenbrand et al., 2003, 2017; Smith et al., 2014; Larter et al., 2014). These studies mainly focused on millennial scale paleoceanography such as grounding line retreat and deglaciation on the Amundsen Sea. Different sedimentation characteristics and trends of OC in the Holocene have not been closely studied. Three gravity cores represents perennial SIZ, inside the ASP, and in front of the Dotson Ice Shelf focusing on the organic carbon cycling in the Holocene since deglaciation was investigated.

To overcome the spatial limitation of gravity core samples, I collected and analyzed short sediment samples by 10s of boxcores from different surface

`

conditions and topographic environments on the western Amundsen Shelf. According to the Kim et al. (2016), the SOC accumulation rates were generally consistent with the spatial distribution of primary productivity in the surface water. Sedimentation characteristics on the Amundsen Shelf from spatially high resolution datasets has been examined.

1.2. Research goals

This dissertation attempted to understand the past and present Amundsen Sea organic carbon cycling based on sinking particles and sediment samples. Sinking particles from perennial sea ice zone, and spatially expanded sinking particle data from the ASP and in front of the Dotson Ice Shelf was studied. With episodically collected benthic invertebrates in sediment trap which is the first reported phenomenon, I attempted to explain the implication of this observation for coastal benthic ecosystem and possibility of anchor ice formation and sea ice habitat. With spatially and temporally extended SOC data by gravity core and boxcore sediments comprehensive information regarding the characteristics of SOC on the Amundsen Shelf in Holocene tried to be obtained. In this dissertation, more comprehensive picture of Amundsen Sea carbon cycling with following key questions were tried to be provided:

1) How different characteristics of sinking particles appeared in the various sea surface conditions on the Amundsen shelf by using spatially and temporally extended sediment trap materials and what kinds of environmental conditions drive this differences?

`

2) How the mysterious marine benthic organisms collected in sediment traps and what would be the plausible mechanisms of their transport? What will be the implications of this finding?

3) After deglaciation, when did the ASP start to develop? And how were these recorded by various biogeochemical and lithological proxy in sediment? How different environment conditions are recorded in each different gravity core sediment?

4) What are the major sources and controlling factors of OC reaching the sea floor? Do multiple biomarker proxies indicate different plankton communities denote surface water productivity? What controls the OC sequestration on the Amundsen Shelf most at different locations?

1.3. Structure of dissertation

Brief background and research goals are presented in Chapter 1. Overall descriptions of the methods are presented in Chapter 2. Chapter 3~6 are written as stand-alone papers. At the end of the dissertation, a summary and outlook for future research (Chapter 7) is presented.

In ***Chapter 2***, sample collections and analysis methods were described. Especially, comparison of two different methods for radiocarbon measurement were explained.

In ***Chapter 3***, the flux and composition of biogenic and non-biogenic components of sinking particles, diatom cell flux, and carbon isotope ratios of sinking POC collected by sediment traps attached to bottom-tethered moorings deployed at depths

`

of 400–500 m from February and March 2012 has been examined. I compared results from three sites (i.e., in a perennial sea-ice-covered area, the central region of the ASP, and close to the Dotson Ice Shelf within the ASP) of different annual sea ice cover and primary production. Time series of multi-year (3 years) sinking particle data at perennial sea ice covered region especially investigated.

In ***Chapter 4***, large benthic invertebrates including juvenile scallops, a sea urchin, and long and slender worms had been collected in sediment traps deployed at 130−567 m above the sea floor at three locations in the Amundsen Shelf, Antarctica. Plausible origin, transport mechanisms, and ecological impacts of these animals has been proposed.

In ***Chapter 5***, three gravity cores were recovered during ANA02C cruise from the shelf break (perennial SIZ), inside the polynya, and near the Dotson Ice Shelf. Compositions (magnetic susceptibility, TOC content, C/N ratio, water content, grain size, $CaCO_3$ content, and metal content) were examined to understand the spatially different paleo-environment on the Amundsen shelf after deglaciation. Br/Ti and Ba/Al ratios, OC normalized brassicasterol, and diatom valve abundances from gravity core collected at ASP also studied to propose the potential timing of ASP development.

In ***Chapter 6***, spatial coverage of boxcore sediment has been extended to overcome the constrains of gravity core as collect sediments at different environment represents

`

the different sea ice concentration and topography. Lipid biomarkers represent mostly diatom (brassicasterol), dinoflagellates (dinosterol), and overall planktons (cholesterol) were analyzed. Preliminary approaches by using surface area measurement and XRD has been tried to understand the relationship between OC cycling and clay mineralogy.

In ***Chapter 7***, the dissertation was concluded by summarizing the findings and their implications in the context of global carbon cycling. Future research directions are presented for remained questions spawning from this research.

`

Chapter 2. Materials and methods

2.1. Sample collection

Amundsen expeditions

Samples were collected from three Amundsen Sea Cruises in 2011-2012 (ANA02C), 2013-2014 (ANA04B), and 2017-2018 (ANA08B) (Figure 2.1). Collected samples include sinking particles and sediment cores. Sample types and collection sites are listed in Table 2.1.

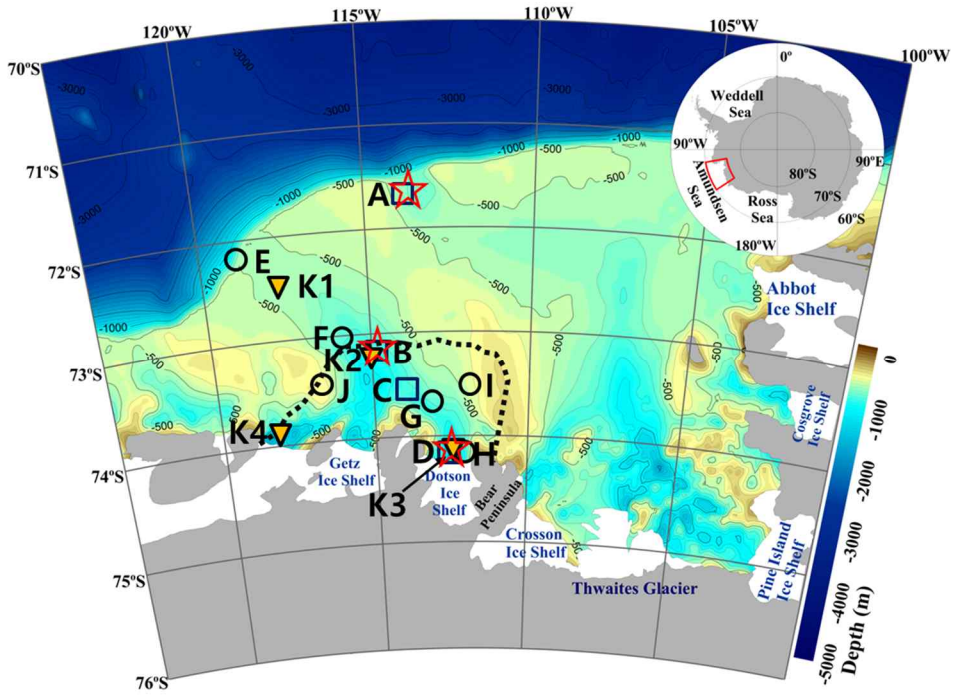

Figure 2.1. Amundsen shelf and sampling locations. Sampling sites for sinking particles (reversed triangle), gravity core (star) and boxcores (circle and square) are indicated.

`

Table 2.1. Amundsen expeditions and collected samples.

Samples collected	Station	Lat (º)	Long (º)	Trap/water depth (m)	Site description	Covered periods (For sediment samples: uncorrected ^{14}C age yrs)	Related publications
Sinking particles	K1	72.40	117.72	400/530	Perennial SIZ	1/5/11~12/28/11 3/7/12~3/16/13	Chap. 3,4 and Kim et al., 2015
	K2	73.28	114.97	410/830	Inside polynya	2/15/12~2/20/13	Chap.3
	K3	74.19	112.54	490/1057	In front of DIS	2/17/12~3/1/13	Chap.3,4
	K4	73.89	118.72	427/688	Near East GIS	2/1/16~2/28/18	Chap.4
Gravity core	A (GC01)	71.70	114.04	543	Shelf break	6921~15098	Chap.5
	B (GC02)	73.23	114.91	802	Inside polynya	3435~16490	Chap.5
	D (GC03)	74.20	112.52	1080	In front of DIS	7161~15290	Chap.5
Box core	A	71.70	114.04	543	Shelf break	3860~15700	Chap 6 and Kim et al., 2016
	B	73.23	114.91	802	periphery polynya	2930~4310	Chap 6 and Kim et al., 2016
	C	74.20	112.52	1080	Inside polynya	3320~6020	Chap 6 and Kim et al., 2016
	D	73.04	115.72	710	In front of DIS	4130~11550	Chap 6 and Kim et al., 2016
	E	72.10	118.88	745	Shelf break	3366~20514	Chap 6
	F	73.62	113.80	777	Perennial SIZ	2994~9247	Chap 6
	G	73.82	113.05	788	Inside polynya	3155~21038	Chap 6
	H	74.17	112.15	1034	In front of DIS	3839~12729	Chap 6
	I	73.50	112	375	boundary polynya, outside DT	3645~16658	Chap 6
	J	73.50	116.50	420	boundary polynya, outside DT	6340~17547	Chap 6
	K1	72.39	117.71	514	Perennial SIZ	2897~9212	Chap 6

`

Sinking particles

Sinking particle samples were collected by deploying time-series sediment traps (McLane, conical type, aperture diameter=80 cm, and height/diameter=2.5) in the SIZ, inside the ASP, near the Dotson Ice Shelf, and near the East Getz Ice Shelf. Sediment traps were all deployed at ~400 m depths. Sampling bottles were filled with filtered seawater collected from the trap depth, with sodium borate buffer and 10 % formalin solution added as a preservative to prevent microbial degradation. After recovery, the samples were kept in the refrigerator at 2~4 °C until further treatment inland.

Sediment

During the ANA02C cruise, sediment samples were collected by a gravity core, multi-core (KC Denmark A/S. Station B only) and box core (Marine Tech. Korea) at three locations (Stations B, C, and D) along the western paleo ice stream trough from the Dotson Ice Shelf (Dotson trough) and one location near the shelf break in the western Amundsen Sea (Station A). Gravity core sampling was only conducted at three sites (Stations A, B, and D). Unfavorable sea ice conditions and coarse sediment composition (suggested by a multibeam survey) discouraged us from collecting sediments near the shelf break inside the Dotson trough at this first cruise.

In cruises ANA04B and ANA08B, we only used a box-core. Boxcore samples were collected in various locations including the shelf break inside the Dotson trough, polynya stations outside the Dotson trough, perennial SIZ, and

`

boundary of the ASP. Unon detachment of the canister, plastic cores (8 cm diameter, 60 cm length) were gently pushed in for sub-cores. Each sediment core was sliced into 1~2 cm thick subsamples on board and stored in pre baked glass jars and kept frozen until further analyses.

2.2. Sample analyses

Details of sample analyses other than the followings are written in each chapter.

Sinking particle sample split

Any conspicuous swimmers (visible zooplankton specimens) were removed by tweezers with the naked eye before dividing the samples into 5 and/or 10 equal aliquots using a wet-sample divider (WSD-10, McLane Research Laboratories) in a land-based laboratory (Figure 2.2). During the processes to remove swimmers we also collected benthic organisms and preserved them in ethanol and/or formalin.

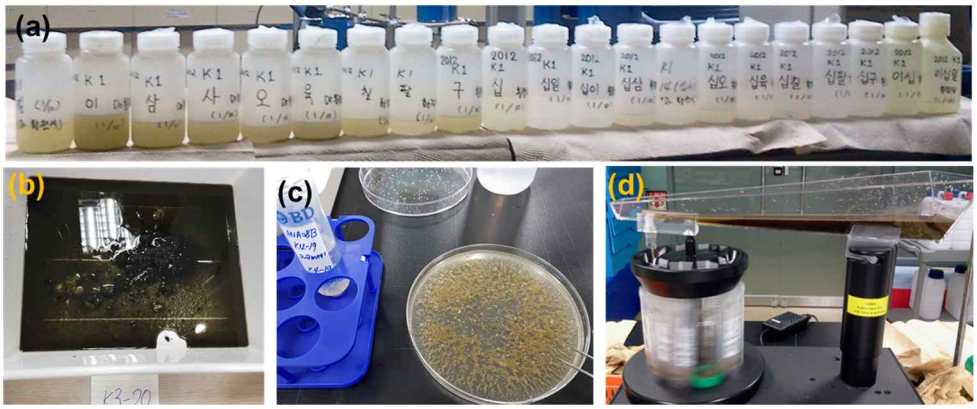

Figure 2.2. Split of sinking particles (a) sample bottles in time series, (b) and (c) removing swimmers (d) splitting of samples into 5~10 equal aliquots.

`

Radiocarbon

Natural levels radiocarbon ($\Delta^{14}C$), with $<10^{-12}$ % relative abundances has been used in this overall dissertation. Within the half-life of 5,730 years, ^{14}C is frequently used as a natural clock to study long time scale processes, and tracer for source regions (primary production, terrestrial source input, resuspension, aeolian input, ice rafted particles and so on).

Reporting of radiocarbon can be done in various ways. $\Delta^{14}C$, a fractionation corrected ($\delta^{13}C$ of −25 ‰) value per mil deviation of $^{14}C/^{12}C$ relative to the Lamont 1890 oak wood/NBS oxalic acid made in 1958 (Broecker and Olson, 1959; Stuiver and Polach, 1977). Fraction modern (Fm) and/or percent modern (pMC) report fraction amount of ^{14}C in a sample relative to that in the standard. It is a linear quantity and can be conveniently used in mass balances. In sediment trap studies (Chapter 3), $\Delta^{14}C$ (‰) was reported to understand the relative portion of two end member sources of sinking POC. In Chapter 5 and Chapter 6, ^{14}C age has been used for age model and chronology. Conventional half-life from Libby (5,568 yrs) adopted for reporting ^{14}C ages. The radiocarbon age (uncorrected ^{14}C age) is not a calendar or chronological age and must be calibrated (details in Chapter 5).

For sinking particles, one aliquot of each sample was used for isotopic analyses. The effect of formalin as a preservative on radiocarbon analysis was determined to be insignificant in a previous study (Otosaka et al., 2008). Each sample with a sizeable amount upon visual inspection was filtered on a pre-cleaned Nuclepore filter (Whatman membrane, 47 mm, 1.0 μm pore size) with rinsing three times with ultrapure (Millipore) water. Samples were freezedried and/or dried at

`

45 °C in an oven, and particles were recovered from the filter pads. Each sample was ground using a mortar and pestle, then ~20 mg dry sample was weighed in a silver cup and fumigated with concentrated HCl in a desiccator for 20 hours (Hedges and Stern, 1984; Komada et al., 2008). If the collected amount of particles are small, the sample was were filtered on pre-combusted 27 mm GF/F filters. These particle samples were not separated from the filter pads. Some pair of samples was combined together to obtain enough carbon for radiocarbon measurements. HCl-fumed samples were then placed on a hot plate at ~45 °C for 4 hours to remove HCl vapor. The sample cup was placed in a quartz tube with CuO. The sample tube was evacuated on a vacuum line and flame-sealed, then combusted at 850 °C for 4 hours (Figure 2.3). Particle samples on GF/F filters were treated in the same way except that silver wire was added instead of a silver cup. Sediment samples were also processed in the same way except enough of samples processed for the ^{14}C detection limit (>100 μgC). The resultant CO_2 was cryogenically purified and stored in a 1/4" size Pyrex tube (Figure 2.3). The resultant CO_2 samples were analyzed for radiocarbon and stable carbon isotopes at the National Ocean Sciences Accelerator Mass Spectrometry Facility at Woods Hole Oceanographic Institution (NOSAMS WHOI) following standard techniques (McNichol et al., 1994). The uncertainty for this type of sample determined by multiple duplicate-analyses in our lab is less than 10 ‰ for $\Delta^{14}C$ and 0.1 ‰ for $\delta^{13}C$. $\Delta^{14}C$ values of OX–I standard processed in the same way in the lab were 36 and 46 ‰, showing that these results were within the error range (< 10 ‰) from the true value.

`

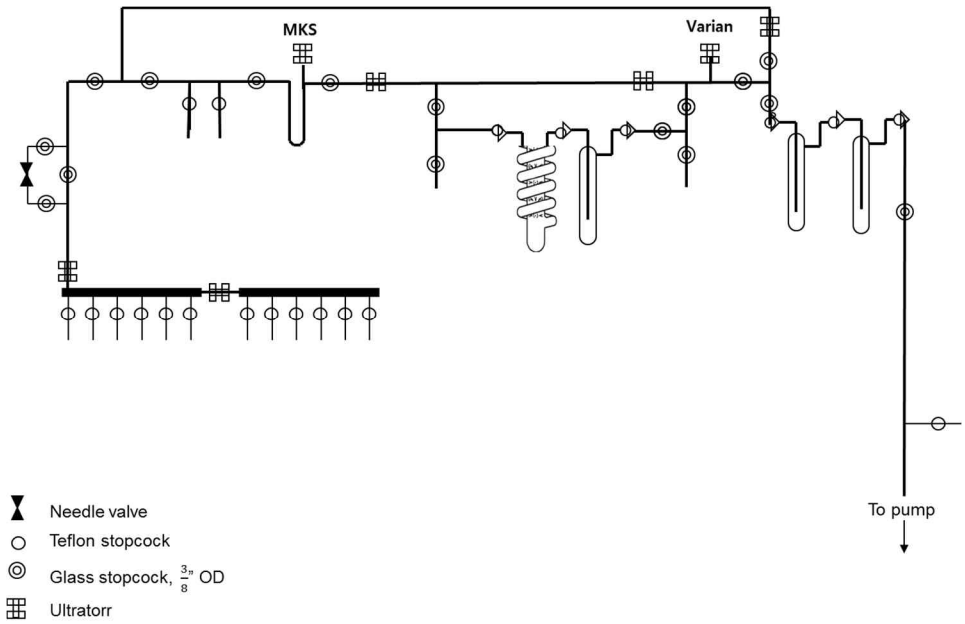

Figure 2.3. Scheme of vacuum manifold system.

Comparison of fuming methods for radiocarbon analyses

In the case of sedimentary organic carbon in chapter 5 and 6, radiocarbon values were measured in Professor Tim Eglinton's lab at ETH Zürich (ETHZ hereafter). The HCl fuming method adopted at ETHZ was slightly different (details below). The results were compared with duplicate samples including sinking particles and sediment samples collected in the Ulleung Basin, East Sea and in the Amundsen Sea.

At ETHZ, each sediment sample was finely ground, weighed in a silver cup, and fumigated with HCl (EMSURE; for hydrochloric acid fuming) in a desiccator for 3 days at 70 ºC. The samples then fumigated with NaOH pellets (Fischer Sceintific; analytical reagent grade) at 70 ºC for more than 3 days to remove HCl vapor (Figure 2.4). Bulk radiocarbon content was measured on a gas-

`

ion source MICADAS (Mini Carbon Dating System) accelerator mass spectrometry (AMS) at the Laboratory for Ion Beam Physics at ETHZ.

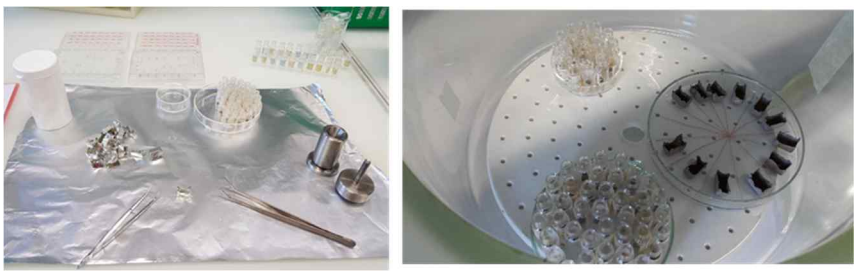

Figure 2.4. Preparation for radiocarbon measurement at ETHZ.

Twelve duplicate samples including 7 sinking particle samples from the Ulleung Basin, East Sea (Kim et al., 2017), 2 sinking particle samples from the Amundsen Sea (Kim et al., 2015), and 3 sediment samples collected from the Amundsen Shelf (Kim et al., 2016) were analyzed again at ETHZ (Figure 2.5; Table 2.2). $\Delta^{14}C$ differences were 15±18 ‰, and except two samples, values from ETHZ were higher.

`

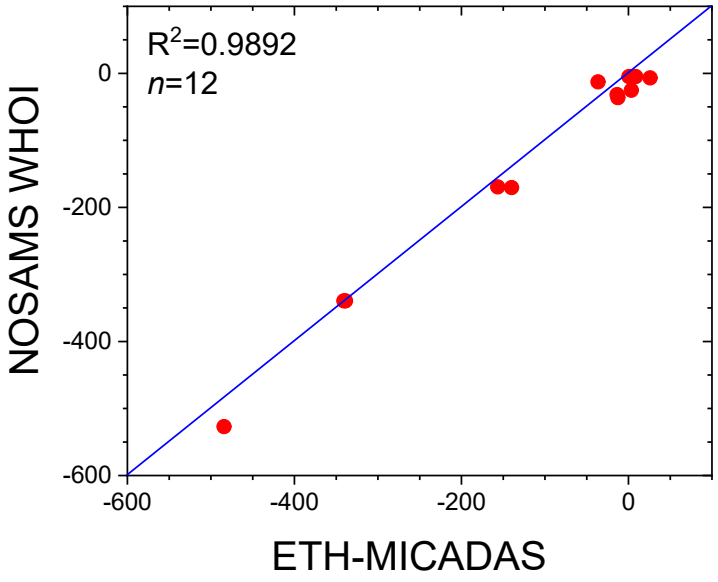

Figure 2.5. Differences in $\Delta^{14}C$ values according to the methods (NOSAMS WHOI at y-axis and ETH-MICADAS at x-axis).

Table 2.2. Different $\Delta^{14}C$ values according to the different methods.

Samples	ETHZ	NOSAMS	Difference
UB sinking particle (1000 m #2)	4	−25	29
UB sinking particle (1000 m #5)	1	−5	5
UB sinking particle (1000 m #5): du	9	−5	14
UB sinking particle (1000 m #16)	26	−7	33
UB sinking particle (2000 m #5)	−14	−32	18
UB sinking particle (2000 m #10)	−36	−13	−24
UB sinking particle (2000 m #16)	−13	−36	24
Amundsen sinking particle (SIZ-#2)	−140	−171	31
Amundsen sinking particle (SIZ-#3)	−157	−169	13
Amundsen sediment (K1 6.5 cm)	−484	−527	43
Amundsen sediment (K2 6.5 cm)	−339	−339	0
Amundsen sediment (K2 6.5 cm): du	−341	−339	−2

`

Lipid biomarkers

For sterol analysis, 5~25 g of freeze dried and homogenized sediments were extracted using a microwave extraction system (MARS6 CEM Corporation; 100 ºC, 20 mins; Figure 2.6) in a dichloromethane:methanol (90:10 v:v) mixture. 20 % of total lipid extract of each sample used for analysis. An internal standard (1-nonadecanol. Aldrich, 99 %) was added to each sample prior to analytical treatment. Sterols were quantified by comparison to Cholesterol external standard (≥99 %). Each total lipid extract was separated into 3 fractions by SiO_2-gel column chromatography. The first fraction was eluted with 100 % hexane and contained alkane and alkenes. The second fraction eluted with 75 % hexane and 25 % Ethyl Acetate and contained sterols. The third fraction eluted with 100 % methanol and contained all remained organic fractions. (Figure 2.4 and 2.5 in Ann Pearson; 2000).

`

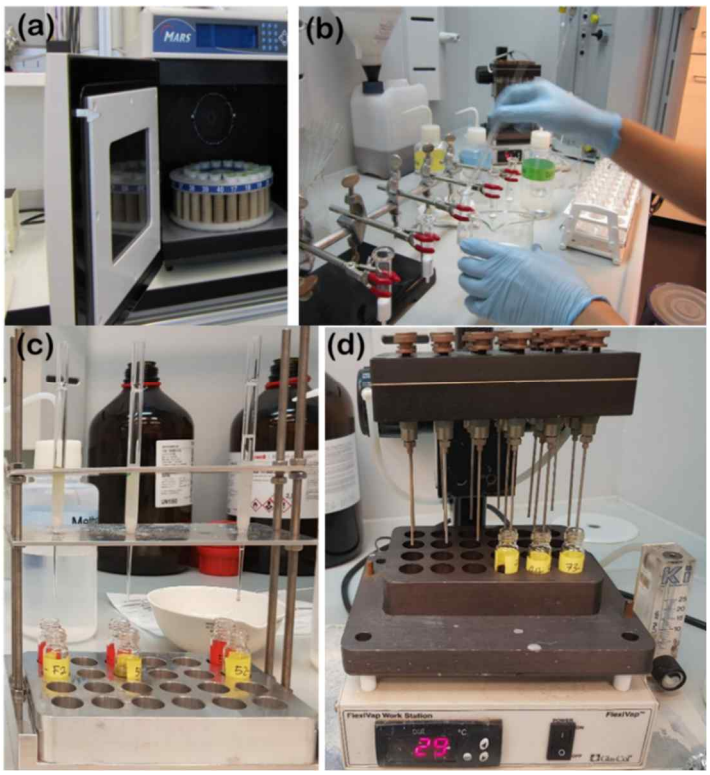

Figure 2.6. Lipid experiment processes from (a) microwave extraction, (b), (c) column chromatographic separation and (d) blow down to analyses.

The second fraction was silylated with bistrimethylsilyl-trifluoroacet-amide (BSTFA) and pyridine (catalyst) at 70 ºC for 30 mins. Derivatized samples were injected into an Agilent 7890A gas chromatograph (GC) equipped with a capillary column (DB-1MS, 0.32 ID, 30 m in length). Compounds were detected and quantified with a time of flight mass spectrometry (TOF-MS, 70 eV constant ionization potential).

The 1 µl was injected to the injector, which was in splitless mode. Injection of 3~5 ng of sterols was aimed for good detection sensitivity. Inlet temperature was

`

programed to increase from 30 to 340 ºC, with a delay at ~115 ºC, holding for 6 min to avoid detection of pyridine tail (boiling point of pyridine; ~115 ºC). The GC analysis was performed with the following temperature program: 40 ºC hold for 1 min, ramping to 130 ºC at a rate of 40 ºC/min, ramping to 320 ºC at a rate of 10 ºC/min, and hold at 320 ºC for 10 min. Scan mass range for bench TOF set as 35~500. Brassicasterol, dinosterol, and cholesterol were identified based on their retention times (Figure 2.7, Figure 2.8). Characteristic mass spectra were 69, 129, 255, 380, 475 for brassicasterol, 129, 329, 360, 450 for cholesterol, and 29, 273, 359, 368 m/z for dinosterol. Due to lack of standard material for each sterol, relative (%) mode on mass spectra for a better resolution was adopted (Figure 2.8). Some peaks were overlapped. To separate overlapped individual paeks, I deconvoluted the data after the analyses (Figure 2.9).

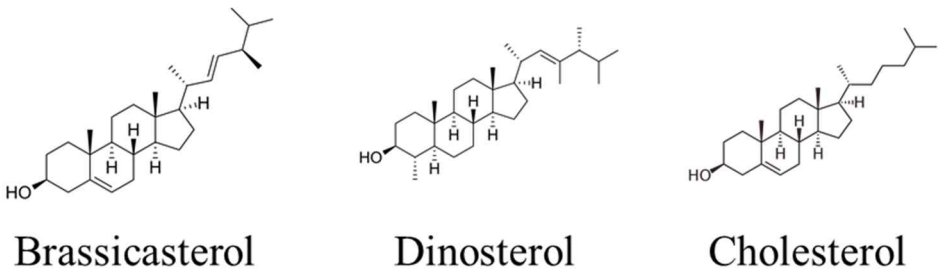

Figure 2.7. Structures of sterols used for analysis.

`

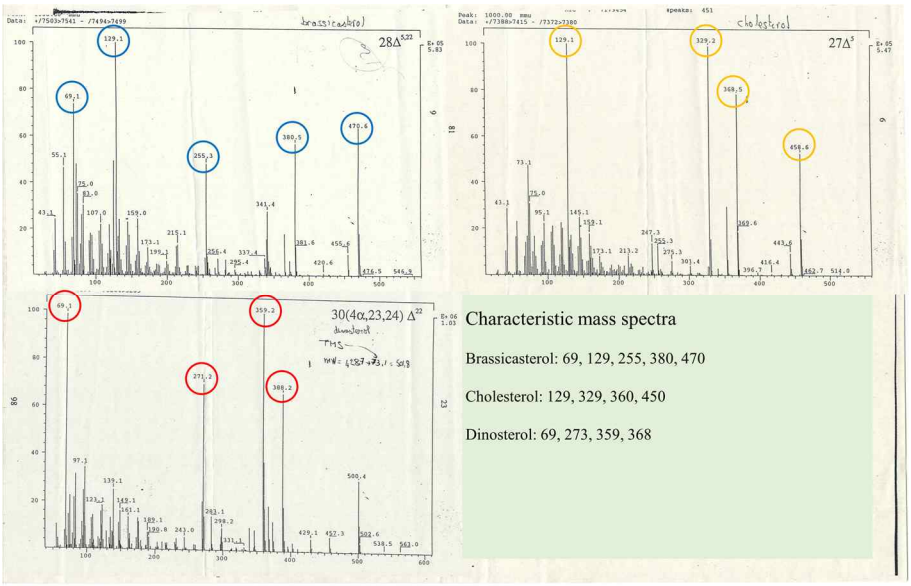

Figure 2.8. Mass spectra for each sterols.

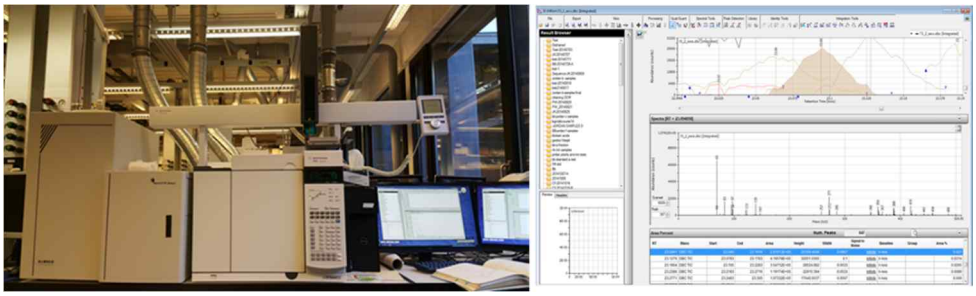

Figure 2.9. GC-TOF-MS system in ETHZ and convolution method after analyses for a better resolution of sterol values.

Grain size analysis

Large particle seems too heavy to be transported by current (Andrews, 2000), and rather to be moved by sea ice and/or icebergs (IRD; Ice Rafted Debris) in this high latitude region. Even though different literature frequently uses different IRD size

`

definition, all sizes of sand and gravel considered as a definition of IRD (Birgel and Hass, 2004). Sediments larger than 2 mm had been separated in a lab in Korea after freeze dried for a better analytical condition with grain size analyzer which prefers particles smaller than 2 mm (Figure 2.10). Samples were mixed and shaken overnight with solution of Sodium polyphosphate (dispersing agents) and distilled water. This homogenized samples socked randomly and put into stirrer and then measured 4 to 5 times repeatedly after checking the background. Mastersizer 2000 was used for interpretation.

Figure 2.10. Grain size analyzer at ETHZ.

Surface area and XRD analyses

Wet chemical oxidation technique using sodium persulfate buffered with sodium bicarbonate for analyses for the effective removal of organic matter removal (Meier and Menegatti, 1997). The experimental were performed based on Dr. Thomas Blattmann's dissertation (Diss. ETH No. 25508). In brief, per 1 g of sediment, 5 g of sodium persulfate ($Na_2S_2O_8$) and 5.5 g of sodium bicarbonate ($NaHCO_3$) as a buffer are added to ~200 ml of deionized water. The sample dispersed using an ultra-

`

sonication finger up to 3 minute to avoid the aggregates. The sample than stored above the hotplate ~100 °C and stirred for 1 hour (Figure 2.11a). Sample particles were collected and shook overnighted with ~20 g of calcium chloride dehydrate, and washed 5 times to remove unused oxidant and dissolved salts then oven dried (Figure 2.11b).

The specific surface area (SA) was determined by 5 points nitrogen-based BET (Brunauer, Emmett, Teller; Brunauer et al., 1938) by the Quantachrome NOVA 4000e (Mayer, 1994). Empty glass cells were weighed first. Well dried samples first transferred into the glass cells and degassed by using a Quantachrome FLOVAC degasser at 150 °C under vacuum overnight. Sample weights were measured after degassing. SA was normalized to degassed sediment masses (Figure 2.11c).

After the surface area measurement, samples were dried again and pulverized using miniature planetary ball mill (Fritsch Pulverisette 23) for 3 minutes at an oscillation frequency of 50 Hz with 3 balls. Samples homogenized and washed with ethanol, transported to large china and dried in oven (Figure 2.11d). The powdered sample was tapped on randomly oriented powder specimens for quantitative X-ray diffraction analysis (Figure 2.11e,f ; Bish and Plötze, 2010). Quantitative mineral content was calculated using Rietveld refinement using BGMN (Bergmann et al., 1996) using the Profex graphical used interface (Doebelin and Kleeberg, 2015).

`

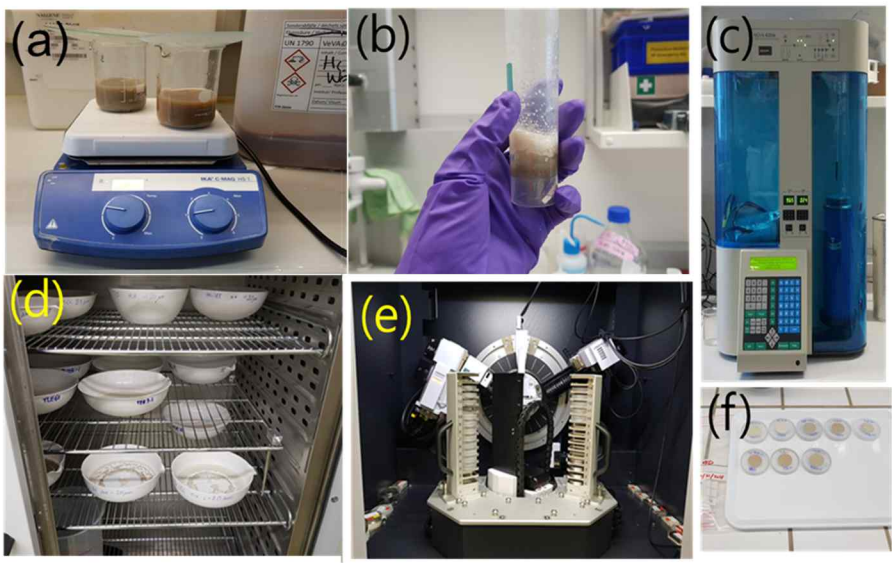

Figure 2.11. (a) Wet chemistry reactions on hotplate (b) sediments reacted with calcium chloride dehydrate (c) surface area measurement (d) samples dried for XRD analyses, (3) XRD machine in geological department, and (f) samples ready for measurement.

^{210}Pb analyses

^{210}Pb has been analyzed in EAWAG aquatic research, with help of Professor Nathalie Dubois and Pascal Rünzi (Figure 2.12). Prior to start to measure sediment core samples, 5 duplicate samples before and after the lipid extraction were analyzed to see the differences. There was some possibility of depleted activities in samples after lipid extraction as during the experiments small size particles may lost and the metal attached into them, too. The activities overall seem very well comparable, except for

`

the top layer (0.5 cm depth), but the difference in the values lines within the standard deviations (Figure 2.12; Table 2.3).

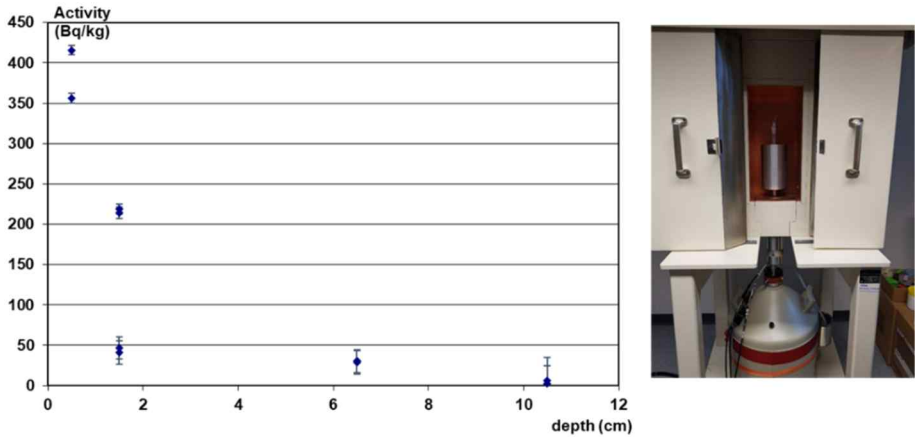

Figure 2.12. Duplicate samples before/after lipid extraction (left) and the beta counter at EAWAG laboratory (right).

Table 2.3. Duplicate results before and after lipid extraction (shaded).

	St. 4		St. 4		St. 4		St. 33		St. 26	
Activity (Gq/kg)	416	356	30	29	6	3	47	41	214	219
Depth (cm)	0.5	0.5	6.5	6.5	10.5	10.5	1.5	1.5	1.5	1.5
Avg.	386		29		4		44		216	
RSD	42		1		3		4		3	

Elemental analyses

Elemental analyses were carried out at KIOST (Korea Institute of Ocean Science & Technology) and KOPRI. Samples were rinsed with MQ water to remove residual formalin solution, then freeze dried. Dried samples were weighed for determination of total mass flux. The dried samples were ground to fine powder in agate mortar

`

and used for elemental analyses. Total carbon (TC) content was determined using a Carlo–Erba 1110 CNS elemental analyzer, with the analytical error smaller than 3 %. Total inorganic carbon content was measured using a UIC coulometrics carbon analyzer with the analytical error smaller than 2 %. OC content was estimated from the difference between total carbon and inorganic carbon contents.

Metal content

Metal content measured by ICP-AES (Optima 8300, PerkinElmer) system at KBSI (Korea Basic Science Institute). Two standard materials (SRM 1646a estuarine sediment and SRM 2702, inorganics of marine sediment supplied by the National Institute of Standards and Technology, USA) were also analyzed for a calibration. Lithogenic material content was estimated as 12.15 times the Al content (%) (Taylor and McLennan, 1985). With these samples, the $CaCO_3$ content was estimated by multiplying the content of biogenic Ca by 2.5 with the latter estimated by subtracting lithogenic Ca (0.5×Al) from the total Ca (%). Opal content was estimated by multiplying the content of biogenic Si by 2.4 with the latter estimated by subtracting lithogenic Si (3.5×Al) from the total Si (%) (Taylor and McLennan, 1985).

Biogenic Si (Opal)

In addition to ICP-AES measurement, biogenic opal content was determined following a wet alkaline extraction (DeMaster, 1981; Mortlock and Froelich, 1989) for sinking particle samples at KIOST. Briefly, ~15 mg of sediment samples were

`

put into the centrifuge with 20 ml of 1N NaOH and shook inside the water bath 85 °C. Every 1 hour after 2 hours of reaction, took 0.1 ml of samples and put into vial with 2 ml of 0.1N HCl and 2 ml of ammonium molybdate solution. After 15 mins, put 3 ml reducing solution and next day, spectrophotometer absorbance was read (wavelength of 812 nm).

Precautions of metal estimated opal

Opal content estimated by wet alkaline extraction and by the Si and Al content measured from ICP-AES were widely used in sinking particles. In deep sediments, however, the opal content with this approach was not consistent to real diatom valve abundances (Figure 2.13). Abnormally highly estimated opal (%) observed at depths below ~100 cm depths. On the other hand, diatom valve abundance was low which is more reliable considering the sediments below ~100 cm depths were glacier deposit. It is probably due to high sand content (%) with SiO_2 while in sinking particles, fine size lithogenic particles (e.g. clay) contain alluminosilicate was dominant in general.

`

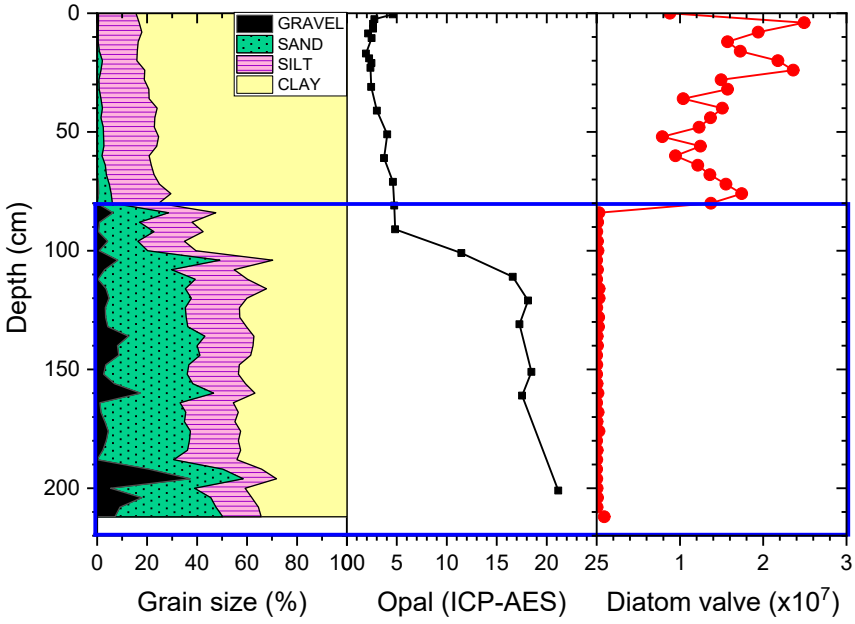

Figure 2.13. Abnormally high opal content below 100 cm (box) was not consistent to diatom valve abundance. This might be because of the grain size dominated by sand. (redrawn gravity core profile in Chapter 5).

`

Chapter 3

Sinking particle flux and composition at three sites of different annual sea ice cover in the Amundsen Sea, Antarctica

Minkyoung Kim[1], Eun J. Yang[2], Dongseon Kim[3], Jin-Hyun Jeong[3], Hyung J. Kim[3], Jisoo Park[2], Jinyoung Jung[2], Hugh W. Ducklow[4], SangHoon Lee[2], Jeomshik Hwang[1*]

Published in *Journal of Marine Systems*, 2019 v. 192 p. 42-50.

[1]School of Earth and Environmental Sciences/Research Institute of Oceanography, Seoul National University, Seoul, 08826, South Korea
[2]Korea Polar Research Institute, Incheon, 21990, South Korea
[3]Korea Institute of Ocean Science & Technology, Ansan, 15627, South Korea
[4]Lamont-Doherty Earth Observatory, Columbia University, Palisades, NY, 10964, USA

Highlights

- Summertime POC flux in the perennial sea ice area is mainly from sea ice diatoms.
- POC flux in the perennial sea ice area is high and similar to the central polynya.
- Interannual variability in the POC flux was large in the perennial sea ice area.
- Reduction in sea ice and sufficient sun light were critical to enhanced POC flux.

`

Abstract

This study examines the sinking particle flux and composition of samples collected at three sites in the western Amundsen Sea, Antarctica: a perennial sea-ice-covered area, the central region of the Amundsen Sea polynya, and close to the Dotson Ice Shelf within the polynya. Time series sediment traps were deployed for one year at depths of 400–500 m from February and March 2012. Observations from the three sites confirm previously reported findings that the majority of annual POC (particulate organic carbon) flux in the Amundsen Sea occurs during the austral summer, with much smaller POC fluxes during other seasons. In the perennial ice-covered area, sea ice diatoms were the dominant source of sinking particles. In this region, the summertime POC flux is similar to that in the central polynya. However, the POC flux exhibited large interannual variability, with the reduction in sea ice cover and sufficient insolation being critical to enhanced sinking POC flux. Within the Amundsen Sea polynya, the sinking POC flux was higher in the central region than near the Dotson Ice Shelf, consistent with spatial variability in primary production. The site near the Dotson Ice Shelf had the lowest contribution of diatoms to sinking particles and the smallest POC flux among the three sites.

Keywords: particulate organic carbon, biological pump, perennial ice-covered area, polynya, Amundsen Sea

`

3.1. Introduction

The Amundsen Sea in the western Antarctic is experiencing rapid declining of sea ice cover and melting of ice shelves (Walker et al., 2007; Stammerjohn et al., 2012). If we are to determine how this region will respond to such changes it is critical to improve our understanding of the ecosystem properties and biogeochemistry of the Amundsen Sea. Because of a lack of field measurements, the biogeochemistry of the Amundsen Sea has been observed primarily using satellite telemetry (Arrigo and van Dijken, 2003; Arrigo et al., 2012). These studies showed that the Amundsen Sea polynya (ASP) in the western Amundsen Sea is the most productive polynya around Antarctica (Arrigo and van Dijken, 2003). Additionally, these polynyas provide environments that facilitate the uptake of atmospheric CO_2 (Arrigo et al., 2012).

The region north of the ASP is perennially covered with pack ice, even during summer (Stammerjohn et al., 2015). This region experiences a reduction in sea ice concentration during summer, but does not usually experience ice-free conditions. This perennial sea-ice-covered area is different from the “seasonal ice zone” (i.e., an area of ocean that extends from the permanent ice zone to the boundary where the winter sea ice extent is at a maximum). Perennial ice-covered regions around Antarctica cover 3–4 million km^2 in February compared with the full extent of 17–20 million km^2 in September (https://earthobservatory.nasa.gov). Therefore, it is important to understand primary production and particle export in the perennial ice-covered area.

`

Recent field campaigns have investigated the role of the biological pump in the Amundsen Sea (Arrigo and Alderkamp, 2012; Yager et al., 2012; Meredith et al., 2016; Yager et al., 2016; Lee et al., 2017). In situ measurements are limited to summer when access via icebreakers is possible. Moorings equipped with time series sediment traps facilitate the annual sampling of sinking particles, with the sinking particle flux providing a direct indication of POC export to the deeper water column.

The flux and biogenic composition of sinking particles was previously reported for two sites, one in the central ASP between December 18, 2010 and January 4, 2012 (Ducklow et al., 2015), and the other in the perennial ice-covered area north of the ASP between January 5, 2011 and January 5, 2012 (Kim et al., 2015). At both sites, an elevated flux of sinking particles was observed during summer, with particle flux remaining low during the other seasons. Peak POC flux in the ASP was roughly twice that in the perennial ice-covered area. Despite in situ primary production being higher in the ASP than in the perennial ice-covered area, POC fluxes at both sites were comparable when integrated over the summer (January and February 2011; Kim et al., 2015).

We expanded the available particle flux and composition dataset by collecting samples at three sites using sediment trap moorings deployed for one year. Building on the previous results, we investigated the following questions. 1) Is the high sinking POC flux in the perennial ice-covered area comparable to that in the center of the polynya a persistent feature? 2) How is POC flux in the perennial ice-covered area associated with the temporal evolution of sea ice? 3) Is spatial

`

variability in satellite-based chlorophyll-*a* concentration within the ASP reflected in the sinking POC flux? 4) How does sinking particle composition vary spatially in the Amundsen Sea and how is this variability related to particle export?

3.2. Materials and methods

Time series sediment traps (McLane PARFLUX Mark 78G; conical type, aperture diameter = 80 cm with a height:diameter ratio of 2.5) were deployed on bottom-tethered hydrographic moorings at three sites (Figure 3.1). Trapping efficiency of the conical type sediment traps has been debated. Regarding this issue, readers are referred to papers such as Buesseler et al. (2007, 2010). An RCM-11 current meter was deployed 2 m below each sediment trap (detailed information on mooring designs can be found in Ha et al., 2014). Station K1 is located in the northern part of the Amundsen Sea, which is mostly covered with perennial sea ice but experiences a reduction in sea ice concentration during summer. Sampling at Station K1 (72.40°S, 117.72°W, trap depth = 400 m, water depth = 530 m) was a continuation from the preceding year (Kim et al., 2015). Sinking particles were sampled from March 7, 2012 to March 16, 2013 (Table 3.1). Station K1 was originally visited in early February 2012; however, thick sea ice cover delayed the mooring turnaround until early March 2012, resulting in a data gap of about 60 days. Station K2 (73.28°S, 114.97°W, trap depth = 410 m, water depth = 830 m) is located in the central region of the ASP, which is characterized by high primary production (Yager et al., 2012). Samples were collected from February 15, 2012 to February 20, 2013. POC flux results at K2 are reported in Lee et al. (2017). Station

`

K3 (74.19°S, 112.54°W; trap depth = 490 m, water depth = 1057 m) is located in front of the Dotson Ice Shelf. This region experiences low sea ice cover, even during winter (Stammerjohn et al., 2015), and primary production is lower than in the central region of the polynya (Yager et al., 2016). Samples were collected from February 17, 2012 to March 1, 2013. The sampling intervals were between 9 and 31 days, depending on the expected particle flux (Table 3.1). Each sample bottle was filled with filtered seawater collected from the trap depth, with sodium borate buffer and 10% formalin solution added as a preservative.

The samples were stored in a refrigerator at 2–4 °C. Upon inspection with the naked eye, any visible zooplankton specimens were removed using tweezers in a land-based laboratory. Each sample was split into five equal aliquots using a wet sample divider (WSD-10, McLane Laboratory). Three of the five equal aliquots were combined. This fraction was rinsed with ultrapure water (Milli-Q water) and the supernatant was removed after centrifugation. This process was repeated three times to remove salts and the residual formalin. The rinsed samples were then freeze dried and weighed for determination of total particle flux. The uncertainty of the particle flux determination is mainly from sample splitting and is <5% (www.mclanelabs.com). One aliquot was used for radiocarbon analysis after rinsing with Milli-Q water and freeze drying. The other aliquot was used for microscopic examination of diatoms.

The dried samples were homogenized in an agate mortar prior to determination of total carbon, inorganic carbon, and biogenic opal content. The chemical analysis procedure is fully described in Kim et al. (2012). Briefly, total

`

carbon content was determined using a Carlo-Erba 1110 CNS elemental analyzer with an analytical error of less than 3% based on a sulfanilamide standard. Inorganic carbon content was measured using a UIC coulometrics carbon analyzer with an accuracy of more than 98%. Organic carbon content was estimated as the difference between the total carbon and inorganic carbon contents. A conservative uncertainty of <10% of the measured values was assigned for organic carbon content estimation. The biogenic opal content was determined following a wet alkaline extraction method with a precision of roughly 5% (DeMaster, 1981). For station K1, biogenic opal analysis was conducted only for the periods with a high particle flux (March to June 2012 and January to March 2013) due to the limited amount of samples available.

Radiocarbon isotope ratios were measured on a subset of samples (6 and 2 results for K2 and K3, respectively). Approximately 20 mg of finely ground particle samples were exposed to HCl fumes to remove inorganic carbon (Hedges and Stern, 1984; Komada et al., 2008) and combusted at 850°C in closed quartz tubes. Cryogenically isolated CO_2 gas was analyzed for radiocarbon and stable carbon isotope ratios using standard techniques at the National Ocean Sciences Accelerator Mass Spectrometry facility at Woods Hole Oceanographic Institution (McNichol et al., 1994). The uncertainty associated with the $\Delta^{14}C$ measurements was less than 10‰.

Particle samples were examined under the microscope for identification and quantification of diatom cells. Diatom enumeration was performed using a biological counting technique (Salter et al., 2012). A 1/5 aliquot of each sample

`

was gently homogenized and 1–2 mL were drawn using a 5 mL standard pipette (ca. 1 cm of the tip was cut off to widen the mouth and thus minimize selective sampling of certain particle sizes) and diluted into a total volume of 20–50 mL of 0.2-mm-filtered preservative solution. The diluted sample was placed in a Sedgewick–Rafter counting chamber. Depending on diatom abundance, one quarter to one half of the chamber was examined with an inverted microscope with phase contrast (Olympus BX51) at 400× or 600× magnification. The uncertainty of cell counting was ~5 % based on multiple analysis.

Sea ice concentration data were retrieved from the European Centre for Medium-Range Weather Forecasts (ECMWF) ERA-Interim reanalysis. We used the daily sea ice concentration with a horizontal resolution of 0.125° × 0.125°. Data were averaged over the regions (72.2–72.7°S, 118.4–117.4°W), (73.0–73.5°S, 115.5–114.5°W), and (74.0–74.25°S, 113.0–112.0°W) for Stations K1, K2, and K3, respectively. MODIS Aqua-derived estimates of surface chlorophyll-*a* concentration were obtained from the Goddard Space Flight Center. The data for the Amundsen Sea were available only between November and February because of low solar elevation and high sea ice cover. We used Level 3, 8-day composite global datasets with a spatial resolution of approximately 4.5 km. Primary production was estimated using the VGPM (vertically generalized production model) method (Behrenfeld and Falkowski, 1997) and MODIS data for the sea surface temperature, photosynthetically available radiation, and chlorophyll-*a*. To compare this data with the sinking POC flux at stations K2 and K3, primary production was estimated by averaging values over a larger region surrounding

`

each station. Primary production was averaged over the regions (112–117°W, 73.0–73.5°S) for K2 and (111–114°W, between 73.75°S and the coast) for K3.

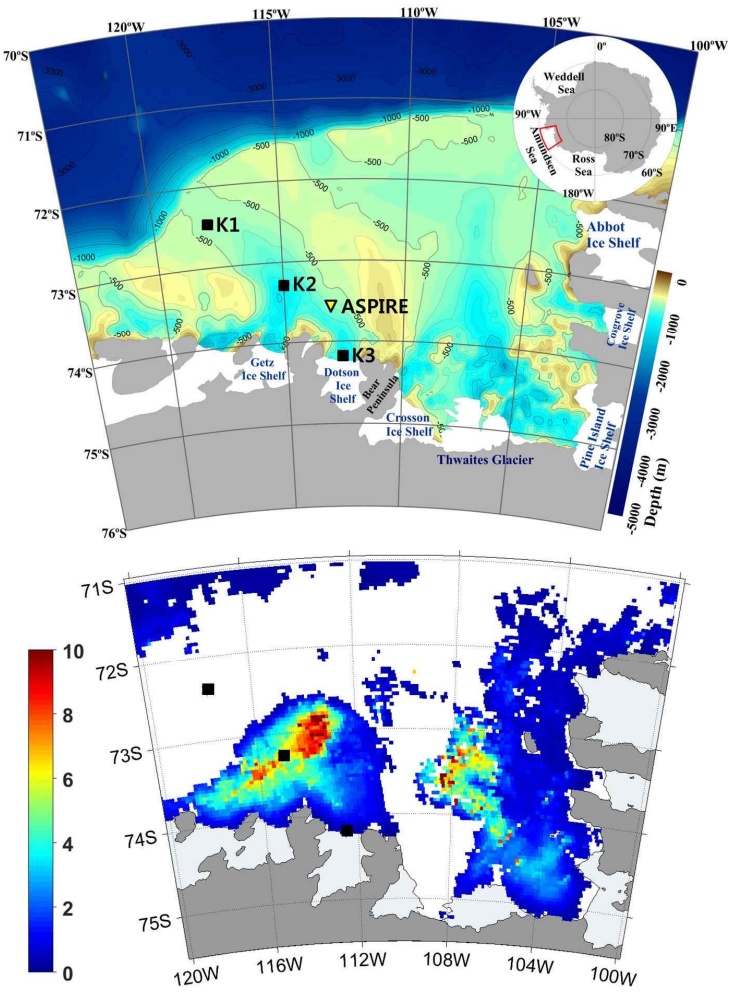

Figure 3.1. (Top) Amundsen Sea bathymetry and the locations of sediment traps from this study (black squares) and the US Amundsen Sea Polynya International Research Expedition (ASPIRE) project (yellow downward-pointing triangle). (Bottom) Chlorophyll-*a* concentration derived from MODIS data (units of mg m^{-3}), averaged over January and February 2013 in the Amundsen Sea polynya (western side). The white region represents the perennial ice-covered area.

`

Table 3.1. Sampling dates, fluxes, and compositions of biogenic particles at three sites in the Amundsen Sea. ND means not determined.

Sample no.	Cup opening date	Sampling Interval	Particle flux	POC flux	TC	POC	TN	Opal	$CaCO_3$	$\Delta^{14}C$	Diatom flux
	mm/dd/yy	days	mg $m^{-2}d^{-1}$	mgC $m^{-2}d^{-1}$	%	%	%	%	%	‰	10^6 cells $m^{-2}d^{-1}$
Station K1											
1	3/7/12–4/1/12	25	396	25	6.6	6.3	0.84	70	2.8	ND	340
2	4/1/12–5/1/12	30	167	9.4	5.9	5.6	0.87	66	2.1	ND	160
3	5/1/12–6/1/12	31	59	3.8	6.6	6.3	1.0	52	2.4	ND	40
4	6/1/12–7/1/12	30	16	1.4	8.5	8.3	1.4	43	1.6	ND	7.8
5	7/1/12–8/1/12	31	2.5	0.7	26.8	26.8	5.1	ND	0.8	ND	0.19
6	8/1/12–9/1/12	31	2.4	0.7	30.7	28.8	5.8	ND	15	ND	0.09
7	9/1/12–0/1/12	30	3.3	0.7	23.5	21.3	4.0	ND	18	ND	0.15
8	10/1/12–11/1/12	31	3.2	0.5	15.0	14.1	2.3	ND	7.5	ND	0.075
9	11/1/12–11/16/12	15	0.7	ND	20.0	ND	2.4	ND	ND	ND	0.016
10	11/16/12–12/1/12	15	1.1	ND	17.9	ND	3.4	ND	ND	ND	0.046
11	12/1/12–12/10/12	9	3.4	ND	11.0	ND	1.7	ND	ND	ND	0.11
12	12/10/12–12/19/12	9	6.8	0.5	8.4	7.5	1.2	ND	7.9	ND	0.19
13	12/19/12–12/28/12	9	7.0	0.4	7.3	6.2	0.93	ND	9.0	ND	0.44
14	12/28/12–1/6/13	9	12	0.9	8.1	7.6	0.99	ND	4.0	ND	0.64
15	1/6/13–1/15/13	9	24	1.3	6.4	5.5	0.78	27	7.8	ND	3.9
16	1/15/13–1/24/13	9	36	1.9	5.8	5.2	0.67	31	4.7	ND	8.1
17	1/24/13–2/2/13	9	25	1.6	7.1	6.4	0.89	28	6.2	ND	9.2
18	2/2/13–2/11/13	9	36	2.2	7.7	6.3	0.84	30	12	ND	14
19	2/11/13–2/20/13	9	32	3.9	13.3	12.1	1.7	51	10	ND	23
20	2/20/13–3/1/13	9	17	1.3	7.2	7.2	0.99	ND	0.2	ND	16
21	3/1/13–3/16/13	15	76	4.7	6.8	6.2	0.90	38	5.0	ND	36
Station K2											
1	2/15/12–3/1/12	15	30	4.3	14.0	14.0	2.1	16	0.2	ND	3.7
2	3/1/12–3/16/12	15	15	3.5	23.5	23.4	3.9	20	0.8	ND	2.9
3	3/16/12–4/1/12	16	17	3.0	17.7	17.6	2.6	28	1.0	−175	3.9
4	4/1/12–5/1/12	30	3.9	0.7	17.9	17.8	3.0	ND	0.6	ND	0.45
5	5/1/12–6/1/12	31	54	3.2	6.1	6.0	0.82	19	1.1	−245	12
6	6/1/12–7/1/12	30	40	2.4	6.2	6.0	0.90	16	1.3	ND	5.5
7	7/1/12–8/1/12	31	42	2.5	6.0	5.8	0.79	14	1.2	−209	6.2
8	8/1/12–9/1/12	31	16	1.8	11.5	11.3	1.3	12	1.5	ND	0.88
9	9/1/12–10/1/12	30	65	2.8	4.7	4.4	0.59	12	2.5	ND	3.6
10	10/1/12–11/1/12	31	29	1.3	4.7	4.4	0.60	11	2.1	ND	1.3
11	11/1/12–11/16/12	15	40	1.5	4.0	3.7	0.47	10	2.4	ND	1.3
12	11/16/12–12/1/12	15	70	2.4	3.9	3.5	0.44	13	3.0	−240	1.9
13	12/1/12–12/10/12	9	87	4.8	5.8	5.5	0.85	16	2.1	ND	5.0
14	12/10/12–12/19/12	9	163	8.9	5.7	5.5	0.77	21	1.6	ND	14
15	12/19/12–12/28/12	9	179	10	5.7	5.6	0.74	21	1.3	−198	27
16	12/28/12–1/6/13	9	273	15	5.7	5.6	0.72	28	1.2	ND	55
17	1/6/13–1/15/13	9	222	13	6.1	6.0	0.87	28	1.4	ND	71
18	1/15/13–1/24/13	9	260	29	11.3	11.2	1.8	27	0.8	−171	69
19	1/24/13–2/2/13	9	4.1	0.5†)	12.7	12.6†)	1.8	ND	ND	ND	0.45
20	2/2/13–2/11/13	9	3.0	0.4†)	14.7	14.6†)	2.1	ND	ND	ND	3.6
21	2/11/13–2/20/13	9	4.7	0.7†)	14.3	14.2†)	2.2	ND	ND	ND	1.6
Station K3											
1	2/17/12–3/16/12	28	2.5	0.5	20.6	20.5	2.7	ND	1.2	ND	2.6
2	3/16/12–4/1/12	16	9.0	1.7	18.9	18.8	2.8	13	1.4	ND	4.7
3	4/1/12–5/1/12	30	8.5	0.9	11.2	11.1	1.9	15	1.2	ND	2.2
4	5/1/12–6/1/12	31	33	2.4	7.6	7.4	1.2	13	1.8	−224	7.4
5	6/1/12–7/1/12	30	26	1.4	5.5	5.3	0.84	9	1.5	ND	6.7
6	7/1/12–8/1/12	31	45	2.7	6.1	6.0	1.0	10	0.3	ND	9.6
7	8/1/12–9/1/12	31	14	0.9	6.5	6.1	1.1	5	3.3	ND	3.5
8	9/1/12–10/1/12	30	16	2.0	13.2	12.9	3.0	3	3.1	ND	1.2
9	10/1/12–11/1/12	31	8.4	0.5	6.6	6.3	1.1	6	2.6	ND	1.0
10	11/1/12–1/16/12	15	14	0.6	4.3	3.9	0.53	7	2.8	ND	1.1
11	11/16/12–12/1/12	15	25	1.5	6.4	5.9	1.1	6	4.6	ND	1.9

`

12	12/1/12–12/10/12	9	25	1.6	7.2	6.6	0.88	6	4.5	ND	2.3
13	12/10/12–12/19/12	9	79	3.2	4.5	4.1	0.62	7	3.2	ND	4.7
14	12/19/12–12/28/12	9	42	1.9	4.9	4.4	0.57	6	3.7	ND	5.2
15	12/28/12–1/6/13	9	47	3.4	7.7	7.2	0.98	5	4.3	ND	4.8
16	1/6/13–1/15/13	9	14	1.1	8.5	7.9	1.2	5	5.0	ND	2.1
17	1/15/13–1/24/13	9	162	16	10.0	9.8	1.4	11	2.2	−197	58
18	1/24/13–2/2/13	9	62	8.2	13.5	13.2	2.1	15	2.9	ND	26
19	2/2/13–2/11/13	9	24	3.8	16.7	16.0	2.6	14	6.2	ND	6.5
20	2/11/13–2/20/13	9	22	3.2	15.0	14.2	2.3	17	6.5	ND	7.6
21	2/20/13–3/1/13	9	22	3.1	15.1	13.9	2.1	12	11	ND	7.0

†) These values are based on estimated POC content under the assumption that inorganic carbon content was 0.1%.

3.3. Results

Sea ice concentration and ocean currents

At K1, sea ice concentration reached minimum values of approximately 50% in February 2012 and 40% in March 2013 (Figure 3.2a). Except during summer, sea ice concentration remained mostly over 90%. Therefore K1 remained in the perennial ice-covered area. At K2, located in the central polynya, minimum sea ice concentration was close to, or lower than 10% in February 2012 (Figure 3.2b). The sea ice concentration started to decrease in early November 2012 and reached about 20% in late December. It recovered to around 70% briefly in early January 2013 and then decreased to the annual minimum in late February 2013. During the year, the surface characteristics of K2 changed from sea ice in winter, to marginal ice in spring, to open sea in summer−early fall. Station K3 was generally free of sea ice for more than three months during summer (Figure 3.2c). This site was never fully covered with sea ice during the remainder of the year, with concentrations fluctuating between 30% and 80%.

`

The arithmetic mean of the current speed measured at 2 m below the trap at K1 was 5.7±3.0 cm s^{-1}. Current direction varied with the integrated flow direction being northwestward (Figure 3.3). At K2, the mean current speed was 5.9±3.0 cm s^{-1}. Here, current direction varied widely with no predominant direction being evident. Integrated flow was southeastward. Current speed was somewhat higher at K3 than at the other stations, and speeds greater than 20 cm s^{-1} were recorded occasionally between July and October 2012. At K3, the mean current speed was 9.7±5.6 cm s^{-1}, and the integrated current direction was northwestward. Considering the settling velocity of particles, estimated to be 10–100 m d^{-1} by McDonnell and Buesseler (2010), and the trap depths, we concluded that the collected biogenic particles originated from within a few tens of km of each site.

`

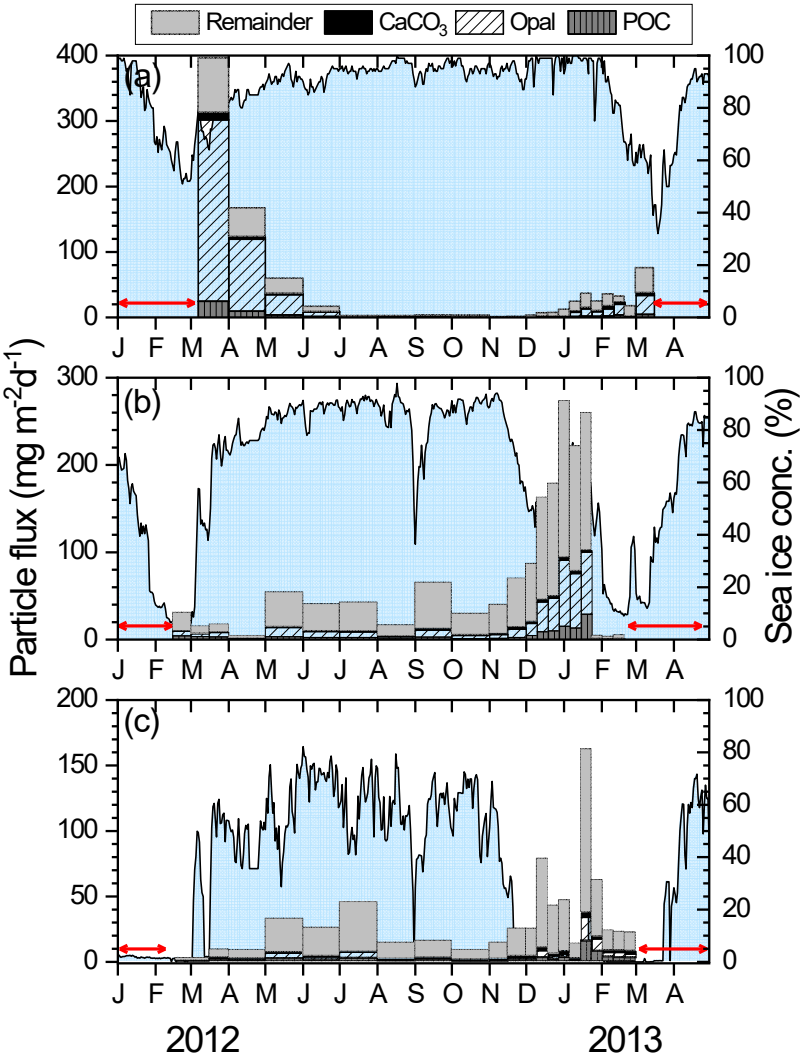

Figure 3.2. Fluxes of each biogenic component (POC, $CaCO_3$, and opal,) and the remainder that is not accounted for by these components at stations (a) K1, (b) K2, and (c) K3. Tick marks on x-axis indicate the start of each month. Note that the y-axis scales are not equal. Horizontal arrows denote periods of no data. Sea ice concentration (blue shading) is represented on the right-hand y-axis.

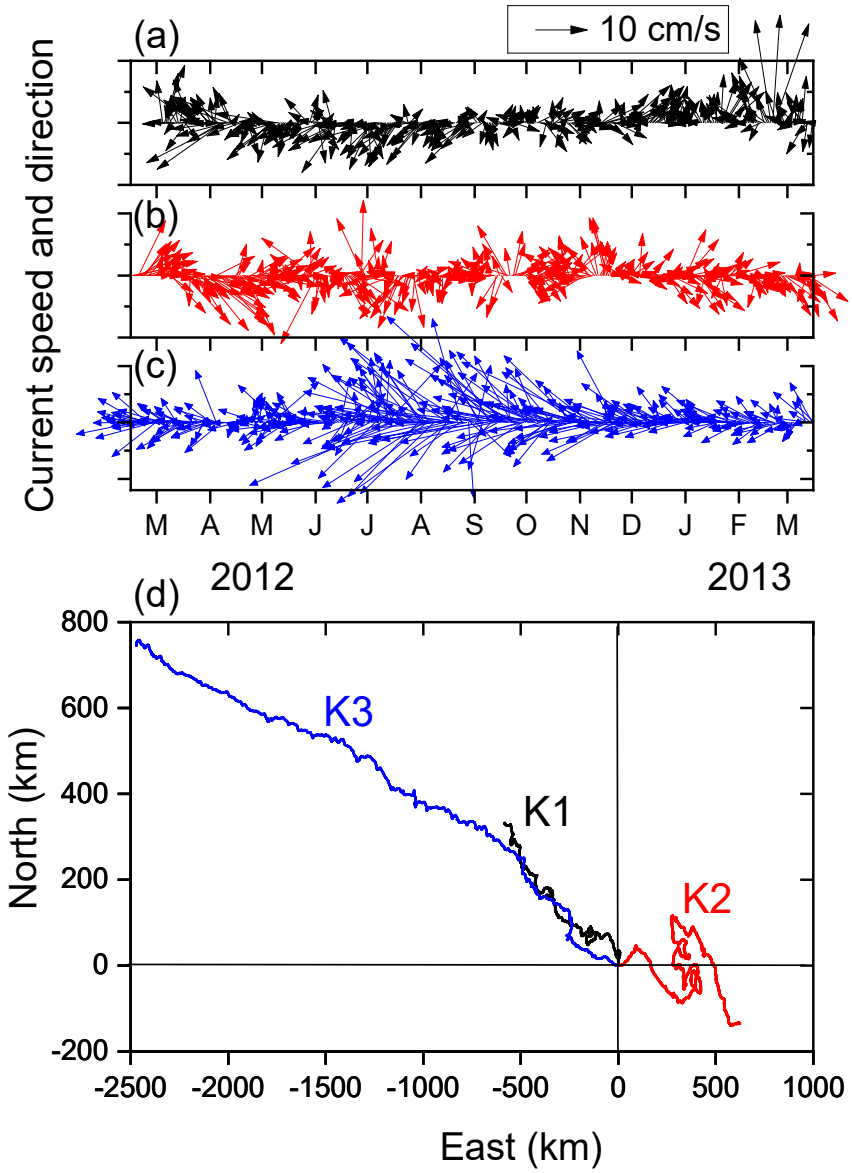

Figure 3.3. Daily current speed and direction measured at 2 m below each trap at stations (a) K1, (b) K2, and (c) K3. (d) Progressive vector diagrams at three stations. The origin indicates the location on the initial day.

`

Flux, biogenic composition, and radiocarbon isotope ratio of sinking particles

Total particle flux at K1 ranged from 0.7 to 396 mg m^{-2} d^{-1}, with high values occurring during March and April 2012 (Figure 3.2a). The particle flux was greatest at the beginning of the sampling period (March 2012) and decreased steadily to 16 mg m^{-2} d^{-1} in June. Low particle flux, ranging from 0.7 to 7.0 mg m^{-2} d^{-1}, persisted from July to December. Total particle flux increased slightly in January 2013 and fluctuated between 12 and 76 mg m^{-2} d^{-1} until the end of the sampling period on March 16. A prominent peak in particle flux, such as that recorded during the previous summer, was not observed. Total particle flux at K2 ranged from 3.0 to 273 mg m^{-2} d^{-1} (Figure 3.2b). Our sample collection, having started in mid-February, most probably missed the peak sinking particle flux during summer 2011–2012. Total particle flux remained low (3.9–70 mg m^{-2} d^{-1}) until November 2012, and then increased steadily to the maximum value in late December 2012 to early January 2013. The flux dropped to less than 5.0 mg m^{-2} d^{-1} from January 24 to the end of the sampling period. We have not determined whether this sudden drop in particle flux was a sampling artifact, although we verified the functionality of the trap carousel (clogging of the funnel is a possibility). Total particle flux at K3 ranged from 2.5 to 162 mg m^{-2} d^{-1}. Temporal variability at K3 was similar to that at K2. A high particle flux was not observed in late February 2012, when sampling began. The flux was low during the winter until November, when the flux started to increase. The highest value was observed in late January 2013, after which the particle flux decreased rapidly.

`

The POC content at K1 ranged between 5.6% and 6.3% during the high particle flux period of March–May 2012 (Figure 3.4), before increasing to high values (up to 29%) in July and August. POC content gradually decreased to about 14% in October 2012. Subsequently, the POC content during the summer generally remained low (5% to 8%). In contrast, higher values were observed at K2 in summer than in winter. The highest POC content of 23% was observed during the period February–April 2012. The values then remained between 3.5% and 6.0% (with an exception of 11% in August) until mid-January 2013, with values increasing to 14.6% during February 2013. At K3, both the temporal variability and magnitude of the POC content were similar to K2. The temporal variability of POC flux resembled that of total particle flux (Figure 3.2). The POC flux varied within the ranges 0.4–25, 0.4–29, and 0.5–16 mgC m^{-2} d^{-1} at K1, K2, and K3, respectively. The sampling-duration-weighted average POC fluxes were 4.0, 3.8, and 2.1 mgC m^{-2} d^{-1}, which correspond to annual fluxes of 1.5, 1.4, and 0.78 gC m^{-2} yr^{-1} at stations K1, K2, and K3, respectively.

$CaCO_3$ accounted for 3.2% (based on annually integrated fluxes) of the particle flux at K1 (Figure 3.4). The duration-weighted average $CaCO_3$ contents at both K2 and K3 (1.5% and 2.7%, respectively) were lower than that at K1. The $CaCO_3$ flux, with a maximum value of 11 mg m^{-2} d^{-1} at K1, accounted for the smallest portion of the mass flux and was almost insignificant at all sites (Figure 3.4).

The biogenic opal content at K1 was the highest (70%) in March 2012, before decreasing to 43% in June 2012 (Figure 3.4). It increased from 27% in

`

January to 51% in mid-February 2013. The biogenic opal flux at K1 ranged from 6.4 to 277 mg m^{-2} d^{-1} (note that opal data are not available for winter; Figure 2). At K2, the biogenic opal content varied between 10% and 28%. The opal content started to increase in November 2012, reaching the highest values during January 2013. The biogenic opal flux ranged from 2.9 to 75 mg m^{-2} d^{-1} (Figure 3.2). Among the three sites, the biogenic opal content and flux were lowest at K3, with the opal flux in the range 0.5–18 mg m^{-2} d^{-1}.

Non-biogenic material was estimated as the difference between the total mass and the sum of biogenic opal, $CaCO_3$, and POC × 1.88 (the ratio 1.88 for particulate organic matter over POC was adopted from Lam et al., 2011). The associated uncertainty is smaller than 10%. Non-biogenic material was dominant at K2 and K3, accounting for up to 80% of the particle flux (Figure 3.4). Non-biogenic material flux was highest during summer at all sites, with the largest fluxes observed at K2 during December to January (Figure 3.2).

The flux of diatom cells was highest at K1, especially in March and April 2012 (Figure 3.5). The diatom flux remained low during winter and increased from January 2013 to the end of sampling in March at K1. However, the highest flux in March 2013 was an order of magnitude lower than that of March 2012. At K2 and K3, no prominent peaks in diatom flux were observed over the period February–April 2012. The diatom flux began to increase in December 2012, and peaked in January 2013, at both K2 and K3. The peak diatom flux occurred much earlier (>1 month) at K2 and K3 than at K1.

`

Viewed under the microscope, the diatom assemblages at all sites were composed primarily of Fragilariopsis cylindrus/curta, Thalassiosira, Chaetoceros, and Pseudonitzschia. Fragilariopsis cylindrus/curta were the most abundant species (accounting for more than 80% of the diatom assemblages) and were therefore primarily responsible for the observed temporal variability in the diatom fluxes. Diatoms did not contain chloroplasts. No hypnospores were observed.

The radiocarbon isotope ratio ($\Delta^{14}C$ values) at K2 ranged between −171‰ and −245‰, with higher values observed during summer (not shown, Table 3.1). At K3, the $\Delta^{14}C$ values observed in May 2012 and late-January 2013 were −224‰ and −197‰, respectively.

`

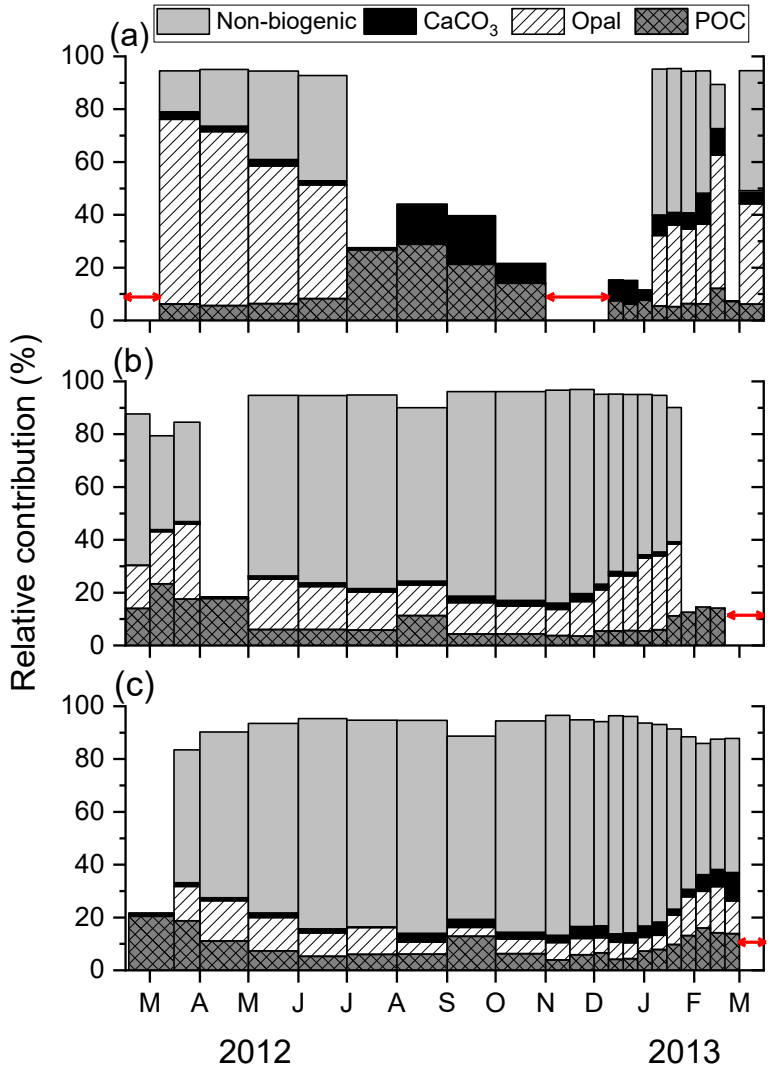

Figure 3.4. Temporal variability in the relative contributions of each biogenic component and the non-biogenic component that is not accounted for by biogenic components (POC×1.88, $CaCO_3$, and opal) at stations (a) K1, (b) K2, and (c) K3. Horizontal arrows denote periods of no data.

`

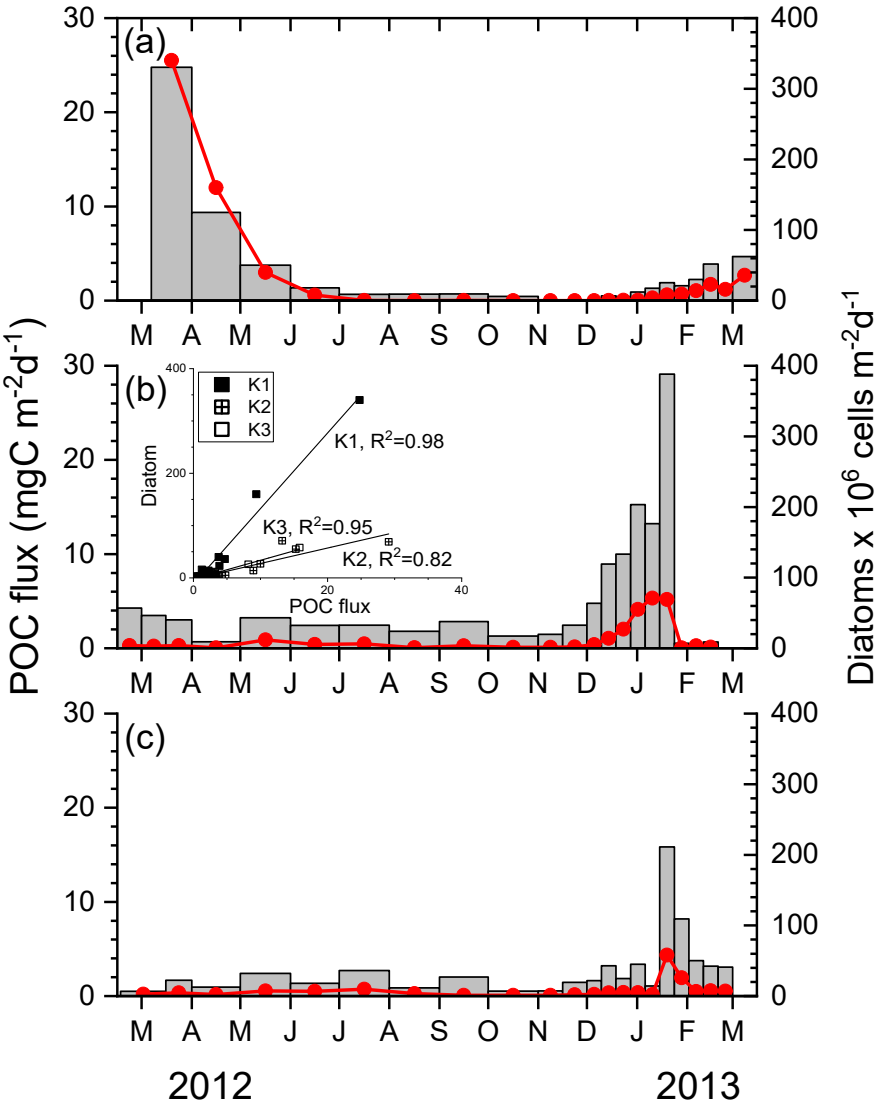

Figure 3.5. Fluxes of POC (bars) and diatom cells (symbols) at Stations (a) K1, (b) K2, and (c) K3. The insert shows the relationship between diatom cell flux and POC flux. R2 values are also shown for each site.

`

3.4. Discussion

Temporal evolution of sea ice and POC flux

Sea ice influences photosynthetically available radiation, primary production, and the dominant primary producers in the near-surface ocean (Smith et al., 2008, 2014) and hence influences the magnitude and efficiency of particle export from the euphotic zone to the deep water column (Ramseier et al., 1999; Garrity et al., 2005). A model was developed to estimate the POC flux as a function of annual sea ice concentration for the seasonal ice zone (Garrity et al., 2005). This model estimated a low POC flux when the annual sea ice concentration was over 80% (<1 gC m^{-2} yr^{-1}). Compared with this model, the annual POC flux at K1 was more than double the expected value at the corresponding sea ice concentration, emphasizing that the perennial ice-covered area behaves differently to the seasonal ice zone, in terms of POC export.

The summer POC flux exhibited high interannual variability at K1 (Figure 3.6). For example, the prominent peak in January 2011 was not observed in January 2013. Also, the POC flux in March 2012 was larger than those in the other two years. The dominant diatoms, Fragilariopsis cylindrus/curta, are known as sea ice algae (Lizotte, 2001). Especially at K1, the water column species Fragilariopsis kerguelensis accounted for less than 5% of the diatom community in the surface waters during the December 2013 to January 2014 cruise (Y.J. Lee, pers. comm.). Diatom cell flux and the POC flux at K1were tightly coupled (R^2 = 0.98, Figure 3.5). POC content in diatoms cells, especially Flagilariopsis spp., reportedly ranges between 128 and 158 pgC per cell (Cornet-Barthaux et al., 2007). When the diatom

`

cell flux was converted to POC flux based on these values, the observed POC flux in March and April 2012 can be fully explained by diatom-derived POC flux.

The sea ice concentration was examined as the major parameter that affects POC production and flux in the perennial ice-covered area. To indicate when sea ice began to decline, we used the day when a 50% sea ice concentration was first reached, as has been used in other studies (e.g., Yager et al., 2016). In 2011, the highest POC flux occurred 34–44 days after the sea ice decline on December 10, 2010 (Figure 3.6). During the following summer, sea ice concentration barely reached 50% on February 23, 2012. As sampling resumed on March 7 in the second year, after a hiatus of around 60 days, our sampling period may not have resolved the peak POC flux and may have occurred during the declining phase of the POC flux. However, if it took about 40 days from sea ice decline to phytoplankton bloom, as we observed during the preceding summer, and as was also observed by Yager et al. (2016), our first sample potentially measured the maximum POC flux. The POC flux of the first sample in March 2012 (24.8 mgC m^{-2} d^{-1}) was about half of the peak POC flux in January 2011 (54.9 mgC m^{-2} d^{-1}) (Figure 3.6). The difference was also conspicuous when monthly-integrated values were compared (768 mgC $m^{-2}month^{-1}$ for March vs. 1140 mgC $m^{-2}month^{-1}$ for January). In 2013, the sea ice concentration reached 50% on March 14 and the POC flux increased until the end of the sampling period. Although diatom cell flux values over 20 million cells $m^{-2}d^{-1}$ indicate that there was a phytoplankton bloom, the POC flux at the end of the sampling was much lower than those in the previous

`

two summers. No data are available after mid-March 2013 to determine whether POC flux increased further or not.

Based on these short time series, the POC flux between December and April appears to be affected by the timing of sea ice reduction, both in terms of the time-integrated flux and peak magnitude. A probable explanation for the time delay between sea ice reduction and peak POC flux may be a “seeding hypothesis”, in which sea ice diatoms released to the water column from sea ice upon its melting, can stimulate subsequent blooms in the water column (Lizotte, 2001). In March 2013, sea ice melting occurred too late in the season, when insolation was diminishing, for a full-fledged bloom to occur. Our preliminary interpretation is that the timing of sea ice reduction, in addition to sea ice reduction itself, is important for a diatom bloom and enhanced POC export in the perennial ice-covered area. Therefore, although high POC flux comparable to that in the central ASP was observed at K1, similar high POC export cannot be equally expected across the perennial ice-covered area because of these restraints. The few locations that were examined under the perennial sea ice cover in the Amundsen Sea suggest low organic carbon accumulation rates compared with the ASP, further supporting this hypothesis (M. Kim et al., 2016). Ultimately, longer time series will be needed to establish a quantitative relationship between sea ice concentration and flux phenology.

`

Spatial variability in sinking particle flux and composition

The annual POC fluxes at stations K1 and K2 were similar; however, the composition of the biogenic particles was differed. The contribution of biogenic opal to the sinking particles was highest at K1, comprising 62% of the total flux for the period when data were available, compared with 20% and 9% at K2 and K3, respectively (Figure 3.4). The biogenic-Si/POC ratio (wt/wt) was 2.8 at K1 compared with 1.2 at K2 and 0.46 at K3. The opal flux was derived mostly from diatoms, because radiolarians and silicoflagellates were seldom observed in the sinking particles. The ratio of diatom cell flux to POC flux was the highest at K1(Figure 3.5). Despite the varying contribution of diatoms to POC flux, the fluxes were tightly coupled at all stations (the insert of Figure 3.5).

The difference in the sinking particle composition can be compared with the distinct phytoplankton compositions observed between the two regions in the upper 100 m layer during expeditions in January 2011 (Yang et al., 2016) and January 2014 (Y. Lee et al., 2016). Yang et al. (2016) reported that in January 2011, diatoms accounted for 90±44% and 24±10% of the total phytoplankton biomass, whereas *Phaeocystis antarctica* (*P. antarctica*) accounted for 2% and 73±32% in the perennial ice-covered area and ASP, respectively. Similar spatial variability in the phytoplankton distribution was also observed based on pigment analysis during expeditions in February 2012 and January 2014 (Y.C. Lee et al., 2016).

While both sites were within the ASP, the POC flux at K3 was roughly half that at K2, reflecting the spatially-heterogeneous distribution of POC production. A different sampling depth at K3, ~80 m deeper than at K2, is not the

`

major cause of the observed difference because the attenuation of POC flux from 410 m to 490 m is ~15% based on Martin curve (we used a b value of –0.8 and calculated the export production value that matches the observed flux at 490 m, after which we calculated the POC flux at 410 m using these values; Berelson, 2001; Martin et al., 1987). At K2, the diatom flux in December and the first half of January was significantly higher than at K3. During summer, when satellite data are available, chlorophyll-a concentrations in surface waters were several times higher in the central region of the ASP than on the periphery (Figure 1b and also Mu et al., 2014; La et al., 2015). Average primary production from November 2012 through February 2013 was estimated to be 760 and 550 mgC m^{-2} d^{-1} for the regions including stations K2 and K3, respectively. The duration-weighted average sinking POC flux over the same period was 7.3 and 3.6 mgC m^{-2} d^{-1} at K2 and K3, respectively, resulting in an export and transfer efficiency (ratio of POC flux to primary production) of ~1% in the ASP.

We were not able to determine the export and transfer efficiency for K1 because no primary production data are available except for a snapshot. However, diatom-dominancy can affect the export and transfer efficiency of POC in favor of Station K1. The diatoms' relatively large volume and siliceous mineral content facilitate settling (Collier et al. 2000). McDonnell and Buesseler (2010) examined the particle size spectrum and their corresponding sinking velocities, finding that diatoms and krill fecal pellets had high sinking velocities across the size spectrum. Factors influencing the export efficiency in the ASP include slow sinking of *P. antarctica*, (Dunbar et al., 1998; Asper and Smith, 1999), and/or efficient

`

remineralization due to prolonged exposure to microorganisms in the water column (Ducklow et al., 2015). Alternatively, *P. antarctica* may be channeled through the microbial food web via zooplankton grazing rather than contributing to vertical carbon flux (Reigstad and Wassmann, 2007; Hyun et al., 2016; Yang et al., 2016).

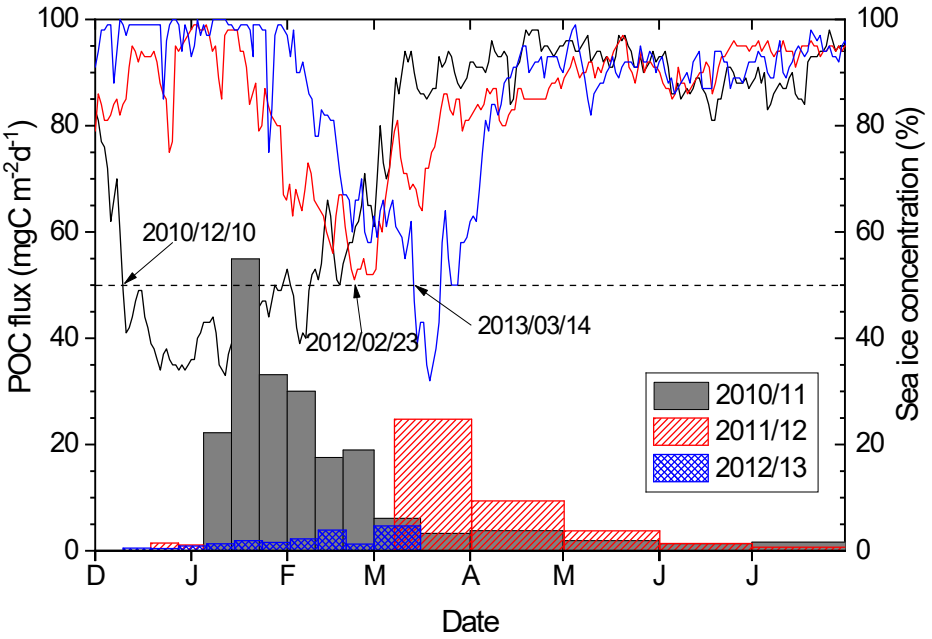

Figure 3.6. Temporal variability of POC flux (bars) and sea ice concentration (lines) at station K1. The data are presented on a common time axis from December to July to show the variability during three summer and fall periods.

`

Contribution of non-biogenic particles

As the sampling sites were located on the continental shelf, the contribution from the lateral supply of allochthonous organic matter and lithogenic particles to the collected sinking particles was expected to be considerable. Radiocarbon analysis of the sinking particle samples collected during the preceding year in the perennial ice-covered area implied that the lateral supply of aged organic carbon could be a considerable source of POC, but only during the winter (Kim et al., 2015).

We used the non-biogenic material as a proxy for lithogenic particles. Non-biogenic material was the dominant component of the sinking particles, especially at K2 (62%, based on annually integrated fluxes, average flux = 41.0 mg m^{-2} d^{-1}) and K3 (68%, 19.0 mg m^{-2} d^{-1}), but was less prominent at K1 (19%, <12 mg m^{-2} d^{-1}; note that an exact flux value was not calculated because there were no data for winter; Figure 3.4). Sources of lithogenic material include aeolian dust deposition, sediment resuspension, and the melting of sea ice, icebergs, and ice shelves (Planquette et al., 2013). Deposition of aeolian dust in Antarctica's coastal regions is negligible compared with the observed non-biogenic material flux (Planquette et al., 2013). Although the K1 trap was the closest to the seafloor (ca. 130 m above the bottom), the total particle flux was extremely low from June to December, suggesting that local resuspension of sediment was not the major source. A much higher value at K2 compared with K1 and K3 suggest that lithogenic particles were released from sea ice melting. The higher non-biogenic material flux during summer compared with other seasons also implies that particles were released by sea ice melting. Fine particles were possibly scavenged

`

more efficiently by the high flux of sinking particles in summer. Planquette et al. (2013) showed that particulate (>5 μm) aluminum concentration was considerably higher (throughout the water column) in front of the Dotson Ice Shelf than at other locations. Aluminum concentration was especially high both near the seafloor and in the near-surface layer, suggesting two distinct sources of particulate aluminum (Planquette et al., 2013).

The $\Delta^{14}C$ values and the contents of the non-biogenic material in sinking particles were negatively correlated (Figure 3.7). The $\Delta^{14}C$ values of dissolved inorganic carbon in surface water collected in 2012 from the study region ranged between −135‰ and −155‰ (n = 4; B. Kim et al., 2016). All observed values of sinking POC were lower than these values, indicating that the sinking POC contained aged POC from allochthonous sources. The $\Delta^{14}C$ values of surface sediments (0–1 cm, n = 4) in the Amundsen Sea ranged between −311‰ at a site near K2 in the ASP and −418‰ near the Dotson Ice Shelf (M. Kim et al., 2016). Therefore, inclusion of resuspended sediments is a plausible explanation of the observed $\Delta^{14}C$ results. In addition, particles from the basal melting of icebergs and ice shelves may also supply aged POC. Exact sources of aged POC and the mode of delivery remain to be determined.

`

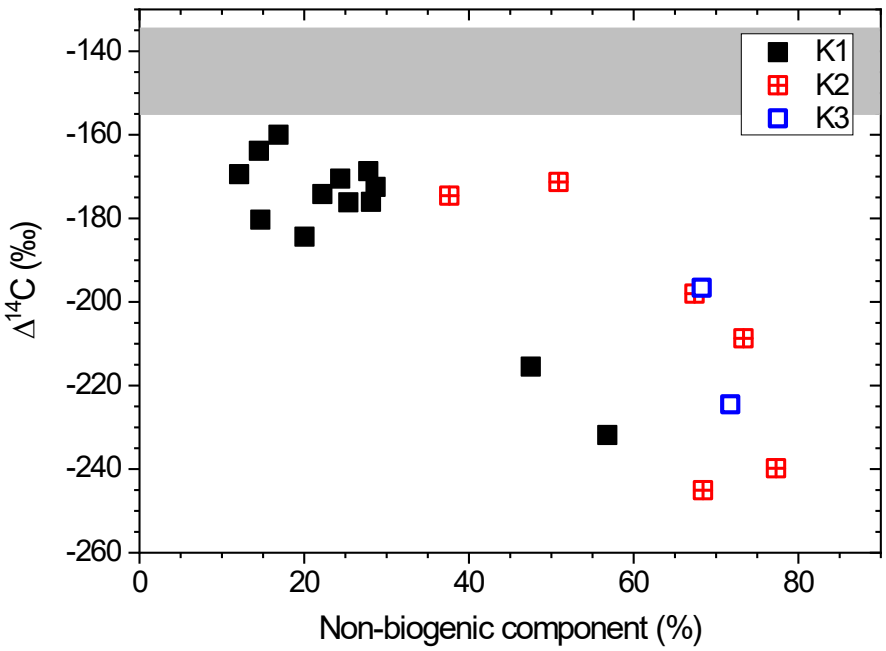

Figure 3.7. Relationship between $\Delta^{14}C$ values of sinking POC and content of non-biogenic particles. Results from the preceding year at K1 are also shown for comparison (Kim et al., 2015). The shaded bar indicates the range of $\Delta^{14}C$ values of dissolved inorganic carbon in the study region (n = 4; B. Kim et al., 2016).

`

3.5. Summary

As observed in previous studies, the POC flux exhibited strong seasonal variability, with most of the annual POC flux occurring during the austral summer when the sea ice concentration was lowest. The ASP showed a high POC flux and is a key component of carbon cycling in the Amundsen Sea. However, the POC flux in the perennial ice-covered area, mostly supplied by sea ice diatoms, was high and comparable with the central region of the ASP, emphasizing the importance of the perennial ice-covered area to Amundsen Sea carbon cycling. However, the summer POC flux in the perennial ice-covered area exhibited high interannual variability. Both the reduction of sea ice cover and the timing when this reduction occurs are important: sea ice reduction in early summer for sufficient insolation appears to be crucial to maintaining high POC fluxes. Particle composition at the perennial ice-covered area and the central ASP was different, reflecting the difference in the phytoplankton community at the two sites: primarily sea ice diatoms in the former and *P. antarctica* in the latter. The importance of the diatom-derived POC flux in the perennial ice-covered area was demonstrated by the biogenic-Si/POC ratio being more than double that in the central ASP. The periphery of the ASP near the Dotson Ice Shelf showed much a smaller particle flux than the center. Lower diatom fluxes especially in early summer, in addition to lower primary production, appear to be responsible for the observed difference in the POC flux.

`

Acknowledgments

We thank Sosul Cho at KIOST for the elemental analysis, Hyoung Sul La for providing sea ice data, and all cruise participants for their help with sampling, the captain and crew of the IBRV Araon for help at sea, and the staff at NOSAMS WHOI for radiocarbon analysis. This work was supported by the Korea Institute of Ocean Science and Technology (PN67330) and the Korea Polar Research Institute (PE18060). H. Ducklow was supported by NSF Award ANT 0839012.

`

Chapter 4

Collection of large benthic invertebrates in sediment traps in the Amundsen Sea, Antarctica

Minkyoung Kim[1], Eun Jin Yang[2], Hyung Jeek Kim[3], Dongseon Kim[3], Tae-Wan Kim[2], Hyoung Sul La[2], SangHoon Lee[2], and Jeomshik Hwang[1*]

Published in *Biogeosciences*, 2019 v. 16 p. 2683-2691.

[1]School of Earth and Environmental Sciences/Research Institute of Oceanography, Seoul National University, Seoul, 08826, South Korea
[2]Korea Polar Research Institute, Incheon, 21990, South Korea
[3]Korea Institute of Ocean Science & Technology, Busan, 49111, South Korea

Short Summary

Unexpectedly, in sediment traps deployed in the Antarctic Amundsen Sea to catch small sinking particles in the water, large benthic invertebrates such as long and slender worms, baby sea urchins, and small scallops were found. We suggest three hypotheses: lifting of these animals by anchor ice formation and subsequent transport by ice rafting, spending their juvenile period in a habitat underneath the sea ice and subsequent falling, or their active use of the current as a means of dispersal.

`

Abstract

To study sinking particle sources and dynamics, sediment traps were deployed at three sites in the Amundsen Sea for 1 year from February–March 2012 and at one site from February 2016 to February 2018. Unexpectedly, large benthic invertebrates were found in three sediment traps deployed 130–567 m above the sea floor. The organisms included long and slender worms, a sea urchin, and juvenile scallops of varying sizes. This is the first reported collection of these benthic invertebrates in sediment traps. The collection of these organisms, predominantly during the austral winter, and their intact bodies suggests they were trapped in anchor ice, incorporated into the overlying sea ice, and subsequently transported by ice rafting. The observations imply that anchor ice forms episodically in the Amundsen Sea and has biological impacts on benthic ecosystems. An alternative hypothesis that these organisms spend their juvenile period underneath the sea ice and subsequently sink to the seafloor is also suggested.

`

4.1. Introduction

The majority of the Amundsen Shelf in the Antarctic is perennially covered with sea ice, except for the two seasonal polynyas. The Amundsen Sea Polynya in the western Amundsen Sea is the most productive polynya around Antarctica (Arrigo and van Dijken, 2003). Intensive flux of particulate organic carbon to the seafloor occurs in the austral summer, while the sea interior is in starvation in the other seasons (Ducklow et al., 2015; Kim et al., 2015, 2019). Biogeochemical processes related to biological pump in the Amundsen Sea have been investigated by recent field campaigns (Arrigo and Alderkamp, 2012; Yager et al., 2012; Meredith et al., 2016; Lee et al., 2017).

Sediment traps were deployed in the Amundsen Sea to study sinking material flux and composition. Sampling occurred from February and March 2012 for 1 year at three locations along the paleoglacier-carved Dotson Trough and from February 2016 to February 2018 in a trap deployed in front of the eastern Getz Ice Shelf, near Duncan Peninsula. Unexpectedly, at three locations macrobenthic organisms were found in the sampling cups, including long and slender worms, a sea urchin, and juvenile scallops of varying sizes. This is the first reported collection of these benthic invertebrates in sediment traps.

This paper reports on details of the benthic invertebrates collected, in addition to sinking particle flux data. The distinct environmental conditions and characteristics of the polar seas relative to temperate and tropical oceans probably explain the unusual occurrence of benthic invertebrates in sediment traps. For example, starvation in the winter due to a reduced supply of organic matter from the

`

overlying water column may stimulate the relocation of benthos. The undersurface of the sea ice may provide a habitat for juvenile benthos before they settle to the seafloor. Anchor ice, which forms at the seafloor in supercooled water, can lift benthos to the overlying sea ice for further transport by ice rafting (Dayton et al., 1969). Studies in the Arctic have shown the incorporation of sediment particles and benthic organisms into sea ice and their subsequent transport (e.g., Nürnberg et al., 1994). Potential transport mechanisms for the collected benthos are considered, and the implications of the surprising observations are discussed.

`

4.2. Methods

Time-series sediment traps (McLane PARFLUX Mark 78G; conical type, 80 cm aperture diameter, height/diameter ratio = 2.5) were deployed on bottom-tethered hydrographic moorings during two cruises in the Amundsen Sea (Figure 4.1). The traps were positioned at four locations with different sea surface conditions: the sea ice region (Station K1), the central Amundsen Sea Polynya (Station K2), near the Dotson Ice Shelf (Station K3), and near the eastern Getz Ice Shelf (Station K4) (Figure 4.1). Station K1 (72.40°S, 117.72°W; water depth = 530 m) was located in the sea ice region, near the northern entrance of a glacier-carved trough (Dotson Trough). A sediment trap was deployed here 130 m above the sea floor at a depth of 400 m and collected samples from 7 March 2012 to 16 March 2013. Station K2 (73.28°S, 114.97°W; trap depth = 410 m; water depth = 830 m) was located in the central region of the Amundsen Sea Polynya. Samples were collected in this trap from 15 February 2012 to 20 February 2013. Station K3 (74.19°S, 112.54°W; water depth = 1057 m) was located ~2 km north of the Dotson Ice Shelf inside the Amundsen Sea Polynya. The trap was deployed here at a depth of 490 m (567 m above the sea floor) and collected samples from 17 February 2012 to 1 March 2013. The trap moorings were equipped with RCM11 current meters placed 2 m below each trap. The flux and composition characteristics of small sinking particles collected at stations K1, K2, and K3 are reported elsewhere in Kim et al. (2019).

Station K4 (73.89°S, 118.72°W; water depth = 688 m) was located ~ 1.3 km off the eastern Getz Ice Shelf near Duncan Peninsula. The sediment trap at this location was deployed at a depth of 427 m from 1 February 2016 to 28 February

`

2018. The sampling intervals at Station K4 varied from 13 to 61 d, depending on the expected particle flux (Table 4.1). Each sample bottle was filled with filtered seawater collected from the same depth as the trap at the sampling site, with a sodium borate buffer and 10 % formalin solution added, the latter as a preservative. Particle samples recovered from the traps were stored at 4 ∘C until analyzed. The particle flux was determined gravimetrically following removal of any conspicuous swimmers. The particulate organic carbon (POC) content was calculated as the difference between the total carbon content and the inorganic carbon content. The details of sample analysis are described in Kim et al. (2015, 2019).

Worm specimens were removed by hand from samples on return to the laboratory and were stored in a 10 % formalin solution. The specimen numbers were determined following visual assessment of whether each specimen was an entire body or a body part. The length and thickness of specimens were measured using a ruler and a Vernier caliper, respectively. At Station K4, juvenile scallops and a sea urchin were collected in addition to worms. The length of each of these organisms was measured using a ruler.

Five worm specimens were freeze dried, weighed, and finely ground using a mortar and pestle. The total carbon content of the ground samples (～0.3 mg) was determined using an elemental analyzer (vario MICRO cube; Elementar, Germany), with an uncertainty of 3 % relative standard deviation (RSD). The inorganic carbon content was determined using the same method but based on ～0.2 mg samples that were ashed at 500 °C for 12 h (Clarke et al., 1997; Obermüller et al., 2013). The inorganic fraction was negligible (0.1 % ± 0.2 % for carbon and 0.1 % ± 0.1 % for

`

nitrogen).

Sea ice concentration data were obtained from the European Centre for Medium-Range Weather Forecasts (ECMWF) ERA-Interim reanalysis (https://www.ecmwf.int, last access: 12 December 2018) and are based on global coverage data (0.75° ×0.75°) received daily from the Operational Sea Surface Temperature and Sea Ice Analysis (OSTIA) system.

`

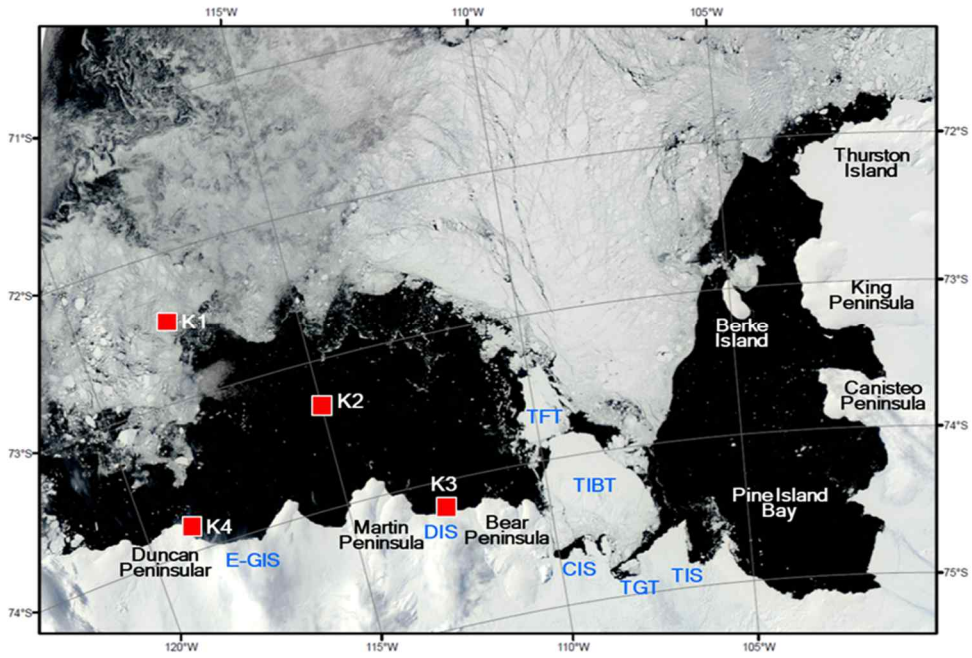

Figure 4.1. Locations of sediment traps deployed in the Amundsen Sea. The satellite image showing the sea ice distribution was taken on 15 February 2012. The satellite image was obtained from Rapid Response imagery from the Land, Atmosphere Near real-time Capability for EOS (LANCE) system, operated by the NASA's GSFC Earth Science Data and Information System (ESDIS). Areas marked from east to west: Thwaites Ice Shelf (TIS), Thwaites Glacier Tongue (TGT), Thwaites Iceberg Tongue (TIBT), Thwaites Fast-ice Tongue (TFT), Crosson Ice Shelf (CIS), Dotson Ice Shelf (DIS), and East Getz Ice Shelf (E-GIS).

`

4.3. Results

Temporal variation in sea ice concentration and fluxes of sinking particles and POC

Station K4 is located within the seasonal Amundsen Sea Polynya, and the sea ice concentration there decreases to zero in summer (Figure 4.2). Ice-free conditions lasted for ～2.5 months from January to March 2016 and for ～4.5 months from late November 2016 to March 2017. In the other seasons the sea ice concentration was generally >85 %. The sinking particle flux varied from 11 to 978 mg m^{-2} d^{-1}, with a sampling duration-weighted average of 70 mg m^{-2} d^{-1}. Relatively high fluxes were found during the austral summer. However, the flux in the 2016/2017 summer was considerably lower than in the preceding summer. The POC flux varied from 1.0 to 37 mg C m^{-2} d^{-1}, with a sampling duration-weighted average of 5.3 mg C m−2 d−1 (Figure 4.2; Table 4.1). The average POC and inorganic carbon contents were 9.2 % ± 4.0 % and 0.3 % ± 0.2 %, respectively (not shown).

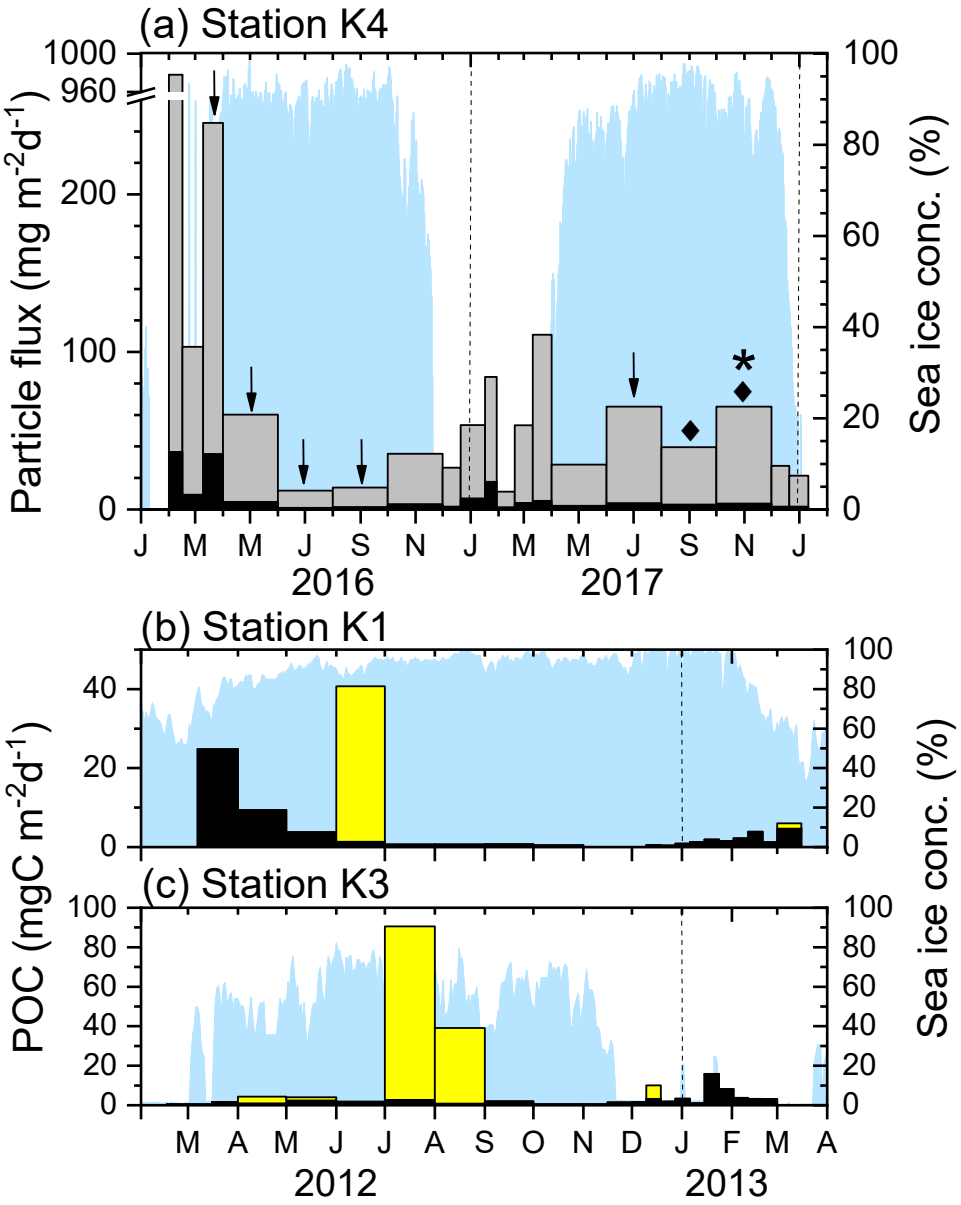

Figure 4.2. (a) Fluxes of sinking particles (gray bars) and POC (black bars) at Station K4. The tick marks on the x-axis indicate the start of each month. The arrows, diamonds, and the star respectively indicate the periods when worms, scallops, and

`

the sea urchin were collected. (b) POC fluxes by worms (yellow bars) and sinking particles (black bars) at Stations K1 and (c) K3. Note that the y-axis scales differ. The dotted vertical lines denote the beginning of each year. The blue shading indicates the sea ice concentration. POC flux and sea ice data for Stations K1 and K3 were redrawn from Kim et al. (2019).

`

Table 4.1. Sequential trap schedules, and organisms collected at Stations K1, K3, and K4 in the Amundsen Sea. Quantity, lengths, and thicknesses of worm specimens collected in the sediment traps are shown. Total particle and POC fluxes are also presented for Station K4.

	Station K1					Station K3					Station K4							
Cup no.	Cup open date (mm/dd/yy)	Interval (d)	Number of whole body/part	Length (cm), thickness (mm)	Worm flux (mg C per bottle)	Cup open date (mm/dd/yy)	Interval (d)	Number of whole body/part	Length (cm), thickness (mm)	Worm flux (mg C per bottle)	Cup open date (mm/dd/yy)	Interval (d)	Total mass flux (mg $m^{-2} d^{-1}$)	POC flux (mg C $m^{-2} d^{-1}$)	Number of whole body/part	Length (cm), thickness (mm)	Worm flux (mg C per bottle)	Number of scallops/ urchin
1	3/7/12	25				2/17/12	28				2/1/16	15	978	37				
2	4/1/12	30				3/16/12	16				2/16/16	23	103	9.4				
3	5/1/12	31				4/1/12	30	1/0	(16.0, 2.8)	52	3/10/16	22	245	35	1/0	(32.0, 1.8)	43	
4	6/1/12	30	1/0	(69.0, 4.6)	590	5/1/12	31	1/0	(6.7, 3.0)	25	4/1/16	61	60	4.8	1/0	(55.0, 2.7)	158	
5	7/1/12	31				6/1/12	30	1/0	(3.7, 2.2)	8	6/1/16	61	12	1.0	0/2	note 3	33	
6	8/1/12	31				7/1/12	31	10/14	note 1	1361	8/1/16	61	14	1.6	1/0	(24.0, 2.6)	67	
7	9/1/12	30				8/1/12	31	1/4	note 2	593	10/1/16	61	35	3.4				
8	10/1/12	31				9/1/12	30				12/1/16	20	27	1.9				
9	11/1/12	15				10/1/12	31				12/21/16	27	54	7.0				
10	11/16/12	15				11/1/12	15				1/17/17	13	84	18				
11	12/1/12	9				11/16/12	15				1/30/17	20	11	1.4				
12	12/10/12	9				12/1/12	9				2/19/17	20	54	4.2				
13	12/19/12	9				12/10/12	9	1/0	(14.0, 2.3)	31	3/11/17	21	111	5.4				
14	12/28/12	9				12/19/12	9				4/1/17	61	29	2.4				
15	1/6/13	9				12/28/12	9				6/1/17	61	65	4.0	2/5	note 4	281	
16	1/15/13	9				1/6/13	9				8/1/17	61	39	3.2		note 5		1/0
17	1/24/13	9				1/15/13	9				10/1/17	61	65	3.7		note 5		10/1
18	2/2/13	9				1/24/13	9				12/1/17	20	28	1.9				
19	2/11/13	9				2/2/13	9				12/21/17	21	21	1.8				
20	2/20/13	9				2/11/13	9				1/11/18	21						
21	3/1/13	15	1/0	(2.5, 2.3)	6	2/20/13	9				2/1/18	27						

note 1: The length in cm and thickness in mm of the 24 specimens collected in cup #6 were (31.5, 4.1), (16.5, 3.5), (19.5, 4.4), (24.5, 3.0), (27.7, 3.8), (31.5, 2.4), (17.5, 2.4), (11.0, 2.2), (9.0, 2.3), (6.0, 2.5), (2.0, 5.1), (3.5, 4.9), (7.9, 3.8), (4.0, 3.5), (1.5, 4.4), (4.8, 3.8), (8.2, 4.6), (2.0, 3.0), (10.0, 4.4), (9.0, 3.9), (5.3, 4.3), (3.5, 3.3), (20.4, 2.9), (3.0, 2.0).

`

note 2: The length in cm and thickness in mm of the 5 specimens in cup #7 were (22.7, 3.4), (53.5, 4.1), (11.8, 4.0), (11.4, 2.2), (7.7, 2.1).

note 3: The length in cm and thickness in mm of the 5 specimens in cup #5 were (4.0, 2.9), (12.0, 1.9).

note 4: The length in cm and thickness in mm of the 7 specimens in cup #15 were (2.0, 1.6), (5.0, 1.5), (8.0, 2.9), (7.0, 1.5), (3.0, 2.6), (12.0, 0.2), (80, 2.7).

note 5: The height and width in cm of the 11 scallops collected in cup #16 and #17 were (1.3, 1.3), (1.2, 0.9), (1.3, 1.1), (1.5, 1.4), (1.5, 1.4), (1.6, 1.5), (1.7, 1.6), (1.9, 1.7), (1.9, 1.6), (2.0, 2.0), (2.8, 2.5). The diameter of the sea urchin was approximately 0.5 cm excluding the spines.

`

Collection of invertebrate specimens

Long and slender worms were found in the sediment traps at Stations K1 and K3 during the 2012–2013 deployments. No worms were found in the traps at Station K2. The worm specimens were either entire bodies or body parts. The specimens were all similar in appearance (Figure 4. 3). All had a rubbery texture and were easily torn apart when gently stretched. The bodies were round and slender and had a body thickness < 5 mm. Species identification based on genetic methods was not successful, probably because the formalin preservative damaged the DNA (Macrogen Inc.; http://www.macrogen.com, last access: 19 April 2018). Identification of the preserved specimens based on morphological characteristics also proved to be difficult because of the storage in formalin preservative for an extended time (> 1 year; Chernyshev Alexei Viktorovich, personal communication, March 2018). Although it was not possible to identify the species, the interpretation of the results might be applicable to studies that involve the collection of any large benthic invertebrates.

In total, 33 specimens (including 18 incomplete bodies) were collected at Station K3 in six sampling bottles from April to August and in mid-December 2012 (Figure 4.2, Table 4.1) and 24 specimens (10 complete and 14 incomplete bodies) were collected in July. Two specimens were collected at Station K1 in two sampling bottles in June 2012 and in early March 2013 (Figure 4.2). The lengths of the specimens collected at Stations K1 and K3 varied from 2 to 69 cm (average: 14±15 cm) (Figure 4.3).

`

The average total carbon and nitrogen contents of five randomly selected worm samples were 44.0 % ± 1.4 % and 7.7 % ± 1.1 %, respectively. The inorganic carbon content was negligible (average: 0.1 %). The POC content, expressed as the difference between the total and inorganic carbon contents, was 43.9 % ± 1.5 %. Considering the high POC content and presumably high protein content of these specimens, their bodies and/or gut content are likely to be mainly organic matter with a relatively small amount of ingested sedimentary material. The POC flux derived from worm specimens was estimated from the length and thickness of each specimen, the dry weight, the POC content, and the linear relationship between the volume of the specimen and the measured amount of POC (POC content in mg = 0.052× volume of worm in mm3 + 0.5498; R^2=0.94, *n*=5, *p value* = 0.0029). The estimated POC fluxes by worm specimens were 1.2 and 4.1 g C m^{-2} yr^{-1} at Stations K1 and K3, respectively. One bottle, deployed for the month of June at Station K1, contained 590 mg C. At Station K3, large quantities of worms were found on two occasions: 1360 mg C in July and 590 mg C in August. The worm specimen flux corresponded to ～ 80 % and 500 % of the annual POC flux of sinking particles at Stations K1 and K3, respectively.

At Station K4 during the 2016–2018 deployment, 11 juvenile scallops and 1 juvenile sea urchin were found, in addition to 12 worm specimens (including 7 incomplete bodies). Worm specimens were found in five samples collected in March–September 2016 and June–July 2017 (Figure 4.2, Table 4.1). These worms were similar in shape to those collected at Stations K1 and K3 (Figure 4.3). A

`

single scallop was collected in August–September 2017 and 10 were collected in October–November 2017. The scallops were all juveniles and varied in size from 1.2 to 2.8 cm. The baffle of the sediment trap (approximately 2.5 cm diameter) would have blocked any larger creatures from falling into the trap. One juvenile sea urchin was also collected in October–November 2017. No specimens were collected under sea-ice-free conditions.

`

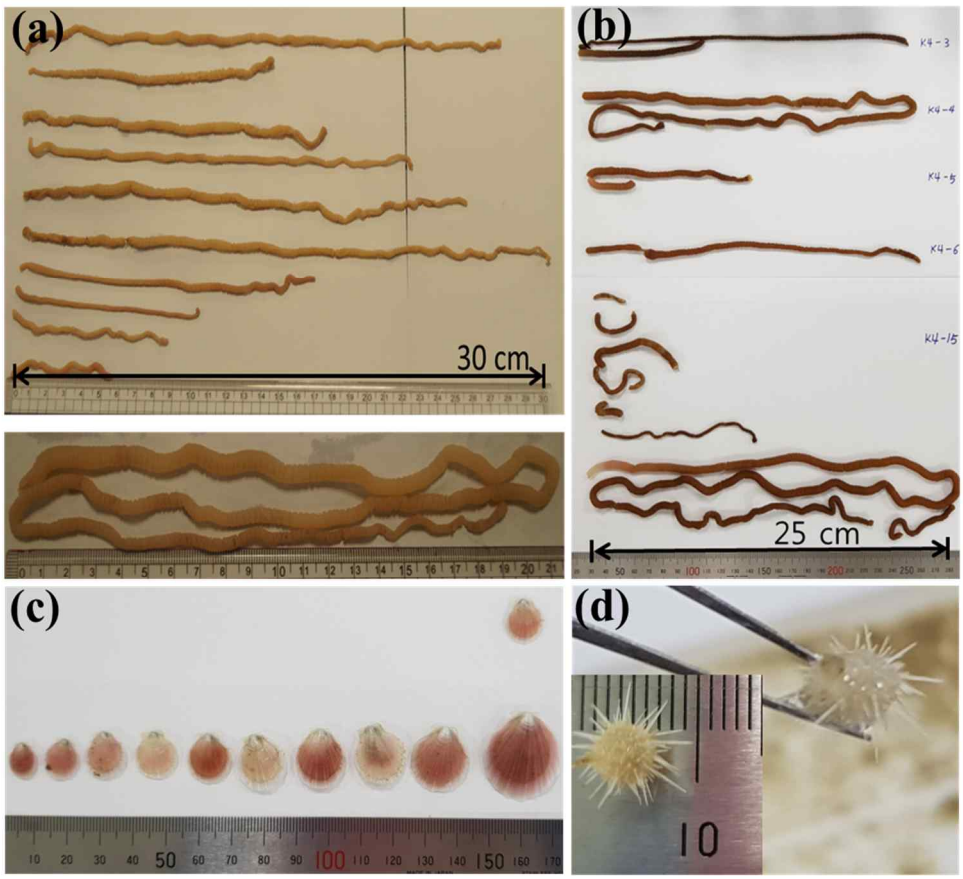

Figure 4.3. (a) Worm specimens collected at Stations K1 and K3, and (b) at Station K4. (c) Scallops and (d) a sea urchin were collected at Station K4.

`

4.4. Discussion

Potential mechanisms for transport of the benthic invertebrates

It is puzzling that large benthic invertebrates lacking swimming capability were collected in sediment traps deployed 130–567 m above the sea floor. The worms had no parapodia or appendages for swimming. It is unlikely that these organisms crawled up the mooring lines to the traps, and human activities were not responsible because the region is not accessible during winter, when most of the specimens were collected. According to the pressure registered to the current meters, ADCPs (acoustic doppler current profilers) and Microcats (Seabird, SBE-37SMP) moored with the sediment traps did not show any sign for considerable tilting of the mooring lines to facilitate better access for the benthos (Kim et al., 2016). Several mechanisms may explain the transport of the collected organisms. Strong currents, especially near Station K3, may have been responsible for swiping and transporting these organisms to the trap sites. Stations K3 and K4 were within ~10 km from the nearest coast. Small juvenile scallops may be particularly affected by strong currents. In addition, scallops may use the current as a means of dispersal and translocation (Picken, 1980). The large size of the worms precludes the possibility that they were passively lifted, but they may actively use the current. The collection of worms in April–August and the period of relatively strong current in July–September partly overlap. However, Station K1 was 200–500 km away from the coast where these worms presumably inhabit and are too remote for transport by current alone.

A likely explanation is that the organisms were transported by and released from sea ice. Two mechanisms could entrain benthic organisms in the sea ice: anchor

`

ice formation and adfreezing of land fast ice. Ice foot formation, fast ice, and subsequent scouring are causes of disturbance of the benthic environment in the Antarctic (Barnes, 1999; Gutt, 2001; Barnes et al., 2011), and benthic organisms can be incorporated into the ice during these processes. For example, adfreezing by bottom fast ice can incorporate benthic organisms in addition to coarse sediment grains (Pfirman et al., 1990; Nürnberg et al., 1994). Several observations indicate that bottom fast-ice formation is not a likely mechanism in this case. Firstly, the collected specimens were intact and well preserved, with no evidence of mechanical abrasion (Reimnitz et al., 1992); breaking of bottom fast ice would have destroyed these soft-bodied benthic organisms. Secondly, no coarse particles (grain size larger than sand) were collected in the sediment traps at the same time; small granules and rock fragments were collected only in one sample at Station K4 in April and May 2016. Thirdly, the organisms were collected mostly in winter; bottom fast ice at the shoreline would remain attached to the land during winter and would thus only release entrained particles near the shore (Reimnitz et al., 1992). In contrast, anchor ice formation could have gently entrained these delicate organisms. Anchor ice forms in supercooled water (Dayton et al., 1969). Any anchor ice that formed on the bodies of benthic organisms would be buoyant and thus able to lift them to the overlying sea ice canopy, in which they could become incorporated (Dayton et al., 1969; Heine et al., 1991). Organisms would be released when the attached anchor ice melted by the heat provided by the underlying water.

Another hypothesis is that the benthic animals actually spend their juvenile period in a habitat underneath the sea ice and fall down to the seafloor. This idea was

`

suggested by a reviewer, Paul Dayton, and we agree that this could be a possibility. This hypothesis is based on his visual inspections in numerous dives at McMurdo Sound that no baby nemerteans were observed and tiny sea urchins and scallops were rare. The undersurface of the sea ice can harbor a thick layer of frazil ice platelets formed by supercooled water and cavities and tunnels formed by brine flow. Diatoms and other algae growing in and/or underneath the sea ice would supply food for juvenile sea urchins and pectins. Also amphipods and small invertebrates would provide food for juvenile nemertean recruits. These organisms may passively sink to the seafloor upon melting of the platelets or actively abandon the sea ice habitat due to depletion of algal food in the winter. This kind of habitat with large populations of these animals has not been observed yet and needs to be verified.

Potential for anchor ice formation in the Amundsen Sea

When ice grows on objects at the seafloor in supercooled water it is called anchor ice (Denny et al., 2011). Anchor ice can grow on epibenthic animals as nucleation sites. Studies of anchor ice formation have focused mainly on sediment entrainment into sea ice in the Arctic (Pfirman et al., 1990; Reimnitz et al., 1992; Nürnberg et al., 1994), where this mechanism is considered to be the most important process for entrainment of sediment into sea ice and subsequent sediment transport (Nürnberg et al., 1994). Arctic sea ice transports well-preserved benthic organisms, including mollusks and sea urchins, in addition to sediments (Reimnitz et al., 1992). Studies of anchor ice in the Antarctic have focused mostly on biological effects (Barnes, 1999).

`

Anchor ice has been reported in McMurdo Sound in the Ross Sea (Dayton et al., 1969; Robinson et al., 2014), Potter Cove in the South Shetland islands (Barrera-Oro and Casaux, 1990), Ellis Fjord, and a few other locations (Kirkwood and Burton, 1988 and references therein). Supercooling has not been reported in the Amundsen Sea because no hydrographic data near the coast are available for seasons other than summer. Observations in summer on the Amundsen Shelf have shown that winter water (water that mimics the properties of water formed in winter) was at near freezing temperature (potential temperature <−1.75 °C; Yager et al., 2016). Surface supercooling over polynyas is one mechanism for anchor ice formation (Mager et al., 2013). Strong winds, subfreezing temperatures, and intense turbulence in an open shallow sea are necessary for anchor ice formation (Reimnitz et al., 1992). Investigation of whether the polynyas in the Amundsen Sea during fall and winter have these conditions is a potential topic for future studies. The majority of the Amundsen Sea Polynya and the Pine Island Polynya is closed in the fall. However, strong katabatic winds generate narrow coastal leads and open spaces (Nihashi et al., 2015; Stammerjohn et al., 2015), where freezing predominates (Assmann et al., 2005).

Another mechanism for anchor ice formation is the so-called “ice pump”, which occurs underneath ice shelves (Mager et al., 2013). Lenard et al. (2014) investigated the potential for anchor ice formation in coastal Antarctic waters, focusing particularly on the ice pump mechanism. They estimated that a wide area of McMurdo Sound is suitable for anchor ice formation. The Amundsen Sea includes several ice shelves. According to a modeling study by Assmann et al. (2005),

`

temperatures below surface freezing were simulated close to the Abbot and Getz Ice Shelves.

4.5. Implications and Conclusions

The observations show that transport and release of benthic invertebrates occurs episodically with potentially high interannual variability. No invertebrates were collected in sediment traps in the preceding year at either Station K1 or the central polynya (Ducklow et al., 2015; Kim et al., 2015). This phenomenon is episodic, probably because particular conditions must occur for anchor ice to form if anchor ice is indeed the mechanism responsible (Kempema et al., 1989; Reimnitz et al., 1992). An implication for coastal benthic ecosystems is that anchor ice formation around Antarctica may be more prevalent than previously thought; the occurrence of many ice shelves and polynyas implies this possibility (Leonard et al., 2014; Mager et al., 2015).

Uplift of benthic organisms to the sea surface by anchor ice has been considered to be important for the Arctic food web (Reimnitz et al., 1992). The role of anchor ice in the transport of benthic organisms off the coast has not been investigated in the Antarctic. Organic carbon supplied by worms accounted for up to 5-fold the POC flux derived from primary production in the overlying water column. This supply of organisms occurred during winter, when little primary production occurs; hence, this flux may provide energy for overwintering organisms. Transport by anchor ice and sea ice rafting may be a means of dispersal for benthic invertebrates (Picken, 1980), provided that the organisms are able to survive this

`

process. In this context, there is no evidence as to whether the organism entered the sediment traps alive or dead.

More studies are needed to clarify the spatial distribution of anchor ice formation. Lenard et al. (2014) noted that detailed information on ice shelf drafts, ground lines, and edges is needed to enable prediction of anchor ice formation, and observations of anchor ice are needed for validation of model outputs. Studies of these aspects of anchor ice formation in the Amundsen Sea would be a useful future study. In parallel, the impact of anchor ice on Antarctic biology, including as a disturbance to benthic ecosystems; a dispersal mechanism for benthic invertebrates; and as a supply of energy, nutrients, and detrital material to the deeper benthic ecosystems, also need to be investigated.

`

Acknowledgements

Junsung Noh is thanked for carbon and nitrogen analyses of the worm specimens; Karen M. Assmann, Okhwan Yu, Dong-Hoon Im, Seung Hee Kim, and Eunah Han for helpful discussion; and the captain and crew of the IBRV Araon for their assistance during fieldwork. Special thanks are given to Alexei Viktorovich Chernyshev, In-Young Ahn, and Francyne Elias-Piera for their contributions to the identification of the worm specimens. We also thank Paul Dayton, Wei-Lei Wang, and Tiantian Tang for their constructive comments. This study made use of rapid response imagery from the Land, Atmosphere Near real-time Capability for EOS (LANCE) system, operated by the NASA's GSFC Earth Science Data and Information System (ESDIS), with funding provided by NASA/HQ.

Financial support

This research has been supported by the Korea Institute of Ocean Science and Technology (grant no. PN67330), the Korea Polar Research Institute (grant no. PE18060), and the National Research Foundation of Korea (global PhD fellowship no. 2015032018).

`

Chapter 5

Changes in sedimentational environment since the last deglaciation in the western Amundsen Sea, Antarctica

In preparation

Highlights

- Gravity cores from distinct surface water condition are examined in Amundsen Sea.
- Sedimentation in the Holocene was higher in the polynya than in the sea ice zone.
- Amundsen Sea Polynya started to develop early on following the deglaciation.
- Diatom valve abundance was correlated with the Antarctic air temperatue anomaly.

`

Abstract

The Amundsen Sea Polynya (ASP) is highly productive and the fourth largest coastal polynya. Organic carbon accumulation rate for the last few thousand years in the ASP was reportedly about 20 times higher than in the perennial sea ice covered region. We examined three gravity cores to investigat whether this characteristics of organic carbon accumulation has persisted since the last deglaciation, with a focus on the timing of the ASP opening. Post glacial sedimentation rate was ~10 times higher in the central ASP than in the ice covered region near the shelf break. In the ASP region, geological and biogeochemical properties showed transition from glacial deposits of terrestrial organic matter to marine production at ~10 kyr cal BP. Since the deglaciation, marine productivity varied in relation with the change in the dominant plankton species and the Antarctic air temperature.

`

5.1. Introduction

The Antarctic polynyas, open water area surrounded by sea ice and land, are characterized with high primary production (PP) in austral summer (Arrigo and Van Dijken 2003; Smith and Barber, 2007) and consequently, are important sites for atmospheric CO_2 absorption (Arrigo et al., 2008). The Amundsen Sea Polynya (ASP) in the western Amundsen Sea is the most productive polynya around Antarctica (Arrigo and Van Dijken 2003; Arrigo et al., 2012; Mu et al., 2014). A few in situ measurements showed that the PP was very high (~2200±1400 mgC $m^{-2}d^{-1}$ in summer bloom; Lee et al., 2012) in the ASP compared with the perennial sea ice covered region where PP was much lower (Lee et al., 2012). These observations are consistent with the sedimentary organic carbon accumulation rates: the linear organic carbon accumulation rate was 1.2 $gCm^{-2}yr^{-1}$, during the period of 3.2~4.7 kyr BP (before present, uncorrected ^{14}C age) in the ASP, and was about 20 times higher than at a site near the shelf break (Kim et al., 2016). TOC (total organic carbon) accumulation in the ASP was estimated to account for ~90 % of the organic carbon burial in the western Amundsen Sea despite the small area, ~30 % (Kim et al., 2016). Sea ice concentration in the Amundsen Sea has been decreasing with the unknown future (Stammerjohn et al., 2012). Therefore, it is important to know the marine production and sediment accumulation since the last deglaciation, especially in terms of the starting time of the ASP opening.

Several studies investigated deglaciation and ice sheet/shelf movement in the Amundsen Sea embayment (Hillenbrand et al., 2003; Larter et al., 2014; Smith et al., 2014). Grounding line passed the shelf break at ~13.8 kyr cal BP and

`

approached the current location of the Dotson Ice Shelf at ~10 kyr cal BP (Kirshner et al., 2012). Deglacial melting of the ice shelves was associated with strong CDW (circumpolar deep water) inflow in the case of the inner Pine Island Bay (Hillenbrand et al., 2017). These studies mainly focused on the ice sheet/shelf retreat and pattern of deglaciation on the Amundsen Sea embayment since the last glacial maximum (Hillenbrand et al., 2013). In this paper we address the sedimentation change since the last deglaciation especially focusing on the following questions: (1) When did the ASP opening start and how did the sedimentation has changed with time? (2) How different were the sedimentational environment in the ASP and in the sea ice region?

`

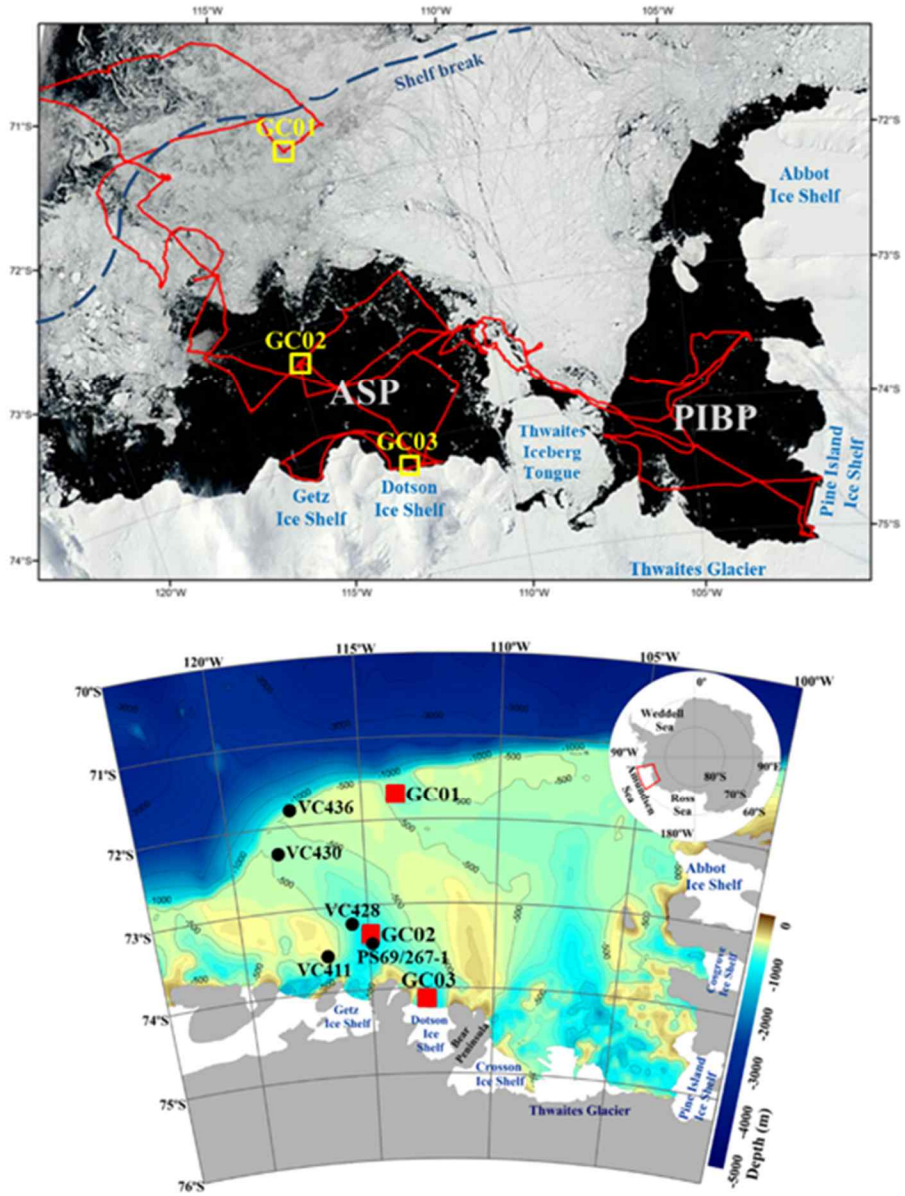

Figure 5.1. (a) Sampling locations (square) and the cruise track of 2011/12 Amundsen Cruise (red line) are shown. The satellite image showing the sea ice distribution was taken on 15 February 2012. The satellite image was obtained from rapid response imagery from the Land, Atmosphere Near real-time Capability for

`

EOS (LANCE) system, operated by the NASA's GSFC Earth Science Data and Information System (ESDIS). ASP and PIBP indicates Amundsen Sea Polynya and Pine Island Bay Polynya, respectively. The shelf break indicated as a dashed line. (b) Locations of other cores from Hillanbrand et al. (2010) and Smith et al. (2011) are also indicated on bathymetry map of the Amundsen Sea.

`

5.2. Materials and methods

Gravity core samples (12 cm diameter) were collected at three locations during a cruise aboard the IBRV Araon from January to March 2012. GC01 was in the perennial sea ice covered region near the shelf break (71.70 ºS, 114.04 ºW; 543 m bottom depth). GC02 was in the centrarl region of the ASP (73.23 ºS, 114.91 ºW; 802 m). GC03 was ~2 km north of the Dotson Ice Shelf (74.20 ºS, 112.52 ºW; 1080 m) inside the ASP (Figure 5.1). These gravity core stations are identical to the sites for which linear sedimentation rates based on box core samples were reported (Kim et al., 2016).

Details of core treatment and analyses for lithogenic and biogenic components of the sediment particles are reported elsewhere (Lee et al., 2010; Kim et al., 2018). Briefly, the cores were cut lengthwise and scanned with a multisensory core logger (Geotek Ltd.) after temperature equilibration overnight in a land-based laboratory. Element content (Br and Ti) of the core sediments was obtained by ITRAX, a multi-function X-ray core scanning system of bulk sediment samples. The samples were scanned from 3 to 50° 2q with a scan speed of 5° 2q per minute under Ni-filtered CuKa radiation. Magnetic susceptibility (MS) reading was made with a Bartington MS-2B susceptibility meter at 1cm interval. Subsamples of 1-cm-thick layer at 4-cm interval were analyzed for grain size distribution (Micrometrics Sedigraph 5000) and water content (Kim et al., 2018). Another set of 1-cm thick layers were subsampled with 2-cm interval for carbon and nitrogen analysis by using a Flash EA 1112 element analyser. $CaCO_3$ content was determine by total inorganic carbon content analyzed using a UIC 5030

`

coulometer. TOC content was determined as the difference between total and inorganic carbon contents. These analyses were performed at Korea Polar Research Institute (KOPRI).

A set of subsamples of 1-cm layer (from surface to 16 cm depth) or 2-cm layer (from 16 cm depth to the bottom) were used for analyses of radiocarbon isotope ratio and element content (Al, Ba and Zr). These subsamples were freeze dried, and sieved to remove ice rafted debris (>2 mm, Grobe, 1987) and stored in pre-baked (450 ºC for 4 hours) glass jars and kept frozen until analyses. Radiocarbon isotope ratio of sedimentary organic carbon was measured on a Mini Carbon Dating System (MICADAS) at the Laboratory for Ion Beam Physics at ETH Zürich (Christl et al., 2013; McIntyre et al., 2017). Each finely ground sediment sample was weighed in a silver cup, and fumigated with HCl vapor in a desiccator for three days at 70 ºC to remove inorganic carbon. The samples then fumigated with NaOH pellets at 70 ºC for over three days to remove HCl vapor. These samples were converted to CO_2 using an elemental analyzer aligned with the MICADAS.

For sterol analysis, about 2~30 g of each freeze dried and homogenized sample was extracted into dichloromethane:methanol (90:10 v:v) mixture using a microwave extraction system (MARS6 CEM Corporation; 100 ºC, 20 mins). An internal standard (1-nonadecanol, Sigma-Aldrich, 99 %) was added prior to analytical treatment for recovery check. Sterols were quantified by comparison to an external cholesterol standard (Sigma-Aldrich, ≥99 %). Total lipid fraction was separated into three fractions by silicagel column chromatography using hexane,

`

hexane:ethyl acetate (75:25 v:v), and methanol. The second fraction were silylated with bistrimethylsilyl-trifluoroacetamide (BSTFA) and pyridine at 70 ºC for 30 mins. Derivatized fraction were injected into an Agilent 7890A GC equipped with a capillary column (DB-1MS, 0.32 ID, 30 m length). Peaks were detected and quantified with a time of flight (TOF)-MS (70 eV constant ionization potential). The GC analysis was performed with the following temperature program: 40 ºC (1 min), 130 ºC (rate: 40 ºC/min), 320 ºC (rate: 10 ºC/min), 320 ºC (10 min). The injection volume was 1 μl with splitless mode. Individual sterols were identified based on their mass spectra and retention times.

Contents of selected metal elements (Al, Ba, and Zr) were analyzed using an ICP-AES (Optima 8300, PerkinElmer) at the Korea Basic Science Institute, with a relative standard deviation (RSD) of 2.8, 4.4, and 7.6 % for Al, Ba, and Zr respectively.

For diatom species identification and quantification, ~2 g of dry samples were heated to 100 °C with 25 ml of hydrogen peroxide (H_2O_2: 30%) and 25 ml of 10 % hydrochloric acid for one day to oxidize organic matter and dissolve the carbonates (Bak et al., 2018). Samples were washed 3 times with distilled water. Slides for quantitative analysis of diatoms were made using the random settling method of Scherer (1994). Diatom counts were conducted using a Nikon E400 microscope at 1000× magnification.

`

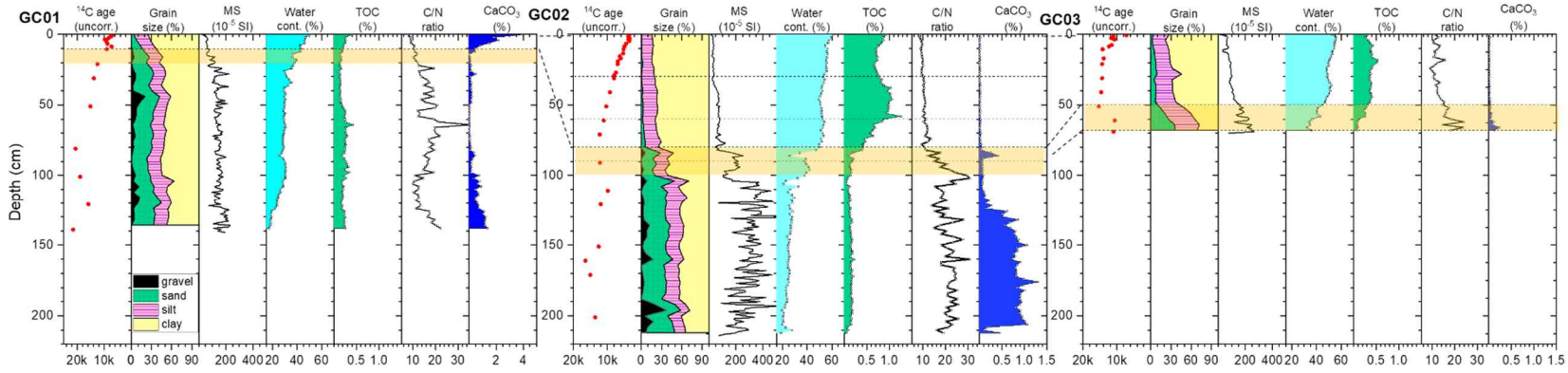

Figure 5.2. Vertical distribution of geological and biogeochemical properties: uncorrected ^{14}C age, grain size distribution, magnetic susceptibility (MS), water content (%), TOC (%), C/N molar ratio, and $CaCO_3$ (%) distribution at GC01, GC02 and GC03. Note that x-axis scales for $CaCO_3$ are different.

`

5.3. Results

The recovered core length at GC01, GC02, and GC03 was 141 cm, 214 cm, and 70 cm, respectively (Figure 5.2). The longest core, GC02, showed both open-marine (0~80 cm), glacial deposits (100~core bottom), and transition in between (80~100 cm). GC01 showed similar characteristics to GC02, but with a much shorter length for open-marine deposits (0~10 cm). In comparison, GC03 showed only open-marine (0~50 cm) and transition (50~core bottom). The open-marine deposits were characterized with high portions of clay, absence or very low content of gravels, low MS, high water content and relatively high TOC content, low C/N ratio. Glacial deposits were characterized with the matrix of diamicton containing >20 % of sand and gravel, low TOC content, high C/N ratio. At GC02, $CaCO_3$ content was low (<1 %) in the glacial deposit and was absent in the open marine deposit. At GC01, $CaCO_3$ content was >1 % (up to 4 %) in the open marine deposit.

Because GC02 shows the change from glacial to interglacial best and the down-core variation of GC01 and GC03 cores resembles that of GC02, characteristics of GC02 are described below in detail. A major down-core change in various properties occurred at ~80 cm. The lithology shifted from fine to coarse. The majority of sediment particles of the upper 80 cm layer were clay and silt (98 % on average), while below that, the portion of sand and gravel accounted for ~37 %. The MS values (<120, $\times 10^{-5}$) changed from low to much higher values (~273). The MS values were well correlated with the fractions of gravel and sand (Figure 5.2). Within the upper layer, perhaps TOC content (%) showed considerable variation. It decreased down-core from 0.9 % to 0.7 % (20 cm depth),

`

then increased to ~60 cm (1.3 %), then decreased rapidly from 60 to 80 cm (0.4 %). Another major change occurred at ~100 cm below which depth to the core-bottom, most properties were distinctly different from those in the upper 80cm layer. Water content (%) decreased from 50-61 % in the upper 80 cm layer to low values (~26 %) in the layer below 100 cm. C/N ratio was low and uniform in the upper 80 cm horizon and fluctuated around a high value (21 on average) in the layer below 100 cm. Between these two demarcations, lay the transition zone.

Sedimentological and biogeochemical properties of our cores were similar to the previously studied ones collected at nearby sites (Figure 5.1, Hillenbrand et al., 2010; Smith et al., 2011). VC436 core collected at shelf break (Smith et al., 2011) showed high CaCO3 content in the upper 10 cm layer (>1 %) above the transition facies. VC430 from the shelf break inside the Dotson trough also contains ~20 cm of sediment layer above the transition zone. PS69/267-1, collected inside the ASP (Smith et al., 2011) showed similar evolution in sedimentation from diamicton (below ~100 cm), transition (80~100 cm), to open marine deposit (0~80 cm). VC428 showed the open marine sediment in the upper 100 cm. Therefore, our cores appear to be representative of the sea ice covered regions and the ASP.

`

Table 5.1.

Fraction modern (Fm), uncorrected radiocarbon age (yrs BP), error (±yr), core-top age-corrected age in calendric age (cal BP) with error range. Core-top ages used for correction was 3860, 2930, and 4290 yrs for GC01, GC02, and GC03, respectively.

Core ID	Depth (cmbsf)	Fm	uncorrected ^{14}C age (yrs BP)	Error (±yr)	Calibrated yrs BP	Calendric Age cal BP
GC01	0.5	0.422	6921	101	3061	3329±176
GC01	1.5	0.393	7497	92	3637	4057±188
GC01	2.5	0.361	8352	104	4492	5174±209
GC01	3.5	0.296	9782	117	5922	6788±201
GC01	4.5	0.319	9180	101	5320	6124±162
GC01	6.5	0.336	8756	103	4896	5677±162
GC01	8.5	0.405	7268	103	3408	3750±191
GC01	10.5	0.326	9013	104	5153	5969±187
GC01	21	0.211	12481	126	8621	9711±248
GC01	31	0.179	13828	148	9968	11470±349
GC01	51	0.153	15098	153	11238	13111±228
GC01	81	0.077	20583	236	16723	20189±412
GC01	101	0.095	18870	171	15010	18232±288
GC01	121	0.139	15827	181	11967	13839±305
GC01	139	0.069	21505	211	17645	21322±420
GC02	0.5	0.640	3590	79	660	615±91
GC02	1.5	0.623	3803	83	873	817±117
GC02	2.5	0.650	3435	81	505	587±16
GC02	3.5	0.619	3849	86	919	854±127
GC02	4.5	0.647	3492	77	562	563±79
GC02	6.5	0.579	4395	88	1465	1416±130
GC02	8.5	0.537	4998	86	2068	2135±165
GC02	10.5	0.524	5185	96	2255	2344±203
GC02	13.5	0.514	5344	91	2414	2571±170
GC02	15.5	0.455	6319	93	3389	3727±171
GC02	17	0.470	6059	86	3129	3431±147
GC02	19	0.421	6944	104	4014	4574±199
GC02	21	0.421	6954	99	4024	4603±179
GC02	27	0.394	7475	96	4545	5302±184
GC02	29	0.372	7951	124	5021	5779±188
GC02	31	0.367	8049	106	5119	5880±190
GC02	41	0.317	9240	101	6310	7250±150
GC02	51	0.276	10336	122	7406	8269±172
GC02	61	0.251	11098	121	8168	9217±213
GC02	71	0.218	12246	127	9316	10610±245

`

GC02	91	0.220	12179	122	9249	10530±224
GC02	111	0.293	9872	105	6942	7807±148
GC02	121	0.226	11953	123	9023	10295±209
GC02	151	0.209	12566	141	9636	11005±243
GC02	161	0.128	16490	155	13560	16335±330
GC02	171	0.154	15045	220	12115	14048±500
GC02	201	0.184	13616	135	10686	12608±187
GC03	0.5	0.410	7161	98	2871	3091±190
GC03	1.5	0.254	11008	118	6718	7588±153
GC03	2.5	0.239	11623	125	7333	8196±183
GC03	3.5	0.262	10766	127	6476	7382±162
GC03	7.5	0.239	11511	139	7221	8079±201
GC03	8.5	0.217	12291	133	8001	8984±283
GC03	10.5	0.171	14171	159	9881	11383±363
GC03	17	0.178	13856	150	9566	10931±257
GC03	21	0.168	14339	164	10049	11577±407
GC03	31	0.168	14331	153	10041	11562±384
GC03	41	0.162	14614	154	10324	12171±397
GC03	51	0.149	15290	172	11000	12884±240
GC03	61	0.268	10587	120	6297	7236±186
GC03	69	0.257	10915	128	6625	7519±156

`

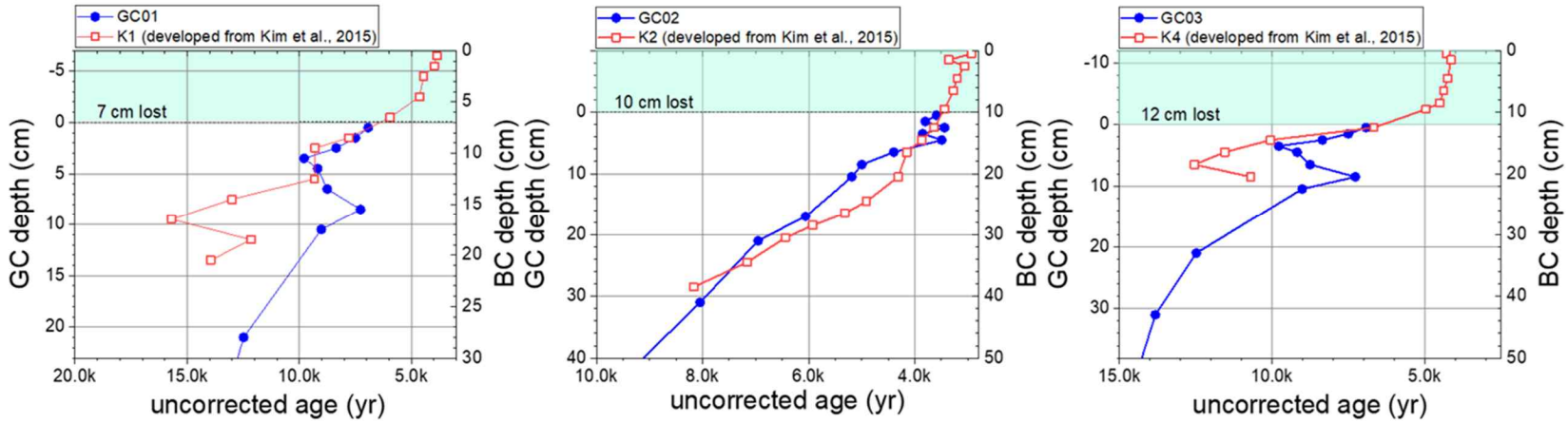

Figure 5.3. Comparison of apparent ^{14}C ages between the gravity cores and the corresponding box cores (Kim et al., 2016). Approximately 7, 10, and 12 cm of the top layers of the gravity cores appear to have been lost.

`

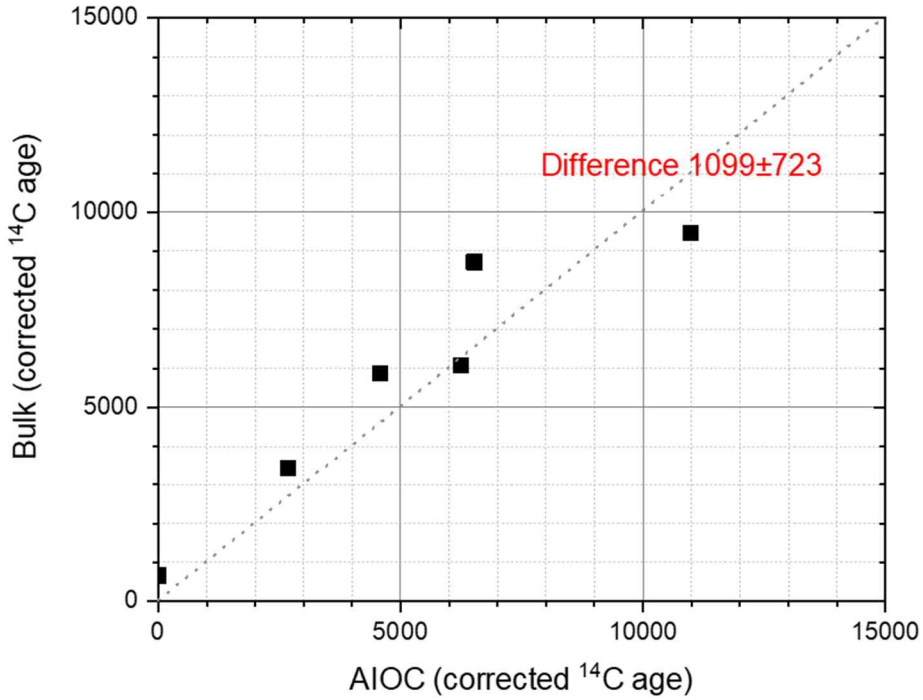

Figure 5.4. Comparison of our core-top corrected ^{14}C ages of bulk TOC with those of the acid-insoluble organic carbon (AIOC) of other cores from VC411 (15 cm), VC428 (38 and 65 cm), PS69/267-1 (0, 40, and 72 cm).

`

5.4. Discussion

Radiocarbon chronology

Chronology was obtained based on radiocarbon measurements of bulk TOC. At GC01, the ^{14}C ages decreased downcore from core top to 80 cm depth (from 6.9 and 20.6 kyr BP), and then age reversal was observed between 80 to 120 cm (from 20.6 to 15.8 kyr BP) (Figure 5.2, Table 5.1). At GC02, the ^{14}C ages the monotonically increased from 4 cm to 91 cm (3.5 to ~12 kyr BP). Age reversal was observed at 110 cm. At GC03, the ^{14}C ages were similar in the upper 1.5 to 7.5 cm layer (11±0.4 kyr BP, n=4), then decreased to 15.3 kyr BP. The 14C ages were almost constant from 10.5 cm to 51 cm layer (14±0.5 kyr BP, n=6) with a reversal at 61 cm depth.

Possibility of loss of the core-top of the gravity cores was examined by comparison of 14C ages to those of box cores, for which preservation of the core-top was visually confirmed (Kim et al., 2016). Based on this comparison, the top parts amounting to ~7, 10, and 12 cm of GC01, GC02, and GC03 appear to have been lost, respectively (Figure 5.3). We correct the observed ^{14}C ages by subtracting that of the core-top sediment of the corresponding box cores. Secondly, potential error in using ^{14}C ages of bulk TOC instead of acid-insoluble organic (AIO) fraction was considered. Bulk TOC can contain both freshly produced labile organic matter and potentially refractory, pre-aged AIO fraction (Hillenbrand et al., 2010, Subt et al., 2016). We compared our core-top value-corrected ^{14}C ages with those of the AIO fraction from cores collected at nearby stations (VC411, VC428, and PS69/267-1, Figure 5.1; Smith et al., 2011). For

`

comparison, we interpolated our results to match the depths. The values did not show any systematic difference (Figure 5.4). The average deviation from the 1:1 line was 1099±723 yrs (total 6 numbers were used). Our core-top corrected ^{14}C ages were converted to calendar years BP (cal BP, years before 1950) using CALIB 7.1 program (http://calib.org).

Difference in sedimentation between the perennial sea ice covered region and inside the ASP

Transition to glacial deposition occurred at depths 10~20 cm at GC01 (corresponding to 6~10 kyr cal BP), while it occurred at depths of 80~100 cm of core GC02 (corresponding to ~10.5 kyr cal BP; Figure 5.2). The timing for this transition is consistent with that of the grounding line retreat (Kirshner et al., 2012). Open marine sedimentation since the end of the transition would be 3.8 cm/kyr (0~10 cm layer) and 9.8 cm/kyr (10~90 cm layer) at GC01 and GC02, respectively, indicating that the two sites have been experiencing very different sedimentational environments (Figure 5.2).

Ultimately, sedimentation reflects the surface water condition. Marine C/N ratio, presence and absence of CaCO3 at GC01 and GC02, respectively, are consistent with the current observation of sinking particles (Kim et al., 2015, 2019). Therefore, the difference in the sediment accumulation rate caused by different marine biological productivity seems to have persisted since the ice shelf retreat. In addition, higher supply of lithogenic material in the ASP than in the sea

`

ice covered region (Kim et al., 2019) may at least partly have contributed to the observed difference in sedimentation rate.

Temporal variation in sedimentation in the ASP since the ice shelf retreat

High sedimentation rate at GC02 enables us to investigate temporal variation in the sedimentational environment. We divide the post glacial period into three stages: transition from glacial to open-marine sedimentation, initiation of marine production, and stable marine production similar to present state. Considering the surface loss of ~10 cm (Figure 5.3), we combined the top 10 cm of the box core with the gravity core and describe the depth as cmcd (centimeter composite depth, Figure 5.5).

Transition from glacial to open-marine sedimentation (110-90 cmcd)

Transition from glacial to open-marine sedimentation seems to have occurred at ~10.5 kyr cal BP. Sedimentation of coarse particles and ^{14}C age reversal was caused by ice shelf retreat process. All biology-related parameters especially extremely low diatom valve abundance indicates low marine production in this period.

Initiation of open-marine sedimentation (90-70 cmcd)

At ~90 cmcd (~10.5 kyr cal BP) abrupt increase in TOC content, Br/Ti, and diatom valve abundance occurred. In comparison, Ba/Al ratio and brassicasterol/OC increased gradually from 80 cmcd. Sedimentation in this period shows building up

`

of marine primary production. By the end of this period, present state of marine production in the ASP seems to have been achieved. Timing suggested for strong CDW intrusion onto the Pine Island Bay (Hillanbrand et al., 2017) overlaps with the transition period and beginning of this period.

Stable condition for high primary production similar to the present state in the ASP (70-0 cmcd)

High TOC content about twice that of GC01 at the corresponding depth horizons indicate that stable and high PP has persisted throughout this period. This period can be subdivided into two periods considering the TOC content, diatom valve abundance, and the sedimentation rate. The lower layer (70~40 cmcd) shows higher TOC content although sedimentation rate was higher than the upper layer (40~10 cmcd). Lower diatom valve abundance is somewhat puzzling. *Chaetoceros resting spores* (CRS) was dominantly observed only in this period. *Thalassiosira antarctica* was also mostly observed in this period (Figure 5.6).

Lower sedimentation rate was at least partly caused by reduced lateral supply of coarse particles. A proxy of current strength, Zr/Al ratio, decreased upcore in general (Figure 5.5) consistent with the decrease in the coarse particle content. Higher diatom valve abundance in the upper layer is consistent with higher brassicasterol/OC ratio. Sea ice species, *Eucampia antarctica, Fragilariopsis kerguelensis* and *Fragilariopsis curta*, were dominant diatom species in this period. Temporal variation of the diatom valve abundance was strongly correlated with the Antarctic air temperature anomaly obtained from Vostok, Dome F, and EPICA

`

Dome C (Marcott et al., 2013; Figure 5.7). The initiation of open-marine sedimentation corresponds with high temperature. The lower layer and upper layer respectively correspond to low and high temperature periods. *F. Kerguelensis* peaked at 20 and 70 cm in the early warm period (Figure 5.6). The cold period is associated with *Thalassiosira antarctica. Chaetoceros resting spores* also peaked in the cold period (Figure 5.6) pointing to less CDW intrusion (Hillanbrand et al., 2017). The ratio of *F. curta/F. kerguelensis* exhibited high values in the cold period. Diatom valve abundance was also lower in the cold period. These lines of information imply that the surface was more heavily populated with sea ice and the condition was adverse for diatom growth in the cold period. A peak of *F. kerguelensis* at ~20 cm implies an open water condition such as a polynya. At the same time, high abundance of *F. curta*, a sea ice proximal species, at 10~20 cm implies coexistence of sea ice. Overall, diatoms seem to have flourished in the warm periods then in the cold period. A puzzling result is high TOC content in the cold period despite the low productivity of diatoms. Flourishment of primary producers other than diatoms such as *phaeocystis* is a possibility. However, at present, *P. antarctica* dominate in the central polynya (Yang et al., 2016) while diatoms dominate sea ice covered region. Sediment trap studies also showed that opal flux was significantly lower in the ASP than in the sea ice covered region (Kim et al., 2019).

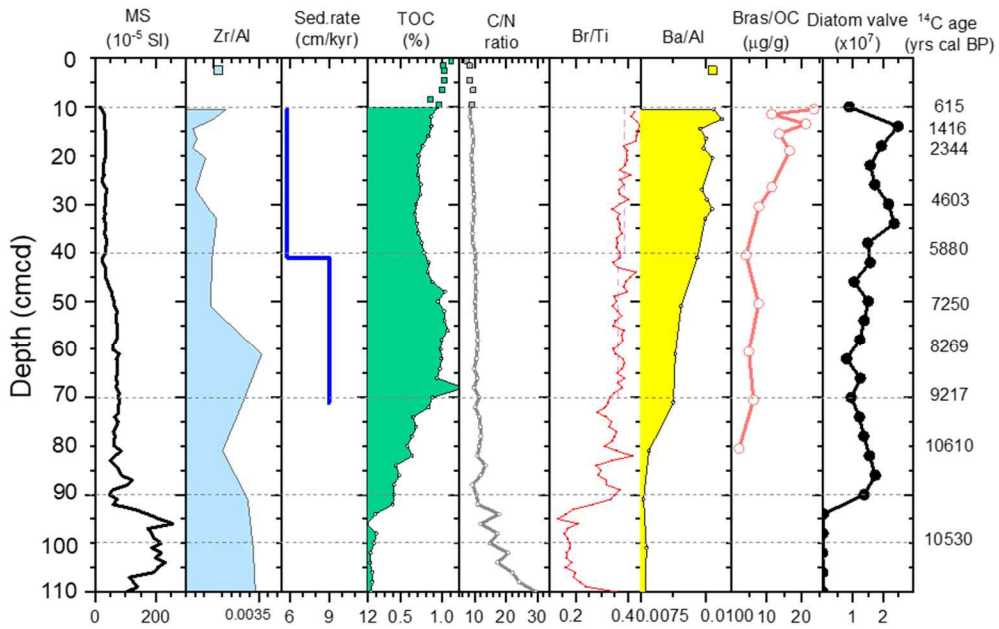

Figure 5.5. Vertical distributions of magnetic susceptibility (MS), Zr/Al ratio as a proxy for current strength, linear sedimentation rate (cm/kyr), TOC (%), C/N molar ratio, Br/Ti, Ba/Al, brassicasterol/OC, and diatom valve abundance in the GC02 core and the corresponding boxcore, against the cm composite depth (cmcd). Core-top-corrected ^{14}C age (yrs cal BP) are also presented.

`

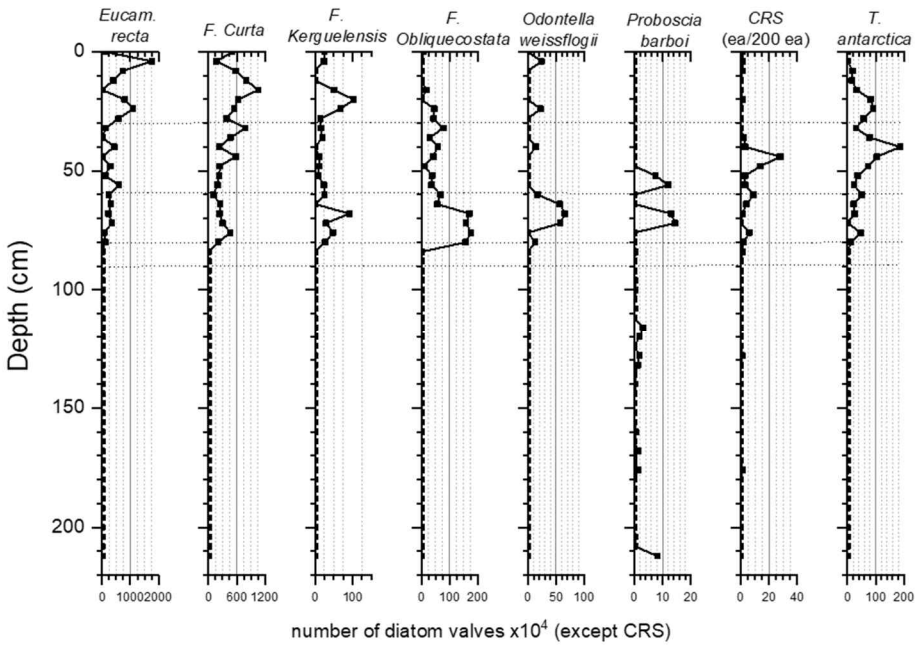

Figure 5.6. Valve abundances of selected diatom species at GC02. Note that the x-axis scales are different. *Chaetoceros resting spores (CRS)* are shown as the number of spores per 200 diatom specimens.

`

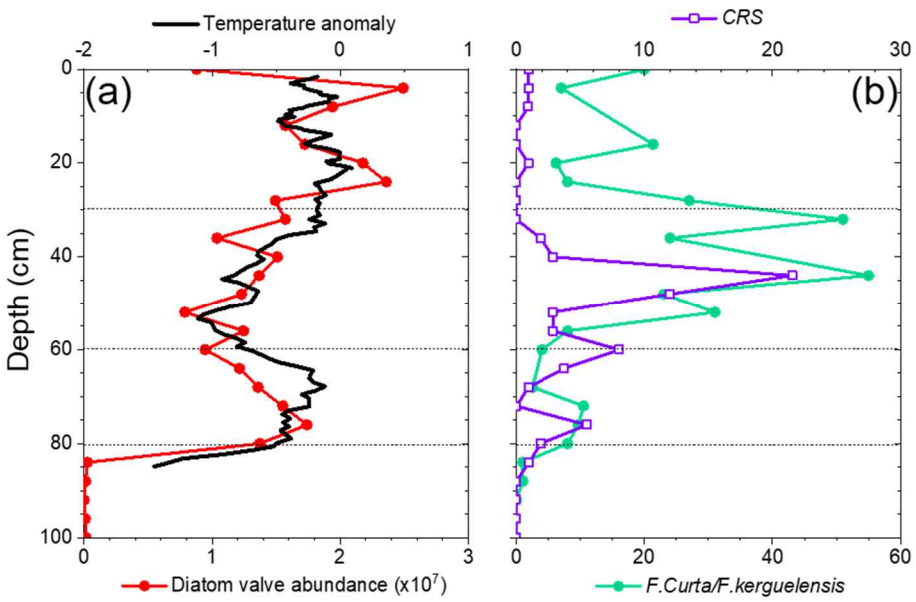

Figure 5.7. Vertical distribution of (a) diatom valve abundances (red line) and air temperature anomaly obtained from Vostok, Dome F, and EPICA Dome C (Marcott et al., 2013) and (b) *F. curta/F. kerguelensis* ratio and *CRS (Chaetoceros resting spores)* abundance at GC02.

`

5.5. Conclusions

We have examined sedimentology and productivity-related proxies in the gravity cores obtained from two different surface water conditions and biological productivity in the western Amundsen Sea. Also, detailed temporal variation of those proxies in the ASP core was investigated. Our results show that the sedimentational environment in the sea ice covered region and in the central ASP was very different since the last ice shelf retreat. The difference observed in primary production in two distinct regions observed in the present has persisted through the Holocene epoch. We suggest that the polynya-like condition for high marine productivity formed early on following the ice shelf retreat. A stable condition for high primary production seems to have persisted at least since 9.2 kyr cal BP. However, there was a significant difference consistently observed in several productivity proxies at least in two periods. Especially, diatom valve abundance was strongly correlated with the Antarctic air temperature anomaly implying that the biological productivity and primary producer communities were somehow related with the variability in the Antarctic climate. Exact processes that connect the biology and air temperature is a future research topic.

`

Acknowledgments

We thank Heung Soo Moon for help with gravity core sampling, staff at the Laboratory for Ion Beam Physics at ETH Zürich for carbon isotope analysis, and the captain and crew of the IBRV Araon for help at sea. This study made use of rapid response imagery from the Land, Atmosphere Near real-time Capa- 70 bility for EOS (LANCE) system, operated by the NASA's GSFC Earth Science Data and Information System (ESDIS), with funding provided by NASA/HQ. This research was supported by the Korea Polar Research Institute (PE 18060 and PE 19030). MK was partly supported by the National Research Foundation of Korea grant funded by the Korean Government (Global PhD fellowship 2015032018) and Young Researcher's Exchange Programme between Korea and Switzerland (NRF-2017K1A3A1A14092122).

`

Chapter 6

Organic carbon sequestration on the Amundsen Shelf: Insights from lipid biomarkers

`

Abstract

High resolution recent history of the sedimentary organic carbon (SOC) on the Amundsen Shelf has been examined. A series of sediment cores cover shelf break, Amundsen Sea Polynya (ASP), and in front of the Dotson Ice Shelf mainly following the right flank of Dotson trough (DT), also outside of DT. OC normalized brassicasterol, dinosterol, and cholesterol also examined. The SOC accumulation rate was similar to the previous study. At new stations at the edge of the ASP, but also outside the DT with shallower depths (~400 m) the SOC accumulation rate were low, might be affected by both low paleoproductivity and/or non-preferred depositional environment. Scattered ^{14}C values at timing of groundling line retreat. A sudden change in SOC accumulation rate observed ~4.7 kyr BP (uncorrected) in previous study also observed in nearby polynya stations. Even though the brassicasterol/OC was high in upper sediment, ratio of brassicasterol among brassicasterol, dinosterol, and cholesterol decreased after this change. This indicates the diatoms will not be a main driver of this increase of sediment accumulation rate.

Keywords: Amundsen Sea Polynya, Dotson trough, sedimentary organic carbon, radiocarbon, sterols

`

6.1. Introduction

Polynya is seasonally open water area surrounded by sea ice and/or land in the polar regions (Smith and Barber, 2007). Being a hot spot during a short periods of summer time, the role of polynya in carbon sequestration and as a food source is important (Arrigo and Van Dijken 2003). The Amundsen Sea Polynya (ASP), in the western Amundsen Sea is one of the most productive polynyas among the Antarctic coastal polynyas. Primary production (PP) and subsequent export of particulate organic carbon in the form of sinking particles, and the SOC (sedimentary organic carbon) accumulation in the most recent ASP (3.1 to 4.7 kyr) has been examined to characterize the biological pump system in this region (Lee et al., 2012; Ducklow et al., 2015; Kim et al., 2015, 2016). Temporally extended SOC study to investigated the history of the ASP has been conducted by using three representative gravity cores: shelf break, ASP, in front of the DIS (Dotson Ice Shelf) (Kim et al., in prep). Different sedimentation characteristics between perennial sea ice covered region and ASP recorded in sediment significantly.

Some differences in SOC accumulation rate and surface $\Delta^{14}C$ values were observed within the boxcore samples both collected inside the ASP (Kim et al., 2016). Ultimately sedimentation reflects the surface water conditions. In previous study, the SOC accumulation rate and surface $\Delta^{14}C$ values in the central ASP was slightly higher, and younger than the values at periphery of the ASP (Kim et al., 2016). Chlorophyll *a* concentration based on satellite observation (Arrigo et al., 2012; La et al., 2015) corresponded well with this spatial heterogeneity. Sediment cores have been collected by various locations on the Amundsen Shelf so far

`

(Smith et al., 2014). However, most of these studies mainly focusing on the ice sheet extent and shelf ice dynamics (Hillenbrand et al., 2010; Smith et al., 2011; Kirshner et al., 2012), and therefore, the characteristics of SOC in recent-past is lack of information. For further understanding of SOC cycling and sequestration on the Amundsen Shelf, spatial extension of high resolution study focusing on recent Holocene is necessary.

In addition to the surface water condition, SOC accumulation in shelf area is controlled by several factors such as potential inflow of ice rafted organic matter, sediment reworking because of physical forcing, bioturbation and so on according to the local geology conditions (Coffin et al., 2017). For example, it is known that the sediment deposition high preferentially accumulates on gentle slope and troughs (Mayer 1981). There could be some possibilities of erosion or lack of redeposited particles due to the bottom water current following the Dotson trough (DT) (i.e. circumpolar deep water inflow) on the Amundsen shelf.

We collected a series of sediment cores mainly following the right flank of DT, starts from the shelf break, elongated into the inner shelf basin including the ASP, to in front of the DIS (Figure 6.1), also outside of DT. OC normalized brassicasterol was a good indicator of paleo productivity on the ASP (Kim et al. in prep). Dinosterol, produced by dinoflagellates which are the major heterotropic mesozooplankton in the Amundsen Sea (Yang et al., 2016, 2018) and cholesterol also examined.

In this study, we address the spatially high-resolution characteristics of SOC together with diverse lipid biomarker indicators of marine phytoplankton in

`

recent Holocene. As one of the highly productive, rapidly changing, and persistently opening polynya among the Antarctic coastal polynyas (Criscitiello et al., 2013), understanding the carbon sequestration on the Amundsen Shelf is important as a biogeochemical standpoint, with implications for the Southern Ocean and the global environment.

`

6.2. Methods

Study region and sample collection

The Amundsen Shelf contains large amount of perennial sea ice and two coastal polynyas (Arrigo and van Dijken, 2003; Arrigo et al., 2012). ASP, exists in the western part of ridge opens ~27,000 km^2, adjacent to the DIS (Dotson Ice Shelf; Figure 6.1, Yager et al., 2012; Jenkins et al., 2018). Below the ASP, on the Amundsen shelf embayment, glacially carved DT exits. DT leads from the DIS to shelf break, with 17~39 m width, maximum 1400 m depth (Ha et al., 2014; Graham et al., 2016).

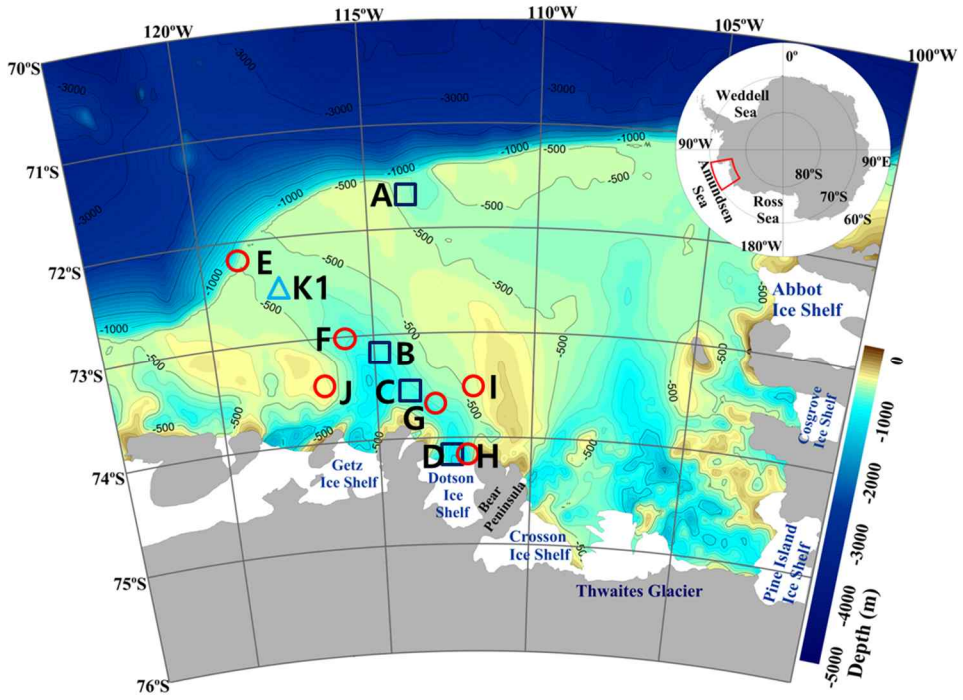

Figure 6.1. Sampling locations on the Amundsen Shelf. Squares (A~D), a triangle (K1), and circles (E~J) indicate different cruises (ANA02C, ANA04B, ad ANA06B), respectively.

`

Sediment samples were collected during three cruises aboard the IBRV *Araon*: four stations A, B, C, and D from January to March 2012 (Kim et al., 2016), one station K1 from December 2013 to January 2014, six stations E, F, G, H, I, and J from January to February 2016 (Figure 6.1, Table 6.1). All stations except A, I, and J was located along the DT. Station E and K1 are located at perennial sea ice zone near the shelf break following the DT. At station K1, the hydrographic mooring has been conducted since 2010 (Kim et al., 2015). Sediment sampling failed in 2012 cruise due to coarse sediment composition (Kim et al., 2016). Station F and G located in the seasonal ice zone and central polynya, respectively. Station H is in front of the DIS, close to the Bear Peninsula. Stations I and J are located at the boundary of the polynya, outside of the DT. Detailed information of the stations from A to D is in the previous paper (Kim et al., 2016). Simply Station A is located in the perennial sea ice zone near the shelf break and Station B and Station C are located at the periphery and center of the ASP, respectively. Station D is located approximated 2 km away from the DIS.

A box-core (Marine Tech. Korea) was used for sediment sampling. Upon detachment of the box-core canister, plastic barrels of 8 cm diameter and 60 cm length were gently pushed in for sub-cores. Each sub-core was sliced into 1 or 2 cm layers on board and stored in pre-baked (450 ºC for 4 hours) glass jars and kept frozen until analysis.

`

Sample analyses

In the laboratory, the frozen sediment samples were thawed and dried in an oven at 45 ºC prior to analyses for stations A to D (Kim et al., 2016). The other sediment samples were freeze-dried (Martin Christ Alpha 1-4 LD plus) and sieved. We separated the particles >2 mm which are presuppose as IRD (ice rafted debris), represents the iceberg activity (Grobe 1987). By using 2 mm sieve (Testing Sieve with wire dia. 0.9 mm, Stainless Steel), large size particles gently sieved, weighed, and stored separately (Grobe, 1987; personal communication with Lora Teitler). Particles smaller than 2 mm were used for the following analyses.

Grains except IRD separated into sand (2000~63 μm), silt (63~2 μm), and clay (<2 μm). Samples were mixed and shaken overnight with solution of Sodium polyphosphate (dispersing agents) and distilled water. This homogenized samples socked randomly and put into stirrer and then measured 4 to 5 times repeatedly after checking the background.

Radiocarbon content of sedimentary organic carbon was measured on a Mini Carbon Dating System (MICADAS) at the Laboratory for Ion Beam Physics at ETH Zürich (Christl et al., 2013; McIntyre et al., 2017). Prior to measurement, each sediment sample was finely ground, weighed in a silver cup, and fumigated with HCl vapor in a desiccator for three days at 70 ºC to remove inorganic carbon (Bao et al., 2016). The samples then fumigated with NaOH pellets at 70 ºC for over three days to remove HCl vapor.

For sterol analyses, about 2~30 g of freeze dried and homogenized sample was extracted into dichloromethol:methanol (90:10 v:v) mixture using a

`

microwave extraction system (MARS6 CEM Corporation; 100 ºC, 20 mins). About 20 % of total lipid extract was used for the GC-MS (gas chromatograph-mass spectrometry) analyses. An internal standard (1-nonadecanol. Aldrich, 99 %) was added prior to analytical treatment. Sterols were quantified by comparison to a Cholesterol external standard (Sigmagrade, ≥99 %). Total lipid fractions were silylated with bistrimethylsilyl-trifluoroacet-amide (BSTFA) and pyridine at 70 ºC for 30 mins. Derivatized total lipids were injected into an Agilent 7890A GC equipped with a capillary column (DB-1MS, 0.32 ID, 30 m length). Peaks were detected and quantified with a time of flight (TOF)-MS (70 eV constant ionization potential). The GC analyses were performed with the following temperature program: 40 ºC (1 min), 130 ºC (rate: 40 ºC/min), 320 ºC (rate: 10 ºC/min), 320 ºC (10 min). The injection volume was 1 µl with a splitless mode. Individual sterols were identified based on their mass spectra and retention times. Recovery efficiencies of the extraction process was obtained by addition of an internal standard.

`

6.3. Results

Radiocarbon age

High resolution radiocarbon values with depth obtained at seven locations (Figure 6.1; Table 6.1). $\Delta^{14}C$ values of the core-top sediment (0-1 cm) ranged from −311 to −549 ‰, the highest value was observed inside the polynya (St. B; Kim et al., 2016) and the lowest value outside the trough (St. J), respectively. The average $\Delta^{14}C$ values from the ice covered region and ASP (−334±14 ‰, *n*=6) were lower than the average from in front of the DIS, and outside of the DT (−422±74 ‰ in average, *n*=5). Surface sediment from shelf break (St. E) inside the DT was ~40 ‰ enriched than the one outside the DT (St. A).

Vertical radiocarbon age (^{14}C age hereafter) showed large spatial variations (Figure 6.2, Table 6.2). The ^{14}C age at St. E (shelf break) decreased linearly with increasing depth from surface down to 18.5 cm (20.5 kyr before present (BP)), and remained low ~19.5 kyr to bottom of core. At St. F (perennial sea ice zone), ^{14}C age were nearly constant from core-top to 10.5 cm depth. The ^{14}C age linearly changed with increasing depth until 18.5 cm. The ^{14}C age almost not changed below that. At St. G (inside the ASP), from core top to 16.5 cm depth (^{14}C age from 3.2 to 7.5 kyr) and from 16.5 to 36.5 cm depth (from 7.5 to 2.1 kyr), ^{14}C age linearly increased with increasing depth. At St. H (in front of the DIS), surface ^{14}C age was similar until 6.5 cm depth (4.1±0.2 kyr, *n*=5) and linearly shifted from 4.4 to 12.5 kyr below 8.5 cm. Stations I and J showed similar vertical sedimentation pattern. ^{14}C age rapidly decreased from 4.3 to 16.7 kyr (correspond

`

to 4.5~14.5 cm layer) at St. I and from 6.6 to 14.9 kyr (correspond to 4.5~10.5 cm layer) at St. J. Values below each depth were scattered.

SOC and biomarker content

SOC (%) in surface sediment ranged between 0.18 to 1.1 % (Table 6.1). Spatially, high SOC (%) observed inside the ASP, followed by the stations near the DIS, shelf break, outside the DT, and perennial sea ice zone. Sterols normalized to SOC were used in this study to eliminate any influence of sedimentation rate and/or sediment size as SOC and biomarkers intent to be absorbed by fine particles. In surface, brassicasterol, dinosterol, and cholesterol ranged from 8.6 to 279 μg/g SOC, 6.4 to 33 μg/g SOC, and 9.8 to 426 μg/g SOC, respectively. Spatially, the lowest and highest content for all sterols observed at St. E (shelf break) and G (ASP) except the lowest dinosterol content was observed at St. I. In general, dinosterol content shows opposite trend with OC % except core E.

`

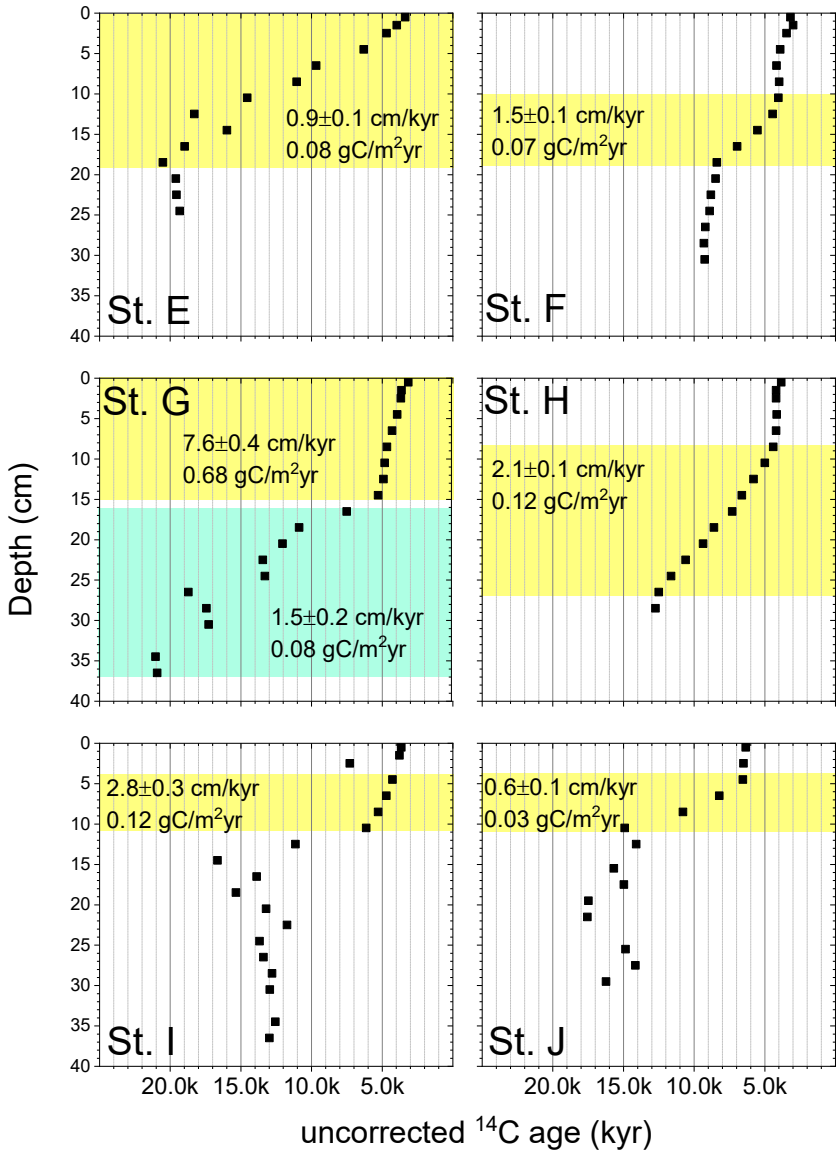

Figure 6.2. Vertical distribution of uncorrected ^{14}C age (kyr) in depth. Shaded layers denote the sediment horizons for linear sedimentation rate were determined.

`

At core E, SOC (%) decreased from 0.2 % to 0.05 % at upper 10.5 cm depth, and low value ≤0.1 % maintained below that. Except a shift at 4.5 cm depth, brassicasterol and dinosterol content were relatively low in upper layer (surface to 10 cm) while dinosterol showed no vertical differences. At core F, SOC (%) decreased from 0.4 to 0.2 % by increasing depth until 18.5 cm. The largest contents observed at core top sediment, and decreased according to depth from surface to 6.5 cm for all sterols. At core G, SOC (%) steadily decreased according to depth until 20.5 cm, and then stayed ~0.3 % until 34.5 cm depth except extremely low value (0.09 %) at 30.5 cm. Sterol contents are high at core top and decrease rapidly until 2.5 cm depth. Below ~6.5 cm, the contents stayed similar to core bottom. At core H, SOC (%) decreased from 0.59 to 0.31 % as increasing depth. The slope was changed in bioturbated layer. Sterols showed high values at upper 4.5 cm depths, and remained low at sediments deeper than 4.5 cm. At core I, SOC (%) decreased from 0.50 to 0.21 % as increasing depth from surface to 12.5 cm, then increased in depth to 36.5 cm (0.40 %). Content of brassicasterol and cholesterol decreased in depth until 6.5 cm, and stayed stable while dinosterol showed no vertical trend. At Core J, SOC (%) stayed same (0.44 %) at upper 4.5 cm depth, and gently decreased to 15.5 cm depth (0.3 %). Brassicasterol and cholesterol contents decreased in depth at upper ~7.5 cm and stayed low. Dinosterol has no vertical trend.

`

IRD and grain size

IRD (%) and relative grain size (sand, silt, and clay) in depth obtained at stations E, G, H, I, and J (Figure 6.3). In general, large size particles observed at shelf break and outside the DT. At core E, IRD content was high at core top (33 %) and below 20.5 cm (>10 %) depth. Sand content (%) was also high (46 %) in surface, and remained high (>20 %) throughout the core. At core G, IRD and sand content were both episodically increased at 16.5 cm and 30.5 cm. Sand maintained low (<10 %) at upper 12.5 cm, and slightly increased (<20 %) below 30.5 cm. At core H, sand (%) maintained <5 % and IRD mostly not existed in whole core. Silt and clay occupied 98 % of grain size in general. At cores I and J, few IRD (<10 %) with ~60 % of silt, sand (20 %) and clay (20 %) observed in whole core.

`

Table 6.1. SOC content (%), $\Delta^{14}C$ (‰) values of surface sediments (0-1cm) and linear sedimentation rates (LRS) with sedimentary organic carbon accumulation rates on the Amundsen Sea.

Station	Cruise ID	Location	Lat.(°)	Long. (°)	Water depth (m)	SOC (%)	$\Delta^{14}C$ (‰)	LSR (cm/kyr)	SOC accu. Rate (gC $m^{-2}yr^{-1}$)
A[1)]	ANA02C	Shelf break	71.70	114.04	543	0.49	−386	1.1±0.3	0.05
E	ANA06B	Shelf break	72.10	118.88	745	0.18	−348	0.9±0.1	0.08
K1	ANA04B	SIZ	72.39	117.71	514	0.40	−334		
F	ANA06B	SIZ	73.04	115.72	710	0.37	−332	1.5±0.1	0.07
B[1)]	ANA02C	Periphery polynya	73.23	114.91	802	1.1	−311	13±2	1.2
C[1)]	ANA02C	Inside polynya	73.62	113.80	777	0.80	−349	12±3	0.9
G	ANA06B	Inside polynya	73.82	113.05	788	0.25	−330	7.6±0.4	0.7
D[1)]	ANA02C	Near iceshelf	74.20	112.52	1080	0.58	−418	1.0±0.6	0.06
H	ANA06B	Near iceshelf	74.17	112.15	1034	0.59	−385	2.1±0.1	0.12
I	ANA06B	Outside DT (Eastern)	73.50	112	375	0.50	−370	2.8±0.3	0.12
J	ANA06B	Outside DT (Western)	73.50	116.50	420	0.44	−549	0.6±0.1	0.03

1) Values from Kim et al. (2016)

`

Table 6.2. Down core SOC content, radiocarbon age (uncorrected) of SOC, and plankton sterol biomarker data (μg/g OC). BS: Brassicasterol, DS: Dinosterol, CS: Cholesterol.

	K1 (SIZ, sediment trap location)					E (shelf break, SIZ)					F (SIZ)					G (Polynya)				
Depth (cm)	SOC (%)	^{14}C age (uncorr.)	BS	DS	CS	SOC (%)	^{14}C age (uncorr.)	BS	DS	CS	SOC (%)	^{14}C age (uncorr.)	BS	DS	CS	SOC (%)	^{14}C age (uncorr.)	BS	DS	CS
0-1	0.36	3204	22	10	28	0.18	3366	8.6	8.0	9.8	0.37	3175	41	14	50	0.25	3155	279	33	426
1-2	0.46	2897	14	12	17	0.20	3964	10	7.9	10	0.58	2994	27	6.1	36	0.61	3635	67	9.0	151
2-3						0.19	4693	28	5.1	79	0.43	3451	22	8.9	19	0.59	3678	15	6.6	12
4-5						0.13	6297	9.3	ND	9.5		3899				0.53	3934	17	6.7	33
6-7						0.15	9668	9.0	8.9	9.3	0.43	4162	6.8	5.5	6.0	0.53	4300	7.7	4.3	15
8-9	0.18	8436	17	17	17	0.09	11048	8.0	8.0	9.1	0.30	3982	17	8.5	10	0.46	4657	10	6.9	9.4
10-11	0.17	9212	24	ND	24	0.05	14552	21	ND	22	0.43	4030	16	11	11	0.49	4815	10	5.9	7.2
12-13						0.11	18297				0.35	4440	10	8.0	8.5	0.47	4908			
14-15						0.07	15982			19	0.21	5522	19	15	17	0.44	5279	8.0	4.9	7.3
16-17						0.10	18971				0.29	6953				0.39	7503	9.1	6.3	7.2
18-19						0.07	20514				0.21	8390	14	ND	14	0.33	10879			
20-21						0.09	19604	13	ND	13	0.26	8472	12	11	12	0.30	12049	10	8.0	8.7
22-23						0.07	19558				0.20	8819	18	15	15	0.29	13445			
24-25						0.06	19320	19	19	21	0.36	8894	11	8.4	9.2	0.31	13305	9.3	7.0	7.7
26-27											0.36	9207	14	9.5	10	0.29	18713	8.4	7.4	7.5
28-29											0.52	9304				0.25	17440			
30-31											0.53	9247	13	7.7	9.2	0.09	17282	ND	19	19
32-33																0.13				
34-35																0.33	21038	10	9.7	11
36-37																0.07	20923			

`

	H (near the DIS)					I (Beside DT)					J (Beside DT)					
Depth (cm)	SOC (%)	^{14}C age (uncorr.)	BS	DS	CS	SOC (%)	^{14}C age (uncorr.)	BS	DS	CS	Depth (cm)	SOC (%)	^{14}C age (uncorr.)	BS	DS	CS
0-1	0.59	3839	21	11	21	0.50	3645	30	6.4	41	0-1	0.44	6340	57	9.5	79
1-2	0.60	4191				0.50	3778	25	7.3	32	1-2					
2-3	0.57	4191	22	8.3	15	0.44	7291	15	5.6	21	2-3	0.44	6340	26	9.0	22
4-5	0.54	4154	7.7	3.7	5.5	0.39	4269	13	5.7	9.1	4-5	0.44	6551	22	7.3	22
6-7	0.53	4195				0.37	4704	8.7	5.0	6.4	6-7	0.40	8213	25	4.2	29
8-9	0.50	4403	6.4	3.9	4.9	0.33	5287	9.0	5.9	7.7	8-9	0.38	10794	16	6.5	10
10-11	0.44	4996	9.8	4.7	8.5	0.26	6120	11	7.3	11	10-11	0.34	14909	14	10	11
12-13	0.41	5790				0.21	11140				12-13		14090			
14-15	0.37	6614	6.1	5.7	6.0	0.25	16658	7.7	7.3	7.7	14-16	0.30	15673	12	7.3	8.4
16-17	0.34	7306	7.5	6.6	7.9		13878				17-18	0.33	14967			
18-19	0.31	8588				0.30	15340				19-20	0.36	17487			
20-21	0.31	9365	5.6	5.3	5.5	0.31	13205	6.9	4.8	5.7	21-22	0.36	17547	4.1	5.8	6.1
22-23	0.31	10593					11729				23-24					
24-25	0.31	11627	6.1	5.9	6.2	0.36	13680	7.6	4.6	5.0	25-26	0.30	14849	14	9.8	11
26-27	0.30	12498				0.33	13402	11	5.9	5.5	27-28	0.33	14153			
28-29	0.31	12729				0.34	12790				29-30	0.31	16233	7.7	4.4	5.4
30-31						0.33	12954									
32-33																
34-35						0.40	12560									
36-37						0.40	12985									

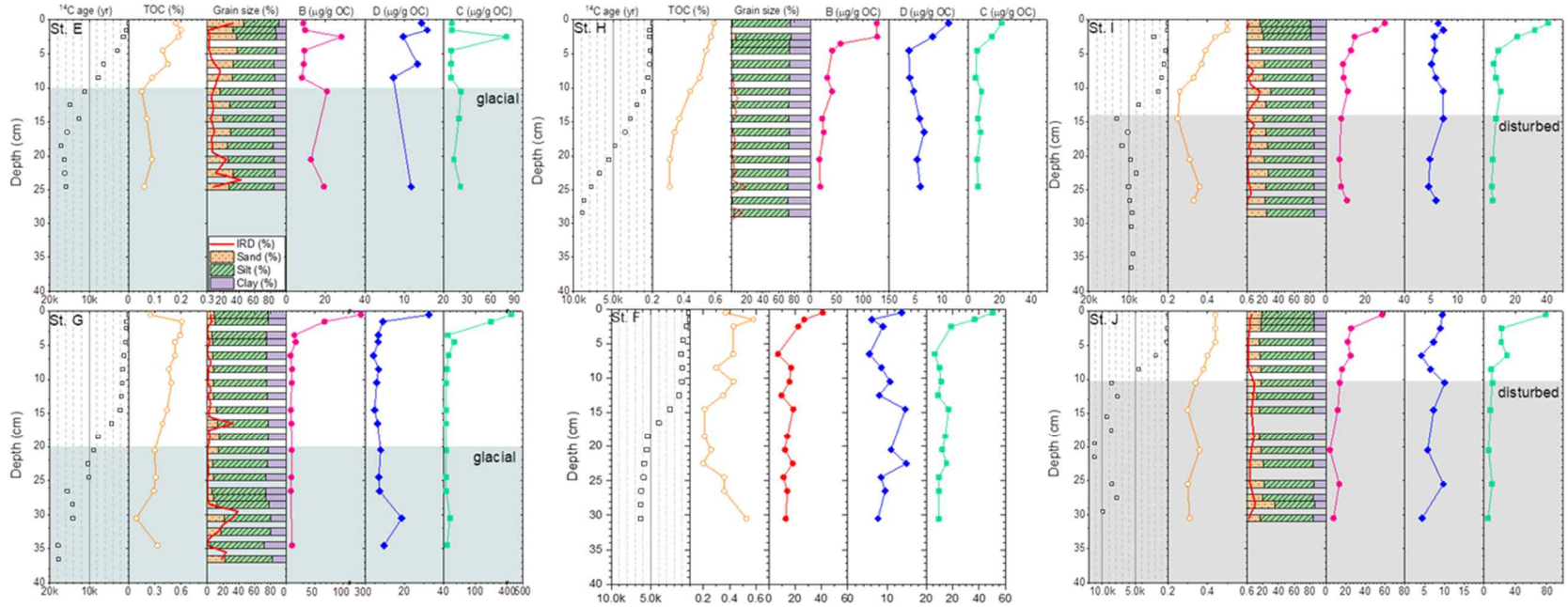

Figure 6.3. Vertical distribution of ^{14}C age (core-top corrected), grain size, and OC normalized sterol contents in depth.

`

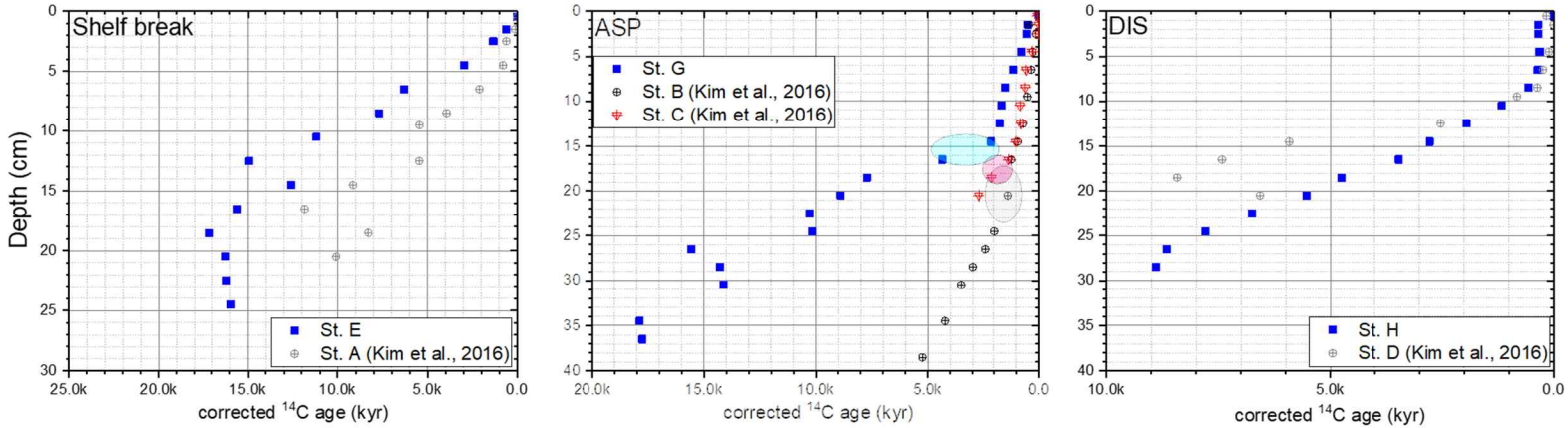

Figure 6.4. Vertical distribution of core-top corrected ^{14}C age (kyr) in depth at shelf break, ASP, and DIS, respectively. Open symbols are redrawn from Kim et al. (2016).

`

6.4. Discussion

Sedimentary organic carbon accumulation on the Amundsen Shelf

Linear sedimentation rate (LSR) were estimated from the slope of the linear regression line between the layers with linearly increasing ^{14}C ages in depth (Figure 6.2). Determined LSR were 0.9±0.1 (from 0.5 to 18.5 cm, *n*=11) at St. E, 1.5±0.1 (from 10.5 to 18.5 cm, *n*=5) at St. F, 7.6±0.4 (from 0.5 to 14.5 cm, *n*=9) at St. G, 2.1±0.1 (from 8.5 to 26.5 cm, *n*=10) at St. H, 2.8±0.3 (from 4.5 to 10.5 cm, *n*=4) at St. I, and 0.6±0.1 cm/kyr (from 4.5 to 10.5 cm, *n*=4) at St. J, respectively. The SOC accumulation rate in the sediment was calculated based on average water content, average SOC content, the LSR, and an estimated sediment density of 2.7±0.2 g/cm^3 (based on the clay mineralogy on the Amundsen Shelf, Ehrmann et al., 2011). Details in Kim et al. (2016). The SOC accumulation rate for stations. E, F, G, H, I, and J were 0.08, 0.07, 0.7, 0.12, 0.12, and 0.03 gC m^{-2}yr^{-1}, respectively (Figure 6.2). LSR and SOC accumulation rate at shelf break (St. E) was similar to the one (St. A) obtained in Kim et al. (2016) even though the location is ~190 km apart (Figure 6.1, Figure 6.4). However, the ^{14}C age in depth were distinctly different: St. E was relatively depleted. Both cores may experience similar sedimentation characteristics, but different sources would be supplied. Consistent LSR at shelf break indicates grounding line retreat (~13.8 kyr BP; Kirshner et al., 2012) and/or deglaciation did not strongly affect to the sedimentation characteristics in this location. Existence of deep bioturbation layer and SOC accumulation rate (~0.1 gC m^{-2}yr^{-1}) in the sea ice zone was similar to in front of the DIS (Figure 6.2, Figure 6.4). SOC accumulation rate inside the ASP (St. G; 0.7 gC

`

$m^{-2}yr^{-1}$) was slightly smaller, but similar to the values obtained by previous studies (1.2 and 0.9 gC $m^{-2}yr^{-1}$; Kim et al., 2016).

The SOC accumulation rate at Stations I and J (0.12 and 0.03 gC $m^{-2}yr^{-1}$) were similar to the non-polynya stations. Station I and J are at the edge of the ASP, but also outside the DT with shallower depths (~400 m), might be affected by both low paleoproductivity and/or non-preferred depositional environment. Scattered ^{14}C values at depths below ~10 cm matches with the timing of groundling line retreat. It is likely the organic carbon sequestration on the Amundsen Shelf is more limited and regional scale even within the boundary of the polynya. In the following session, we investigated the SOC characteristics on the ASP on fine scale with various environmental settings.

Environmental conditions affect to SOC acc. rate

Amundsen Sea embayment contains three 1000-1600 m deep tributary troughs extend seawards from the modern ice shelf fronts, eventually merging into a single cross shelf trough approximately 65 km wide and 600 m deep. Grain size at station G (inside the DT) is significantly different to stations I, and J (Figure 6.4, outside DT). Average sand content (%) within the upper 12.5 cm layer was 8 % at core G while it is 22 and 17 at stations I and J. Average clay content at core G was 24 % while 16 and 18 % at stations I and J.

Variation of relative contribution of planktons

Sedimentation rates were commonly changed at 2100~2400 (core top corrected ^{14}C age) BP at stations B, C, and G located inside the polynya. The shift was also

`

observed in station K2 and K3 in Kim et al. (2016), and upper part (10 cm of the GC02; Kim et al., in prep.) of the gravity core. In this study we investigated the factors affect to this shift in high spatial and temporal resolutions.

Two phytoplankton communities *P. antarctica* (*Phaeocystis Antarctica*) and diatoms are dominant while the majority of plankton biomass was spatially different in the Amundsen Sea (Yang et al., 2016). Heterotrophic dinoflagellates are the major mesozooplankton in the Amundsen Sea (Yang et al., 2018). Abundance of dinoflagellates is low in front of the DIS, high inside the polynya (Lee et al., 2016). Because of the hardness of seeking siliceous frustules due to the bad preservation of diatoms in sediment (YS Bak, personal communications), stable and well preserved biomarker proxies derived by plankton species have been investigated. Dinosterol is a specific biomarker for dinoflagellates and almost exclusive produced by dinoflagellates (Volkman, 1986). Brassicasterol used here as a biomarker for diatoms. But it also found in other microalgae, such as haptophytes and cryptophytes (Volkman et al., 1998). Cholesterol is the biomarker for the eukaryotic marine community produced by some algae, but also related to zooplankton (Volkman, 1986; 2003).

`

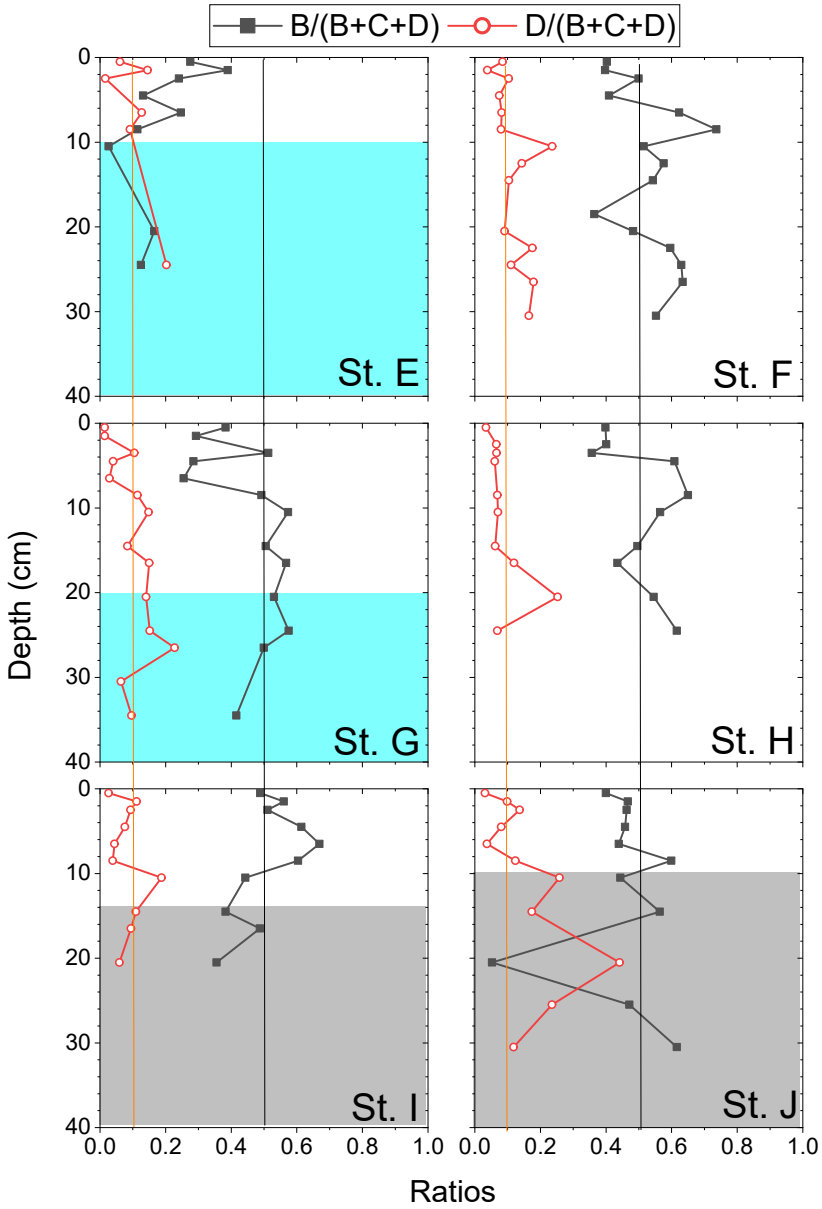

Figure 6.5. The variations of brassicasterol/(brassicasterol+cholesterol+dinosterol) and dinosterol/(brassicasterol+cholesterol+dinosterol) ratio in each cores.

`

Acknowledgements

We thank the captain and the crew of the IBRV *Araon* for help at sea; Prof. Nathalie Dubois and Pascal Rünzi for ^{210}Pb analyses; Dr. Thomas Blattmann and clay lab members at ETH Zürich for the clay mineralogy; Baozhi Lin for the grain size analyses. MK was partially supported by Korean Government (Global PhD fellowship 2015032018) and Young Researcher's Exchange Program Between Korea and Switzerland (2017K1A3A1A14092122). This research was supported by the Korea Polar Research Institute (PE 18060).

`

Chapter 7. Summary and future research directions

The Southern Ocean, and the polynyas are one of the regions affected by climate changes the most rapidly and significantly. This dissertation explored the present and past carbon cycling and its integrated response to climate change on the Amundsen Sea, Antarctica through multi-dimensional and multi-disciplinary scales and levels.

In Chapter 3, "*How different characteristics of sinking particles appeared in the various sea surface conditions on the Amundsen shelf by using spatially and temporally extended sediment trap materials and what kinds of environmental conditions drive this differences*?" were attempted to be resolved. Majority of sinking particles in the perennial sea ice zone during summertime was opal. This is represented as high opal content (%) and amount of ice diatoms. On the other hand, contribution of lithogenic materials were significant among the particles collected inside the ASP and in front of the Dotson Ice Shelf. Fecal pellets are the dominant material contributing to sinking particles. Spatially, the POC flux in the perennial ice-covered area is high and similar to the central ASP. Temporally, interannual variability in the summertime POC flux was large in the perennial ice-covered area, with the reduction in sea ice cover and sufficient insolation being critical to enhanced sinking POC flux.

In Chapter 4, the questions "*How the mysterious marine benthic organisms collected in sediment traps and what would be the plausible mechanisms of their transport? What will be the implications of this finding?"* were attempted

`

to be resolved. I investigated potential mechanisms for transport and release of these organisms. The collection of these organisms predominantly during the austral winter, and their intact bodies, suggest that they were trapped in anchor ice, incorporated into the overlying sea ice, and subsequently transported by ice rafting. The observations imply that anchor ice forms episodically in the Amundsen Sea and has impacts on Antarctic biology, as a disturbance to benthic ecosystems, a dispersal mechanism for benthic invertebrates, and an energy supply to the deeper benthic ecosystems.

In Chapter 5, with sediment samples collected by gravity core, "*After deglaciation, when did the ASP start to develop? And how were these record by various biogeochemical and lithological proxy in sediment? How different environment conditions are recorded in each different gravity core sediment?*" were attempted to be resolved. I obtained high resolution radiocarbon age in depth for three gravity cores. After the deglaciation ~10.5 kyr cal BP, the ASP is likely to be initiated. MS, grain size, TOC (%) and diatom valve abundances all drastically shifted in this layer. In 9~6 kyr cal BP, there exists another shift in biogeochemical compositions: high TOC (%), high productivity, but low diatom valve abundance. The layer proposed as the plausible timing of shift in dominant phytoplankton. Different sedimentation characteristics on the Amundsen Shelf after the deglaciation signal was also investigated. Shelf break and ASP are exposed at distinctively different environment and this represented as biogeochemical compositions and length of sediment layer.

`

In Chapter 6, by sediment samples collected by boxcore "*What are the major sources and controlling factors of OC reaching the sea floor? Do multiple biomarker proxies indicate different plankton communities denote surface water productivity? What controls the OC sequestration on the Amundsen Shelf most at different locations?*" were attempted to be resolved. The preservation and sequestration of SOC were explained focusing on spatial variation of radiocarbon and sterol biomarker according to characteristic surface primary productivity, sea ice concentration, and topography. Sediment accumulation characteristics are not homogeneous inside the ASP and the cause for the heterogeneous nature was tried to be explained by different productivity based on satellite PP observation and topography.

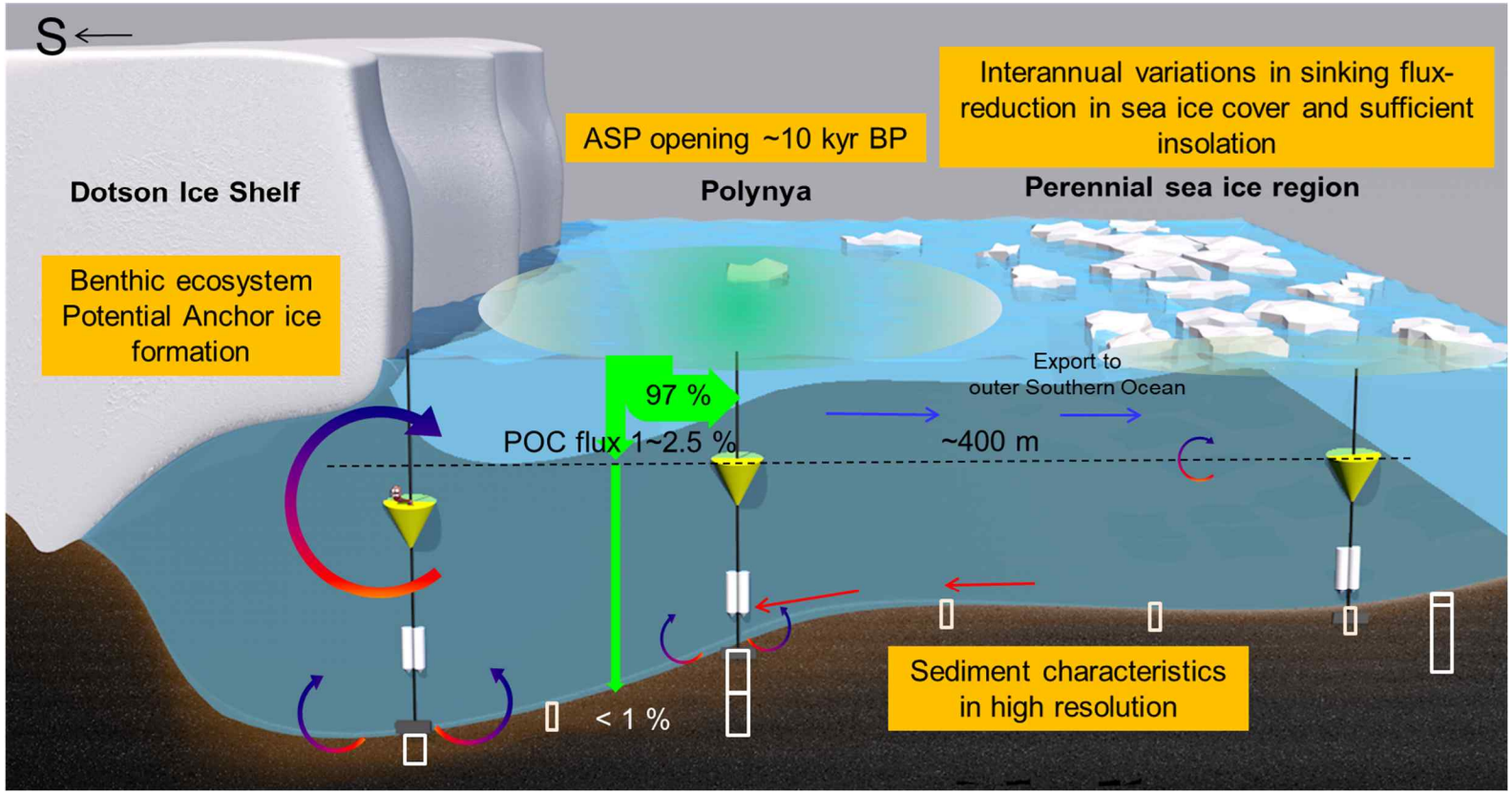

Figure 7.1. Synthesis cartoon of the organic carbon cycling in the Amundsen Sea.

`

Through the several years of sediment trap deployment on the Amundsen Shelf, it was revealed that the timely decreasing sea ice concentration, sunlight, proper input of nutrients is all important for a summer primary production bloom. Long-term sediment trap study is necessary in this region to better understand the interannual variations of sinking particles and the physical and biological controlling factors. Especially perennial sea ice zone occupies a large portion around the Antarctic, 3~20 million km^2 with seasonal variation. Sinking particle flux and compositions together with sea ice concentration in various oceanic settings around the Antarctic need to be investigated to better understand the biological pump operation in the changing Antarctic regions.

Intensive studies on utilizing various biomarkers in this region is also necessary, especially related to the specific plankton species. As the coverage of sea ice is the critical environmental factor controlling the PP and sinking particle flux in this region, comprehensive study on sea ice diatoms will be necessary. Because of the hardness of seeking siliceous frustules due to the bad preservation of diatoms in sediment on the Amundsen Sea, plankton species specific biomarker study is essential.

Another unresolved question is how to distinguish resuspended SOC and the setting OC with ice rafted particles. Not likely the marine system in low and mid latitudes, the particles transported by sea ice is another important source of OC in high latitude regions. It is not clearly defined how much organic materials are transported and how old their ^{14}C age are. Multidisciplinary geological approach, isotopic analyses, and satellite observation is necessary to understand and track the

`

effect of ice rafted particles. This will provide one case represent the high latitude region to characterize and understand the contribution of resuspended and ice rafted particles to sinking particles and the ocean carbon cycling.

`

References

Andrews, J. T. 2000. Icebergs and iceberg rafted detritus (IRD) in the North Atlantic: Facts and assumptions, Oceanography, 13, 3, 100-108.

Arrigo, K. R., van Dijken, G. L., 2003. Phytoplankton dynamics within 37 Antarctic coastal polynya systems. J. Geophys. Res., 108, 27-21.

Arrigo, K. R., van Dijken, G. L. and Long, M. 2008. Coastal Southern Ocean: A strong anthropogenic CO_2 sink. Geophys. Res. Lett., 35. https://doi.org/10.1029/2008GL035624.

Arrigo, K. R., Alderkamp, A.-C., 2012. Shedding dynamic light on Fe limitation (DynaLiFe). Deep-Sea Res. II., 71, 1-4. https://doi.org/10.1016/j.dsr2.2012.03.004.

Arrigo, K. R., Lowry, K. E., van Dijken, G. L., 2012. Annual changes in sea ice and phytoplankton in polynyas of the Amundsen Sea, Antarctica. Deep-Sea Res. II., 71-76, 5-15. https://doi.org/10.1016/j.dsr2.2012.03.006.

Asper, V. L., Smith Jr, W. O., 1999. Particle fluxes during austral spring and summer in the southern Ross Sea, Antarctica. J. Geophys. Res., 104, 5345-5359.

Assmann, K. M., Hellmer, H. H., and Jacobs S. S., 2005. Amundsen Sea ice production and transport, J. Geophys. Res., 110(C12). C12013. https://doi.org/10.1029/2004JC002797.

Bak, Y.-S., Yoo, K.-C., Lee, J. I. and Yoon, H. I., 2018. Glacial–interglacial records from sediments in Powell Basin, Antarctica. Antarct. Sci., 30(6): 371-378. https://doi.org/10.1017/S0954102018000408.

`

Bao, R., McIntyre, C., Zhao, M., Zhu, C., Kao, S.-J. and Eglinton, T. I., 2016. Widespread dispersal and aging of organic carbon in shallow marginal seas. Geology, 44(10): 791-794. https://doi.org/10.1130/G37948.1.

Barnes, D. K., 1999. The influence of ice on polar nearshore benthos, J. Mar. Biolog. Assoc. U.K., 79(3), 401-407. https://doi.org/10.1017/ S0025315498000514.

Barnes, D. K., and Souster, T., 2011. Reduced survival of Antarctic benthos linked to climate-induced iceberg scouring, Nat. Clim. Chang., 1(7), 365-368. https://doi.org/10.1038/nclimate1232.

Barrera-Oro, E., and Casaux R. J., 1990. Feeding selectivity in Notothenia neglecta, Nybelin, from Potter Cove, South Shetland Islands, Antarctica, Antarct. Sci., 2(3), 207-213. https://doi.org/10.1017/S0954102090000281.

Behrenfeld, M. J. and Falkowski, P. G., 1997. Photosynthetic rates derived from satellite-based chlorophyll concentration. Limnol. Oceanogr. 42, 1-20.

Berelson, W. M., 2001. The flux of particulate organic carbon into the ocean interior: A comparison of four US JGOFS regional studies. Oceanogr. 14, 59-67.

Blattmann, T. M., 2018. Topics on radiocarbon geochemistry and organic matter-mineral interactions, PhD. Thesis, ETH No. 25508, ETH Zürich.

Birgel, D., and Hass, H. C., 2004. Oceanic and atmospheric variations during the last deglaciation in the Fram Strait (Arctic Ocean): A coupled high-resolution organic geochemical and sedimentological study, Quat. Sci. Rev. 23, 29-47.

Bish D. L. and Plötze M. 2010. X-ray powder diffraction with emphasis on qualitative and quantitative analysis in industrial mineralogy. Christidis GE (eds), EMU Notes Mineral 9: 35–76.

`

Broecker, W.S., and Olson, E.A., 1959. Lamont radiocarbon measurements VI. Am. J. Sci., 1, 111-132.

Brunauer, S., 1938. Adsorption of gases in multimolecular layers. J. Am. Chem. Soc., 60, 309–319.

Buesseler, K. O., Antia, A. N., Chen, M., Fowler, S. W., Gardner, W. D., Gustafsson, O., Harada, K., Michaels, A. F., van der Loeff, M. R., Sarin, M., Steinberg, D. K., Trull, T., 2007. An assessment of the use of sediment traps for estimating upper ocean particle fluxes. J. Mar. Res. 65, 345-416.

Buesseler, K. O., McDonnell, A. M. P., Schofield, O. M. E., Steinberg, D. K., Ducklow, H. W., 2010. High particle export over the continental shelf of the west Antarctic Peninsula. Geophys. Res. Letters 37, L22606.

Criscitiello, A. S., Das, S. B., Evans, M. J., Frey, K. E., Conway, H., Joughin, I., Medley, B. and Steig, E. J., 2013. Ice sheet record of recent sea ice behavior and polynya variability in the Amundsen Sea, West Antarctica. J. Geophys. Res.118(1): 118-130. https://doi.org/10.1016/j.pocean.2018.12.003.

Christl, M., Vockenhuber, C., Kubik, P. W., Wacker, L., Lachner, J., Alfimov, V., Synal, H.-A., 2013. The ETH Zürich AMS facilities: Performance parameters and reference materials. Nucl. Instrum. Methods Phys. Res. 294: 29-38. https://doi.org/10.1016/j.nimb.2012.03.004.

Clarke, A., and Prothero-Thomas E., 1997. The influence of feeding on oxygen consumption and nitrogen excretion in the Antarctic nemertean Parborlasia corrugatus, Physiol. Zool., 70(6), 639-649. https://doi.org/10.1086/515868.

`

Collier, R., Dymond, J., Honjo, S., Manganini, S., Francois, R., Dunbar, R., 2000. The vertical flux of biogenic and lithogenic material in the Ross Sea: moored sediment trap observations 1996–1998. Deep-Sea Res. II 47, 3491-3520.

Cornet-Barthaux, V., Armand, L., Quéguiner, B., 2007. Biovolume and biomass estimates of key diatoms in the Southern Ocean. Aquat. Microb. Ecol. 48, 295-308.

Dayton, P. K., Robilliard, G. A., and Devries A. L., 1969. Anchor ice formation in McMurdo Sound, Antarctica, and its biological effects, Science, 163(3864), 273-274. https://doi.org/10.1126/science.163.3864.273.

DeMaster, D. J., 1981. The supply and accumulation of silica in the marine environment. Geochim. Cosmochim. Ac. 45, 1715-1732.

Denny, M., Dorgan, K. M., Evangelista, D., Hettinger, A., Leichter, J., Ruder, W. C., and Tuval, I., 2011. Anchor Ice and Benthic Disturbance in Shallow Antarctic Waters: Interspecific Variation in Initiation and Propagation of Ice Crystals, Biol. Bull. 221, 155-163. https://doi.org/10.1086/BBLv221n2p155.

Doebelin, N. and Kleeberg, R. 2015. Profex: a graphical user interface for the Rietveld refinement program BGMN. J. Appl. Crystallogr., 48, 1573-1580.

Ducklow, H. W., Wilson, S. E., Post, A. F., Stammerjohn, S. E., Erickson, M., Lee, S., Lowry, K. E., Sherrell, R. M., Yager, P. L., 2015. Particle flux on the continental shelf in the Amundsen Sea Polynya and Western Antarctic Peninsula. Elementa 3, 000046.

`

Dunbar, R. B., Leventer, A. R., and Mucciarone, D. A., 1998. Water column sediment fluxes in the Ross Sea, Antarctica: Atmospheric and sea ice forcing. J. Geophys. Res. 103, 30741-30759.

Dutrieux, P., Rydt, J. D., Jenkins, A., Holland, P. R., Ha, H. K., Lee, S. H., Steig, E. J., Ding, Q., Abrahamsen, E. P., and Schoroder, M., 2014. Strong sensitivity of Pine Island Ice-Shelf melting to climate variability. Science 343, 174-178.

Ehrmann, W., Hillenbrand, C.-D., Smith, J. A., Graham, A. G., Kuhn, G. and Larter, R. D., 2011. Provenance changes between recent and glacial-time sediments in the Amundsen Sea embayment, West Antarctica: clay mineral assemblage evidence. Antarct. Sci. 23(5): 471-486.

Garrity, C., Ramseier, R., Peinert, R., Kern, S., Fischer, G., 2005. Water column particulate organic carbon modeled fluxes in the ice-frequented Southern Ocean. J. Mar. Syst. 56, 133-149.

Grobe, H. J. P., 1987. A simple method for the determination of ice-rafted debris in sediment cores. Polarforschung, 57(3): 123-126. hdl:10013/epic.11658.d001.

Graham, A. G., Nitsche, F. O., Larter, R. D. and Gohl, K., 2016. Submarine landform assemblage produced beneath the Dotson–Getz palaeo-ice stream, West Antarctica. Geological Society, London, Memoirs,46(1): 345-348. https://doi.org/10.1144/M46.176.

Gutt, J. 2001. On the direct impact of ice on marine benthic communities, a review, Polar Biol. 24(8), 553-564. https://doi.org/10.1007/s003000100262.

`

Ha, H. K., Wåhlin, A. K., Kim, T. W., H., L. S., Lee, J. H., Lee, H. J., Hong, C. S., Arneborg, L., Bjork, G., Kalen, O., 2014. Circulation and modification of warm deep water on the central Amundsen Shelf. J. Phys. Oceanogr. 44, 1493-1501.

Hedges, J. I., and Stern, J. H., 1984. Carbon and nitrogen determinations of carbonate-containing solids. Limnol. Oceanogr. 29, 657-663.

Heine, J., McClintock, J., Slattery, M., and Weston J., 1991. Energetic composition, biomass, and chemical defense in the common Antarctic nemertean Parborlasia corrugatus McIntosh, J. Exp. Mar. Biol. Ecol., 153(1), 15-25. https://doi.org/10.1016/S0022-0981(05)80003-6.

Hillenbrand, C. D., Grobe, H., Diekmann, B., Kuhn, G., Fütterer, D. K., 2003. Distribution of clay minerals and proxies for productivity in surface sediments of the Bellingshausen and Amundsen seas (West Antarctica)–Relation to modern environmental conditions. Mar. Geol. 193, 253-271. https://doi.org/ 10.1016/S0025-3227(02)00659-X.

Hillenbrand, C. D., Smith, J. A., Kuhn, G., Esper, O., Gersonde, R., Larter, R. D., Maher, B., Moreton, S. G., Shimmield, T. M., and Korte, M., 2010. Age assignment of a diatomaceous ooze deposited in the western Amundsen Sea Embayment after the Last Glacial Maximum. J. Quat. Sci., 25(3): 280-295. https://doi.org/10.1002/jqs.1308.

Hillenbrand, C. D., Kuhn, G., Smith, J. A., Gohl, K., Graham, A. G. C., Larter, R. D., Klages, J. P., Downey, R., Moreton, S. G., Forwick R., and Vaughan, D. G., 2013. Grounding-line retreat of the West Antarctic Ice Sheet from inner Pine Island Bay. Geology 41, 35–38. https://doi.org/10.1130/G33469.1.

`

Hillenbrand, C., Smith, J. A., Hodell, D., Greaves, M., Poole, C. R., Kender, S., Williams, M., Andersen, T. J., Jernas, P. E., Elderfield, H., Klages, J. P. Roberts, S. J., Gohl, K., Larter, R. D., and Kuhn, G. 2017. West Antarctic Ice Sheet retreat driven by Holocene warm water incursions. Nature, 547 (7661), 43-48. https://doi.org/10.1038/nature22995.

Hyun, J.-H., Kim, S.-H., Yang, E. J., Choi, A., Lee, S. H., 2016. Biomass, production, and control of heterotrophic bacterioplankton during a late phytoplankton bloom in the Amundsen Sea Polynya, Antarctica. Deep-Sea Res. II 123, 102-112.

Jenkins, A., Shoosmith, D., Dutrieux, P., Jacobs, S., Kim, T. W., Lee, S. H., Ha, H. K. and Stammerjohn, S., 2018. West Antarctic Ice Sheet retreat in the Amundsen Sea driven by decadal oceanic variability. Nat. Geosci. 11: 733-738. https://doi.org/10.1038/s41561-018-0207-4.

Joughin, I., Smith, B. E., and Medley, B., 2014. Marine ice sheet collapse potentially under way for the Thwaites Glacier Basin, West Antartica. Science 344, 735-738. DOI: 10.1126/science.1249055.

Kempema, E., Reimnitz, E., and Barnes P. W., 1989. Sea ice sediment entrainment and rafting in the Arctic, J. Sediment. Res., 59(2). https://doi.org/10.1306/212F8F80-2B24-11D7-8648000102C1865D.

Komada, T., Anderson, M. R., and Dorfmeier, C. L., 2008. Carbonate removal from coastal sediments for the determination of organic carbon and its isotopic signatures, $\delta^{13}C$ and $\Delta^{14}C$: comparison of fumigation and direct acidification by hydrochloric acid. Limnol. Oceanogr. Methods 6, 254-262.

`

Kim, B., 2016. Distribution of dissolved inorganic radiocarbon in the Amundsen Sea, Antarctica. MSc Thesis, Seoul National University.

Kim, M., Hwang, J., Kim, H. J., Kim, D., Yang, E. J., Ducklow, H. W., La H. S., Lee, S. H., Park, J., and Lee, S., 2015. Sinking particle flux in the sea ice zone of the Amundsen shelf, Antarctica. Deep-Sea Res. I 101, 110-117.

Kim, M., Hwang, J., Lee, S. H., Kim, H. J., Kim, D., Yang, E. J., and Lee, S., 2016. Sedimentation of particulate organic carbon on the Amundsen Shelf, Antarctica. Deep-Sea Res. II. 123, 135-144.

Kim, M., Hwang, J., Rho, T. K. Lee, T., Kang, D. J., Chang, K. I., Noh, S., Joo, H. T., Kwak, J. H., Kang, C. K., Kim, K. R., 2017. Biogeochemical properties of sinking particles in the southwestern part of the East Sea (Japan Sea). J. Mar. Syst. 167, 33-42.

Kim, M., Yang, E. J., Kim, D., Jeong, J.-H., Kim, H. J., Park, J., Jung, J., Ducklow, H. W., Lee, S., and Hwang J. 2019. Sinking particle flux and composition at three sites of different annual sea ice cover in the Amundsen Sea, Antarctica, J. Mar. Syst., 192, 42-50. https://doi.org/10.1016/j.jmarsys.2019.01.002.

Kim, S., Yoo, K. C., Lee, J. I., Lee, M. K., Kim, K. Yoon, H. I., and Moon, H. S., 2018. Relationship between magnetic susceptibility and sediment grain size since the last glacial period in the Southern Ocean off the northern Antarctic Peninsula–Linkages between the cryosphere and atmospheric circulation. Palaeogeogr. Palaeoclimatol. Palaeoecol., 505, 359-370. https://doi.org/10.1016/j.palaeo.2018.06.016.

`

Kirkwood, J., and Burton H. J., 1988. Macrobenthic species assemblages in Ellis Fjord, Vestfold Hills, Antarctica, Mar. Biol., 97(3), 445-457. https://doi.org/10.1007/BF00397776.

Kirshner, A. E., Anderson, J. B., Jakobsson, M., O'Regan, M., Majewski, W., and Nitsche, F. O., 2012. Post-LGM deglaciation in Pine Island Bay, West Antarctica. Quat. Sci. Rev. 38, 11-26. doi.org/10.1016/j.quascirev.2012.01.017.

Komada, T., Anderson, M. R., and Dorfmeier, C. L., 2008. Carbonate removal from coastal sediments for the determination of organic carbon and its isotopic signatures, $\delta^{13}C$ and $\Delta^{14}C$: comparison of fumigation and direct acidification by hydrochloric acid. Limnol. Oceanogr. Methods 6, 254-262.

La, H. S., Lee, H., Fielding, S., Kang, D., Ha, H. K., Atkinson, A., Park, J., Siegel, V., Lee, S., and Shin, H. C., 2015. High density of ice krill (Euphausia crystallorophias) in the Amundsen sea coastal polynya, Antarctica. Deep-Sea Res. I 95, 75-84.

Lam, P. J., Doney, S. C., and Bishop, J. K., 2011. The dynamic ocean biological pump: Insights from a global compilation of particulate organic carbon, CaCO3, and opal concentration profiles from the mesopelagic. Global Biogeochem Cy 25, GB3009, doi:10.1029/2010GB003868.

Larter, R. D., Anderson, J. B., Graham, A. G., Gohl, K., Hillenbrand, C. D., Jakobsson, M., Johnson, J. S., Kuhn, G., Nitsche, F. O., Smith, J. A., 2014. Reconstruction of changes in the Amundsen Sea and Bellingshausen Sea sector of the West Antarctic Ice Sheet since the Last Glacial Maximum. Quat. Sci. Rev. 100, 55-86. https://doi.org/10.1016/j.quascirev.2013.10.016.

`

Lee, J. I., Bak, Y.-S., Yoo, K.-C., Lim, H. S., Yoon, H. I. and Yoon, S. H., 2010. Climate changes in the South Orkney Plateau during the last 8600 years. Holocene, 20(3): 395-404. https://doi.org/10.1177/0959683609353430.

Lee, S., Hwang, J., Ducklow, H. W., Hahm, D., Lee, S. H., Kim, D., Hyun, J. H., Park, J., Ha, H. K., and Kim, T. W., 2017. Evidence of minimal carbon sequestration in the productive Amundsen Sea polynya. Geophy. Res. Lett. 44, 7892-7899.

Lee, S.H., Kim, B.K., Yun, M.S., Joo, H., Yang, E.J., Kim, Y.N., Shin, H.C., Lee, S., 2012. Spatial distribution of phytoplankton productivity in the Amundsen Sea, Antarctica. Polar Biol. 35, 1721-1733. https://doi.org/10.1007/s00300-012-1220-5.

Lee, Y., Yang, E. J., Park, J., Jung, J., Kim, T. W., and Lee, S., 2016. Physical-biological coupling in the Amundsen Sea, Antarctica: Influence of physical factors on phytoplankton community structure and biomass. Deep-Sea Res. I 117, 51-60.

Lee, Y. C., Park, M. O., Jung, J., Yang, E. J., and Lee, S. H., 2016. Taxonomic variability of phytoplankton and relationship with production of CDOM in the polynya of the Amundsen Sea, Antarctica. Deep-Sea Res. II 123, 30-41.

Leonard, G., Mager, S., Pauling, A., Hughes, K., and Smith I. J.,2014. Towards a process model for predicting potential anchor ice formation sites in coastal Antarctic waters, J. Spat. Sci., 59(2), 297-312.

Lizotte, M.P., 2001. The contributions of sea ice algae to Antarctic marine primary production. Amer. Zool. 41, 57-73.

`

Mager, S. M., Smith, I. J., Kempema, E. W., Thomson, B. J., and Leonard G. H., 2013. Anchor ice in polar oceans, Prog. Phys. Geogr., 37(4), 468-483. https://doi.org/10.1177/0309133313479815.

Mager, S. M., Leonard, G. H., Pauling, A. G., and Smith I. J., 2015. A framework for estimating anchor ice extent at potential formation sites in McMurdo Sound, Antarctica, Ann. Glaciol., 56(69), 394-404. https://doi.org/10.3189/2015AoG69A711.

Marcott, S. A., Shakun, J. D., Clark, P. U. and Mix, A. C. 2013. A reconstruction of regional and global temperature for the past 11,300 years. Science, 339(6124): 1198-1201. https://doi.org/10.1126/science.1228026.

Martin, J. H., Knauer, G. A., Karl, D. M., and Broenkow, W. W., 1987. VERTEX: carbon cycling in the northeast Pacific. Deep-Sea Res. I., 34, 267-285.

Massom, R., Harris, P., Michael, K., and Potter, M., 1998. The distribution and formative processes of latent-heat polynyas in East Antarctica. Ann. Glaciol., 27, 420-426. doi:10.3189/1998AoG27-1-420-426.

Mayer L. M., 1994. Surface area control of organic carbon accumulation in continental shelf sediments. Geochim. Cosmochim. Acta, 58, 4, 1271-1284.

McDonnell, A. M. P. and Buesseler, K. O., 2010. Variability in the average sinking velocity of marine particles. Limnol. Oceanogr. 55, 2085-2096.

McIntyre, C. P., Wacker, L., Haghipour, N., Blattmann, T. M., Fahrni, S., Usman, M., Eglinton, T. I. and Synal, H.-A., 2017. Online ^{13}C and ^{14}C Gas Measurements by EA-IRMS–AMS at ETH Zürich. Radiocarbon, 59(3): 893-903. https://doi.org/10.1017/RDC.2016.68.

`

McNichol, A., Osborne, E., Gagnon, A., Fry, B., and Jones, G., 1994. TIC, TOC, DIC, DOC, PIC, POC−unique aspects in the preparation of oceanographic samples for ^{14}C-AMS. Nucl. Instrum. Methods Phys. Res., Sect. B: Beam Interact. Mater. At. 92, 162-165.

Meier L. P. and Menegatti A. P., 1997. New, efficient, one step method for the removal of OM from clay-containing sediments, Clay Minerals, 32. 557-563.

Meredith, M. P., Ducklow, H. W., Schofield, O., Wåhlin, A., Newman, L., and Lee, S., 2016. The interdisciplinary marine system of the Amundsen Sea, Southern Ocean: Recent advances and the need for sustained observations. Deep-Sea Res. II, 123, 1-6. https://doi.org/10.1016/j.dsr2.2015.12.002.

Mortlock, R. A., and Froelich, P. N., 1989. A simple method for the rapid determination of biogenic opal in pelagic marine sediments. Deep-Sea Res. I., 36, 1415-1426.

Mu, L., Stammerjohn, S., Lowry, K., and Yager, P., 2014. Spatial variability of surface pCO_2 and air-sea CO_2 flux in the Amundsen Sea Polynya, Antarctica. Elementa, 3. http://doi.org/10.12952/journal.elementa.000036.

Nelson, D. M., DeMaster, D. J., Dunbar, R. B. and Smith Jr, W. O., 1996. Cycling of organic carbon and biogenic silica in the Southern Ocean: Estimates of water-column and sedimentary fluxes on the Ross Sea continental shelf. J. Geophys. Res., 101, 18519-18532. doi:10.1029/95JC01573.

Nihashi, S., and Ohshima K. I., 2015. Circumpolar mapping of Antarctic coastal polynyas and landfast sea ice: relationship and variability, J. clim., 28(9), 3650-3670. https://doi.org/10.1175/JCLI-D-14-00369.1.

`

Nürnberg, D., Wollenburg, I., Dethleff, D., Eicken, H., Kassens, H., Letzig, T., Reimnitz, E., and Thiede, J., 1994. Sediments in Arctic sea ice: implications for entrainment, transport and release, Mar. Geol., 119(3), 185-214. https://doi.org/10.1016/0025-3227(94)90181-3.

Obermüller, B. E., Truebano, M., Peck, L. S., Eastman, J. T., and Morley S. A., 2013. Reduced seasonality in elemental CHN composition of Antarctic marine benthic predators and scavengers, J. Exp. Mar. Biol. Ecol., 446, 328-333. https://doi.org/10.1016/j.jembe.2013.06.001.

Otosaka, S., Tanaka, T., Togawa, O., Amano, H., Karasev, E. V., Minakawa, M., and Noriki S., 2008. Deep sea circulation of particulate organic carbon in the Japan Sea. J. Oceanogr., 64, 911-923.

Pearson, A. 2000. Biogeochemical applications of compound-specific radiocarbon analysis, PhD Thesis, Woods Hole Oceanographic Institution/Massachusetts Institute of Technology.

Pfirman, S., Lange, M., Wollenburg, I., and Schlosser P. 1990. Sea ice characteristics and the role of sediment inclusions in deep-sea deposition: Arctic—Antarctic comparisons, in: Bleil U., Thiede J. (eds) Geological History of the Polar Oceans: Arctic versus Antarctic. NATO ASI Series, (Vol. 308, pp. 187-211), Springer. https://doi.org/ 10.1007/978-94-009-2029-3_11.

Picken, G. B., 1980. Reproductive adaptations of Antarctic benthic invertebrates, Biol. J. Linnean. Soc., 14(1), 67-75. https://doi.org/10.1111/j.1095-8312.1980.tb00098.

`

Planquette, H., Sherrell, R. M., Stammerjohn, S. E., and Field, M. P., 2013. Particulate iron delivery to the water column of the Amundsen Sea, Antarctica. Mar. Chem. 153, 15-30.

Pritchard, H. D., Arthern, R. J., Vaughan, D. G., and Edwards, L. A., 2009. Extensive dynamic thinning on the margins of the Greenland and Antarctic ice sheets. Nature, 461, 971-975.

Pritchard, H. D., Ligtenberg, S. R. M., Fricker, H. A., Vaughan, D. G, van den Broeke, M. R., and Padman, L., 2012. Antarctic ice-sheet loss driven by basal melting, Nature, 484, 502-505, doi:10.1038/nature10968.

Ramseier, R. O., Garrity, C., Bauerfeind, E., Peinert, R., 1999. Sea-ice impact on long-term particle flux in the Greenland Sea's Is Odden-Nordbukta region, 1985–1996. J. Geophys. Res. 104, 5329-5343.

Reigstad, M., and Wassmann, P., 2007. Does Phaeocystis spp. contribute significantly to vertical export of organic carbon? Biogeochemistry 83, 217-234.

Reimnitz, E., Marincovich Jr, L., McCormick, M., and Briggs W., 1992. Suspension freezing of bottom sediment and biota in the Northwest Passage and implications for Arctic Ocean sedimentation, Can. J. Earth Sci., 29(4), 693-703. https://doi.org/10.1139/e92-060.

Rignot, E., Bamber, J. L., Van Den Broeke, M. R., Davis, C., Li, Y., Van De Berg, W. J., Van Meijgaard, E., 2008. Recent Antarctic ice mass loss from radar interferometry and regional climate modelling. Nature Geosci. 1, 106-110.

Robinson, N. J., Williams, M. J., Stevens, C. L., Langhorne, P. J., and Haskell T. G., 2014. Evolution of a supercooled Ice Shelf Water plume with an actively

growing subice platelet matrix, J. Geophys. Res.,119(6), 3425-3446. https://doi.org/10.1002/2013JC009399.

Salter, I., Kemp, A. E., Moore, C. M., Lampitt, R. S., Wolff, G. A., and Holtvoeth, J., 2012. Diatom resting spore ecology drives enhanced carbon export from a naturally iron-fertilized bloom in the Southern Ocean. Glob. Biogeochem. Cycles 26. GB1014.

Scherer, R. P., 1994. A new method for the determination of absolute abundance of diatoms and other silt-sized sedimentary particles. J. Paleolimnol. 12(2): 171-179. https://doi.org/10.1007/BF00678093.

Smith Jr, W. O. and Barber, D. 2007. Polynyas: Windows to the World. Elsevier Oceanographic Series, 74. Elsevier. 458. Amsterdam, ISBN: 978-0-444-52952-7.

Smith Jr, W. O., and Comiso, J. C., 2008. Influence of sea ice on primary production in the Southern Ocean: A satellite perspective. J. Geophys. Res. 113. C05S93.

Smith Jr, W. O., Ainley, D. G., Arrigo, K. R., and Dinniman, M. S., 2014. The oceanography and ecology of the Ross Sea. Ann. Rev. Mar. Sci. 6, 469-487.

Smith, J. A., Hillenbrand, C. D., Kuhn, G., Larter, R. D., Graham, A. G., Ehrmann, W., Moreton, S. G., and Forwick, M., 2011. Deglacial history of the West Antarctic Ice Sheet in the western Amundsen Sea embayment. Quat. Sci. Rev. 30, 488-505. https://doi.org/10.1016/j.quascirev.2010.11.020.

Smith, J. A., Hillenbrand, C. D., Kuhn, G., Klages, J. P., Graham, A. G., Larter, R. D., Ehrmann, W., Moreton, S. G., Wiers, S., and Frederichs, T., 2014. New constraints on the timing of West Antarctic Ice Sheet retreat in the eastern

Amundsen Sea since the Last Glacial Maximum. Glob. Planet Change, 122: 224-237. https://doi.org/10.1016/j.gloplacha.2014.07.015.

Stammerjohn, S., Massom, R., Rind, D., and Martinson, D., 2012. Regions of rapid sea ice change: An inter hemispheric seasonal comparison. Geophys. Res. Lett. 39, L0501. doi:10.1029/2012GL050874.

Stammerjohn, S., Maksym, T., Massom, R., Lowry, K., Arrigo, K., Yuan, X., Raphael, M., Randall-Goodwin, E., Sherrell, R., and Yager, P., 2015. Seasonal sea ice changes in the Amundsen Sea, Antarctica, over the period of 1979–2014. Elementa, 3:000055.

Stuiver, M., and Polach, H.A., 1977. Discussion; reporting of ^{14}C data. Radiocarbon 19, 355-363.

Subt, C., Fangman, K. A., Wellner, J. S. and Rosenheim, B. E. 2016. Sediment chronology in Antarctic deglacial sediments: Reconciling organic carbon ^{14}C ages to carbonate ^{14}C ages using Ramped PyrOx. Holocene, 26(2): 265-273. https://doi.org/10.1177/0959683615608688.

Taylor, S. R., and McLennan S. M., 1985. The continental crust: its composition and evolution. Blackwell Sci., Oxford, U.K.

Thomas, R., E. Rignot, G. Casassa, P. Kanagaratnam, C. Acuna, T. Akins, H. Brecher, E. Frederick, P. Gogineni, W. Krabill, S. Manizade, H. Ramamoorthy, A. Rivera, R. Russell, J. Sonntag, R. Swift, J. Yungel, and J. Zwally. Accelerated Sea-level rise from West Antarctica. 2004, Science 306, 255, doi:10.1126/science.1099650.

`

Turner, J., Comiso, J. C., Marshall, G. J., Lachlan-Cope, T. A., Bracegirdle, T., Maksym, T., Meredith, M. P., Wang, Z. and Orr, A., 2009. Non-annular atmospheric circulation change induced by stratospheric ozone depletion and its role in the recent increase of Antarctic sea ice extent. Geophys. Res. Lett., 36. doi:10.1029/2009GL037524.

Volkman, J. K., 1986. A review of sterol markers for marine and terrigenous organic matter. Org. Geochem. 9(2): 83-99. https://doi.org/10.1016/0146-6380(86)90089-6.

Volkman, J. K., Barrett, S. M., Blackburn, S. I., Mansour, M. P., Sikes, E. L., and Gelin, F., 1998. Microalgal biomarkers: a review of recent research developments. Org. Geochem. 29(5-7): 1163-1179. doi.org/10.1016/S0146-6380(98)00062-X.

Volkman, J. K., 2003. Sterols in microorganisms. J. Appl. Microbiol Biotechnol. 60(5): 495-506. https://doi.org/10.1007/s00253-002-1172-8.

Walker, D. P., Brandon, M. A., Jenkins, A., Allen, J. T., Dowdeswell, J. A., and Evans, J., 2007. Oceanic heat transport onto the Amundsen Sea shelf through a submarine glacial trough. Geophys. Res. Lett. 34, 1-4.

Yager, P. L., Sherrell, L., Stammerjohn, S., Alderkamp, A., Schofield, O., Abrahamsen, E., Arrigo, K., Bertilsson, S., Garay, D., and Guerrero, R., 2012. ASPIRE: The Amundsen Sea Polynya International Research Expedition. Oceanogr. 25, 40-53.

Yager, P. L., Sherrell, R. M., Stammerjohn, S. E., Ducklow, H. W., Schofield, O. M. E., Ingall, E. D., Wilson, S. E., Lowry, K. E., Williams, C. M., Riemann, L.,

`

Bertilsson, S., Alderkamp, A.-C., Dinasquet, J., Logares, R., Richert, I., Sipler, R. E., Melara, A. J., Mu, L., Newstead, R. G., Post, A. F., Swalethorp, R., and van Dijken, G. L., 2016. A carbon budget for the Amundsen Sea Polynya, Antarctica: Estimating net community production and export in a highly productive polar ecosystem. Elementa 4, 00140.

Yang, E. J., Jiang, Y., and Lee, S., 2016. Microzooplankton herbivory and community structure in the Amundsen Sea, Antarctica. Deep-Sea Res. II 123, 58-68. https://doi.org/10.1016/j.dsr2.2015.06.001.

Yang, E. J., Lee, Y. and Lee, S., 2018. Trophic interactions of micro-and mesozooplankton in the Amundsen Sea polynya and adjacent sea ice zone during austral late summer., https://doi.org/10.1016/j.pocean.2018.12.003.

`

ABSTRACT (in Korean)

서남극 아문젠해는 현재 진행되고 있는 기후변화로 인한 빙붕과 해빙의 급격한 감소를 겪는 등 민감하게 반응하고 있으며, 이에 따라 일차생산과 이산화탄소 흡수 등 탄소순환 양상이 급격하게 변화할 것으로 예상된다. 지구 온난화에 따른 이러한 변화는 일차원적으로 일어나지 않으며, 따라서 보다 정확한 미래 예측을 위해서는 과거와 현재 아문젠해 탄소순환을 이해하는 것이 중요하다.

본 연구는 이러한 아문젠해에서의 탄소순환 양상 변화를 밝히기 위한 국제적이고 다학제적인 연구의 일환으로 극지연구소, ETH Zürich, 그리고 BAS(British Antarctic Survey) 팀과 함께 진행하였다. 2011년부터 2018년에 걸쳐 아문젠해역 전역에서 획득한 침강 입자와 퇴적물 시료를 이용하여 현재와 과거, 홀로세 동안 아문젠해 유기탄소순환을 다층 중장기적으로 해석하였다.

아문젠 해역은 남반구의 여름을 제외하고는 접근이 힘든 지역이기 때문에 퇴적물 트랩은 이 해역의 생물학적 펌프 작용을 살펴볼 수 있는 유일한 방법이다. 2015년 해빙역에서 최초로 이루어진 1년간의 침강입자 연구를 시공간적으로 확대하여, 본 학위논문에서는 해빙역과 아문젠해 폴리냐 내부, 닷슨 빙붕 앞에서 획득한 침강입자 퇴적물 시료를 해석하였다. 아문젠해 전반적으로는 규조류가 우점하는 해빙역이 폴리냐 내부와 빙붕 앞쪽에 비해 침강입자 플럭스가 높게 관측되었다. 다년간의 해빙역 침강입자 자료를 통해 해빙역에서의 침강입자의 플럭스는 해빙이 녹는 정도와 더불어 시기가 매우 중요함을 시사하였다.

또한 해빙역과 빙붕 앞쪽의 퇴적물 트랩에서 2년에 걸쳐

`

거대 저서동물과 가리비, 성게가 발견되었는데, 이는 퇴적물 트랩 연구 사상 최초로 보고되는 현상이다. 이 저서동물 시료의 길이와 두께를 측정하여 유기탄소량으로 환산한 값은 일차생산으로 공급되는 유기탄소의 5배에 달했다. 본 연구에서는 이러한 형태의 유기물 공급이 주로 남반구의 겨울철에 관측되었음을 제시하며, 이 현상이 아문젠 해역, 나아가 남극주변 대륙붕의 저서생태계에 미치는 영향을 고찰하였다. 또한 아문젠해에서의 anchor ice의 형성 가능성을 제시하며 이 생물들의 수송 기작에 대하여 고찰하였다.

한편 중력코어와 박스코어 퇴적물 분석을 통해 홀로세 동안 아문젠 해역 내 유기탄소 퇴적양상을 연구하였다. 이를 위하여 최장 200cm 깊이의 중력코어 시료를 분석하였다. 이전까지 이 해역에서의 고기후 연구와는 차별적으로 깊이에 따른 고해상도의 방사성탄소동위원소 값을 얻었다. 아문젠해 해빙역, 폴리냐 내부와 닷슨 빙붕 앞에서 획득한 각각의 퇴적물에는 아문젠 해역의 해빙역과 폴리냐가 빙하의 후퇴와 해빙 이후 겪은 서로 다른 표층 환경이 반영되어 나타났다. 또한 폴리냐 내부 퇴적물의 다양한 생지화학적 근거(Br/Ti, Ba/Al, 지방계 바이오마커와 규조류 개체 수 등)를 바탕으로 아문젠해 폴리냐의 형성 시기와 과거 환경 변화를 유추하였다. 아문젠해 폴리냐는 해빙 직후 형성되기 시작한 것으로 예상되며 9~6 kyr cal BP 무렵 우점종의 변화가 있었던 것으로 보였다.

중력코어의 공간적 한계를 보완하고자 아문젠 폴리냐 내/외부와 닷슨 트러프의 내/외부 다양한 정점에서 박스코어 퇴적물을 획득하였다. 방사성탄소동위원소, 지방계 바이오마커, 입자사이즈

`

등을 분석함으로써 과거 아문젠 해역의 고환경과 퇴적양상을 보다 고해상도로 추정하였다.

기후변화에 의한 영향을 가장 첨예하게 받음과 동시에, 접근의 어려움으로 인간활동의 영향을 가장 적게 받은 해역 중 한 곳인 서남극 아문젠해에서 현재와 과거 유기탄소 순환을 다층 중장기적으로 이해하고자 했던 본 학위논문은 미래 기후 온난화에 따른 남극 탄소순환양상을 예측하고 기후 모델을 제시하는 데 있어 중요한 자료를 제공하였다.

주요어: 입자성유기탄소, 방사성탄소동위원소, 퇴적물 트랩, 중력코어, 아문젠해

학번: 2014-31014